Uncertainty modeling, propagation, and quantification techniques with applications in engineering dynamics

Thesis submitted in accordance with the requirements of
the University of Liverpool for the degree of Doctor in Philosophy
by

Yuanjin Zhang

March 2017

Acknowledgements

I would like to express my sincere thanks to my research supervisor Assistant Professor Ioannis A. Kougioumtzoglou for his inspiring mentorship and invaluable help during my PhD studies at the University of Liverpool. He has always been available to provide help and discuss academic matters. Further, he has provided the necessary academic freedom to develop myself into an independent researcher.

Further, I also want to express my thanks to my supervisors Professor Michael Beer and Dr. Edoardo Patelli. They have provided with useful advice and allowed me to find my own way to perform research. Special thanks go to Dr. Liam Comerford for his help in editing and co-authoring our research papers.

Finally, I would like to express my gratitude to my family for their unconditional support both materially and spiritually.

Abstract

In the field of engineering dynamics, three of the main challenges associated with stochasticity relate to a) uncertainty modeling, b) uncertainty quantification, and c) uncertainty propagation. Addressing challenge a) relates to the development of methodologies for the interpretation/analysis of measured/available data, as well as for subsequent estimation of pertinent stochastic models, i.e. quantification of the underlying stochastic process/field statistics, while challenge b) relates to quantifying the error of those estimates in a priori, if possible, manner. However, in several engineering applications large amounts of data can be difficult to acquire for several reasons, such as cost, data loss or corruption, as well as limited bandwidth/storage capacity. Furthermore, available data can often be highly limited and irregularly sampled, and thus, standard techniques for spectral estimation, (e.g. Fourier decomposition), can demonstrate poor performance. Further, addressing challenge c) relates to the development of methodologies for determining complex system response/reliability statistics, i.e. development of analytical/numerical methodologies for solving nonlinear high-dimensional stochastic (partial) differential equations efficiently. In this regard, the Monte Carlo simulation (MCS) has been perhaps the most versatile tool. Nevertheless, there are cases, especially for large-scale systems, where the MCS can be computationally prohibitive. Thus, there is a need for developing efficient approximate analytical and/or numerical approaches. In this thesis, techniques are developed for addressing selected aspects of challenges a, b), and c).

First, a general L_p norm ($0 < p \leq 1$) minimization approach is proposed for estimating stochastic process power spectra subject to realizations with incomplete/missing data. Specifically, relying on the assumption that the recorded incomplete data exhibit a significant degree of sparsity in a given domain, employing appropriate Fourier and wavelet bases, and focusing on the L_1 and $L_{1/2}$ norms, it is shown that the approach can satisfactorily estimate the spectral content of the underlying process. Finally, the effect of the chosen norm on the power spectrum estimation error is investigated, and it is shown that the $L_{1/2}$ norm provides almost always a sparser solution than the L_1 norm. Numerical examples consider several stationary, non-stationary, and multi-dimensional processes for demonstrating the accuracy and robustness of the approach, even in cases of up to 80% missing data.

Second, the challenge of quantifying the uncertainty in stochastic process spectral estimates based on realizations with missing data is addressed. Specifically, relying on relatively relaxed assumptions for the missing data and on a Kriging modeling scheme, utilizing fundamental concepts

from probability theory, and resorting to a Fourier based representation of stationary stochastic processes, a closed-form expression for the probability density function (PDF) of the power spectrum value corresponding to a specific frequency is derived. Next, the approach is extended for determining the PDF of spectral moments estimates as well. Clearly, this is of significant importance to various reliability assessment methodologies that rely on knowledge of the system response spectral moments for evaluating its survival probability. Further, it is shown that utilizing a Cholesky-like decomposition for the PDF related integrals the computational cost is kept at a minimal level. Several numerical examples are included and compared against pertinent Monte Carlo simulations for demonstrating the validity of the approach.

Third, a Wiener path integral (WPI) technique based on a variational formulation is developed for nonlinear oscillator stochastic response determination and reliability assessment. This is done in conjunction with a stochastic averaging/linearization treatment of the problem. Specifically, first the nonlinear oscillator is cast into an equivalent linear one with time-varying stiffness and damping elements. Next, relying on the concept of the most probable path a closed-form approximate analytical expression for the oscillator joint transition probability density function (PDF) is derived for small time intervals. Finally, the transition PDF in conjunction with a discrete version of the Chapman-Kolmogorov (C-K) equation is utilized for advancing the solution in short time steps. In this manner, not only the non-stationary response PDF, but also the oscillator survival probability and first-passage PDF are determined. In comparison with existing numerical path integral schemes, a significant advantage of the proposed WPI technique is that closed-form analytical expressions are derived for the involved multi-dimensional integrals; thus, the computational cost is kept at a minimum level. The hardening Duffing and the bilinear hysteretic oscillators are considered in the numerical examples section. Comparisons with pertinent Monte Carlo simulation data demonstrate the reliability of the developed technique.

Finally, an approximate analytical technique for assessing the reliability of a softening Duffing oscillator subject to evolutionary stochastic excitation is developed. Specifically, relying on a stochastic averaging treatment of the problem the oscillator time-varying survival probability is determined in a computationally efficient manner. In comparison with previous techniques that neglect the potential unbounded response behavior of the oscillator when the restoring force acquires negative values, the herein developed technique readily takes this aspect into account by introducing a special form for the oscillator non-stationary response amplitude probability density function (PDF). A significant advantage of the technique relates to the fact that it can readily handle cases of stochastic excitations that exhibit strong variability in both the intensity and the frequency content. Numerical examples include a softening Duffing oscillator under evolutionary earthquake excitation, as well as a softening Duffing oscillator with nonlinear damping modeling the nonlinear ship roll motion in beam seas. Comparisons with pertinent Monte Carlo simulation data demonstrate the efficiency of the technique.

Contents

List of Figures

List of Notations

Chapter 2:

x: discrete time signal vector

A: full measurement matrix

B: reduced measurement matrix

y: sparse coefficient

r, s: iteration index

λ: Lagrangian coefficient

S_X: power spectrum

T: sigal duration

$x(t)$: sigal realization

$W^G_{(m,n),k}$: Harmonic wavelet transform coefficient

ω, t: frequency and time

$(.)^T$: non-conjugate transpose of matrix $(.)$

Chapter 3:

$(.)^T$: non-conjugate transpose of matrix $(.)$

$S_f(\omega_k)$: power spectrum value at frequency ω_k

$\mathbf{X}_\alpha, \mathbf{X}_\beta$: known points vector and missing points vector

$\boldsymbol{\mu}, \boldsymbol{\Sigma}$: mean vector and variance matrix of missing points

N : length of the signal

λ_m : m-th spectral moments

$f_X(x), \Phi_X(\omega)$: probability density function and characteristic function of random variable X

B : barrier level

$H(\omega)$: frequency response function

$P_B(t)$: survival probability

Chapter 4:

$x_n(t)$: system response process

$x(t)$: equivalent system response process

$w(t)$: white excitation process

β, β_{eq} : damping coefficient, equivalent damping coefficient

A : amplitude of the system response

ω_0, ω_{eq} : natural frequency, equivalent frequency

S_0 : power spectral value

$W(x(t))$: probability density functional

$p_B(t)$: first passage probability

$H_u(.)$: unit step function

$K_1(A,t), K_2(A,t)$: Fokker-Planck equation coefficients

Chapter 5:

$x_n(t)$: system response process

$x(t)$: equivalent system response process

ε: duffing nonlinearity coefficient

$w_x(t)$: non-stationary excitation process

A : amplitude of the system response

$\omega_0, \omega_{eq}, \omega_{eq,B}$: natural frequency, equivalent frequency, bounded equivalent frequency

ζ_0 : damping ratio

$\beta_{eq}, \beta_{eq,B}$: equivalent damping coefficient, bounded equivalent damping coefficient

A_{cr} : critical response amplitude

$I_0(.)$: Bessel function of the first kind and of zero order

$T_{eq}(t)$: equivalent natural period

$\Gamma[.,.]$: incomplete Gamma function

Chapter 1

Introduction

1.1 Motivation and objectives

Quantification and management of risk becomes increasingly important in many scientific and technical fields such as engineering, economics and material science, where the effect of uncertainty cannot be neglected. In the field of engineering dynamics, two of the main challenges associated with uncertainty quantification relate to the modeling, and the propagation of the uncertainties. Addressing the challenge of uncertainty modeling relates to the development of methodologies (e.g. spectral analysis techniques) for the interpretation/analysis of measured/available data, as well as for subsequent estimation of pertinent stochastic models, i.e. quantification of the underlying stochastic process/field statistics. These uncertainties are mainly associated with (i) excitations, i.e. environmental processes such as winds, sea waves, seismic motions, extreme events due to climate change, etc, (ii) system parameters, i.e. geometry, material properties, etc, and (iii) system response as a result of (i) and (ii), and (iv) model error, which are the differences between the actual system and the model used to describe the actual system, and the differences between the real excitation and excitation model utilized in the simulations. Clearly, based on available data (ordinarily acquired via experimental set-ups, e.g. sensors), there is a need to translate the above uncertainties into engineering stochastic models so that structural systems are efficiently designed, monitored, and maintained. In real-life situations, however, measured/available data most often exhibit a time/space-varying behavior. For instance, most environmental processes/excitations (and subsequently the system responses) can be realistically described as non-stationary stochastic processes, i.e. their statistics (as well as their frequency content potentially) vary with time. Similarly, in cases of composite/functionally-graded materials for instance, properties such as the Young's modulus, can be realistically modeled as non-homogeneous stochastic fields, i.e. their statistics vary with space. Further, most often there are limited, incomplete and/or missing data. In several engineering applications large amounts of data can be difficult to acquire for several reasons, such as cost (e.g. expensive sensor maintenance in harsh conditions/remote areas), frequency and unpredictability of the effect (e.g. earthquakes), data loss or corruption (e.g. sensor failures, power out-

ages, etc), as well as limited bandwidth/storage capacity. Furthermore, available data can often be highly limited and irregularly sampled. When working with limited data, standard techniques for spectral estimation, (e.g. Fourier decomposition), can demonstrate poor performance, and without any prior knowledge of the underlying statistics of the process, alternative (less general) analysis techniques can be problematic in certain cases. For instance, autoregressive methods can be used often assuming the time record is relatively long and missing data are grouped [10]. Addressing the challenge of the uncertainty propagation relates to the development of methodologies for determining complex system response/reliability statistics, i.e. development of analytical/numerical methodologies for solving nonlinear high-dimensional stochastic (partial) differential equations efficiently. In this regard, the Monte Carlo simulation (MCS) has been perhaps the most versatile tool. Nevertheless, there are cases, especially for large-scale systems, where the MCS can be computationally prohibitive. Thus, there is a need for developing efficient approximate analytical and/or numerical approaches.

In uncertainty modeling, incomplete data is often a big issue to tackle, such as the missing data in wireless sensor networks for structural health monitoring [143] and in spectral estimation (eg. [24] ; [25]). In many cases, stochastic processes are most often described by statistical quantities such as the power spectrum. For instance, a Fourier basis is typically utilized in the spectral estimation of stationary processes [80]. Further, similar to the stationary case, the evolutionary power spectrum related to non-stationary processes can be estimated by employing wavelet (e.g. [115]; [62]) or chirplet bases [90] among other alternatives; see also [93] for a detailed presentation of joint time-frequency analysis techniques. It is noted that the above spectral estimation approaches often require a large number of complete data samples for attaining a predefined adequate degree of accuracy. However, missing data in measurements is frequently an unavoidable situation, especially in the cases where the measurement cost is very high or the data transition loss such as in structure health monitoring [54]. In fact, missing data are possible in almost any situation where data are collected and stored. Indicative reasons in engineering dynamics measurement applications include failure and/or restricted use of equipment, as well as data corruption and cost/bandwidth limitations. Thus, standard spectral analysis techniques that inherently assume the existence of full sets of data, such as those based on Fourier, wavelet and chirplet transforms, cannot be used in a straightforward manner.

To address this challenge, a large number of methods subject to missing / incomplete data (e.g. Lomb-Scargle periodogram, iterative deconvolution method CLEAN, ARMA-model based techniques, etc) have been developed with various degrees of accuracy; see [136] for a review. In general, the power spectrum of many excitations in engineering applications, such as the Jonswap spectrum [51] in sea wave modelling, can be treated as sparse. That is the dominant frequencies of the spectrum are distributed within a relatively small interval in the frequency domain. Based on the above sparsity property, a compressive sensing [37] based approach has recently been developed to reconstruct the missing data by utilizing a L_1-norm optimization technique for both

stationary and nonstationary stochastic processes [25]. According to the compressive sensing concept and assuming a sparse signal, fewer measurements are required compared with conventional recovery algorithms based on Shannon theorem. Nevertheless, on one hand, reconstructing the available records, and thus, deterministically estimating/predicting missing values, rarely accounts for the inherent uncertainty associated with the missing data. Hence, there is merit in developing a methodology for quantifying the uncertainty in a given spectral estimate as a result of the uncertainty related to the missing data in the time/space domain. On the other hand, for those signals which are not sparse enough, L_1 norm based compressive sensing method does not preform well enough in terms of accuracy. Thus, there is still a need to improve the accuracy and efficiency of the above method, especially for the less sparse signals.

To deal with the challenge of the propagation of the uncertainties, Monte Carlo simulation (MCS) (eg. [102], [103], [107]), is often utilized to determine the system response statistics such as the mean and variance (eg. [42], [96], [49]). Undoubtedly, Monte Carlo simulation is the most versatile solution tool since it can readily address complex system and excitation modeling. In general, the essential idea of Monte Carlo simulation (MCS) is to propagate the uncertainty from either the input excitation or the system itself to the final output. In essence, MCS involves a number of deterministic experiments and subsequent statistical analysis on the output responses.

With the increase of computing capacity over the past decades, MCS is widely utilized in tackling various engineering problems. Among them, assessing the reliability of structural systems has been a persistent challenge in the field of engineering dynamics with diverse applications. Further, assessing the risk of failure, or performing a reliability based analysis of dynamical systems is closely related to the determination of the probability that the response of the system stays below a prescribed threshold over a given time interval. This time-dependent probability is also known as survival probability. In this regard, several research efforts have focused on developing versatile MCS based techniques such as importance sampling, subset simulation and line sampling for reliability assessment applications; see (eg. [11],[3], [2],[106]) for some indicative references. Nevertheless, there are cases, especially for large scale complex systems or when the quantity of interest has a relatively small probability of occurrence, where MCS techniques can be computationally prohibitive. In this regard, there is a need for developing alternative efficient approximate analytical and/or numerical solution techniques [70]. In [61] and [63], an analytical stochastic average statistical linearization is used to determine the response statistics. And this method is also applied to obtain the survival probability [118] and is extended to multiple dimension cases [65].

In this regard, in the first half of this thesis, the problems of power spectrum estimation subject to missing data and of assessing the accuracy of the estimates are considered. Thus, a sparsity optimization based method called Lp norm is proposed (eg. [94], [15], [139]) for re-constructing the missing data, whereas the uncertainty of the power spectrum estimates is quantified as well. This method can be used in cases such as structure health monitoring [54], and response system power spectrum estimation subject to the stochastic excitations. After discussing the excitation

estimation, the system response problem can be considered accordingly. Further, in the second half of the thesis, approximate semi-analytical techniques are developed for stochastic response determination and reliability assessment of structural systems. This is done in conjunction with a stochastic averaging/linearization treatment of the problem (eg. [63], [100]), while the recently developed path integral technique([138], [41]) is extended and employed to describe the response of the nonlinear system as well (eg. [14], [64], [67]). It provides an analytical tool to deal with the reliability assessment of the system response subject to stochastic excitations, such as energy harvesting [46], earthquake engineering applications (eg. [18], [116]) the ship rolling motion in the unidirectional beam waves [68].

1.2 Organization of the thesis

This thesis includes six chapters and two appendixes, followed by the list of cited references. The first chapter and the last one present the general introduction section and concluding remarks section respectively, while the rest four chapters, contain their own individual preliminary introduction part, theoretical background and pertinent numerical examples demonstrating the accuracy and efficiency of the developed techniques in each of the chapters.

Chapter 1 introduces the motivation and objectives of the current research. Besides the brief introduction, it also provide the organization and basic contents of each chapter.

Chapter 2 presents the $L_{1/2}$ norm based power spectral estimation method to deal with recorded process realizations suffering from the missing data. Basically, it apples linear transforms such as the discrete Fourier transform or wavelet transform, as the standard spectral estimation methods. Relying on the $L_{1/2}$ norm optimization for the sparse signal, missing data could be reconstructed to the sparse form in the frequency domain. Compared with the compressive sensing method which is based on the L_1 norm optimization, the solution from $L_{1/2}$ norm enhances the peak frequencies parts, making them approach to the level of the original spectrum. To improve the power spectral estimation performance of $L_{1/2}$ norm method, an iterative reweighing procedure is applied before the optimization of $L_{1/2}$ norm to deal with the multiple samples case. In this reweighing procedure, a least square method is utilized repetitively until the error of reweighing coefficients is below the prescribed tolerance. The reconstruction methods are shown to be extremely effective in cases where up to 80% of the data has been lost. Further, the effect of the choice of minimization procedure on the final reconstruction error is investigated, demonstrating a definitive link between available sample size and most effective norm algorithm.

In Chapter 3, the challenge of quantifying the uncertainty in stochastic process spectral estimates based on realizations with missing data is addressed. Specifically, relying on relatively relaxed assumptions for the missing data and on a Kriging modeling scheme, utilizing fundamental concepts from probability theory, and resorting to a Fourier based representation of stationary stochastic processes, a closed-form expression for the probability density function (PDF) of the

power spectrum value corresponding to a specific frequency is derived. Next, the approach is extended for determining the PDF of spectral moments estimates as well. Clearly, this is of significant importance to various reliability assessment methodologies that rely on knowledge of the system response spectral moments for evaluating the survival probability. Further, it is shown that utilizing a Cholesky kind decomposition for the PDF related integrals the computational cost is kept at a minimal level. Several numerical examples are included and compared against pertinent Monte Carlo simulations for demonstrating the validity of the approach.

In chapter 4, a Wiener path integral (WPI) technique based on a variational formulation is developed for nonlinear oscillator stochastic response determination and reliability assessment. This is done in conjunction with a stochastic averaging/linearization treatment of the problem. Specifically, first the nonlinear oscillator is cast into an equivalent linear one with time-varying stiffness and damping elements. Next, relying on the concept of the most probable path a closed-form approximate analytical expression for the oscillator joint transition probability density function (PDF) is derived for small time intervals. Finally, the transition PDF in conjunction with a discrete version of the Chapman-Kolmogorov (C-K) equation is utilized for advancing the solution in short time steps. In this manner, not only the non-stationary response PDF, but also the oscillator survival probability and first-passage PDF are determined. In comparison with existing numerical path integral schemes, a significant advantage of the proposed WPI technique is that closed-form analytical expressions are derived for the involved multi-dimensional integrals; thus, the computational cost is kept at a minimum level. The hardening Duffing and the bilinear hysteretic oscillators are considered in the numerical examples section. Comparisons with pertinent Monte Carlo simulation data demonstrate the reliability of the developed technique.

Chapter 5 focuses on Softening Duffing oscillator reliability assessment subject to evolutionary stochastic excitation. Specifically, relying on a stochastic averaging treatment of the problem the oscillator time-varying survival probability is determined in a computationally efficient manner. In comparison with previous techniques that neglect the potential unbounded response behavior of the oscillator when the restoring force acquires negative values, the herein developed technique readily takes this aspect into account by introducing a special form for the oscillator non-stationary response amplitude probability density function (PDF). A significant advantage of the technique relates to the fact that it can readily handle cases of stochastic excitations that exhibit strong variability in both the intensity and the frequency content. Numerical examples include a softening Duffing oscillator under evolutionary earthquake excitation, as well as a softening Duffing oscillator with nonlinear damping modeling the nonlinear ship roll motion in beam seas. Comparisons with pertinent Monte Carlo simulation data demonstrate the efficiency of the technique.

Chapter 6 contains concluding remarks and some suggestions for potential future work, while two Appendices related to Chapters 3 and 4 are included as well.

Chapter 2

Uncertainty modeling: L_p-norm minimization for stochastic process power spectrum estimation subject to incomplete data

2.1 Preliminary remarks

Reconstruction of discrete time/space signals that suffer from missing data has long been a topic of interest across a range of fields. Whilst the most effective way to address such problems is to sample signals more reliably, under controlled conditions, this is not always possible. 'Missing data' in general, refers to situations in which undesirable gaps occur in data sets. For example, in wireless sensor network for structure health monitoring [54], such problems may be caused by sensor failures or sampling / threshold limitations on the equipment, acquisition or usage restrictions on sensing or on the data itself, and even from data corruption. Re-sampling missing data can be difficult in many cases, and often impossible when working with time-dependent stochastic processes. For this reason, there are numerous approaches to addressing these problems by predicting missing datum values based on the available data. These include zero-padding of missing data [76], least-squares spectral analysis [72], [105], [132], iterative spectral de-noising [53], [4], [97], interpolative as well as autoregressive methods [39]. Clearly, in most cases the choice of the approach is problem-dependent, and typically depends on a priori known information such as the arrangement and amount of missing data. This chapter focuses on a class of missing data problems for which the property of 'sparsity' is exploited to reconstruct records. A sparse discrete-time signal can be characterized by a relatively small number of coefficients with respect to its sample length. This sparsity may be apparent in the sampling domain, for which the majority of the data is zero except for a handful of spikes, or sparsity can occur in some other basis or frame, such as the frequency domain. Signal reconstruction methods that take advantage of sparsity have received increased interest with the advent of Compressive Sensing (CS) [12], [36], a signal processing technique in which data are purposely under-sampled.

Regarding applications in structural engineering/dynamics, so far CS has been mostly applied in situations where some saving in data capture time or data size is useful. For example, sensors (especially wireless ones) that capture data for real-time structural health monitoring can be designed to capture only a fraction of the data, reducing manufacturing cost. By utilizing CS with an appropriate compression basis (in which the signal has a sparse representation), data series with far higher resolution than those originally captured could be reconstructed. Not only would the sensors not need to capture as much data, but also the stored data would have a small file size, negating the requirement for compression processing at the sensor. In this regard, some preliminary recent results exist in the literature for structural system parameters identification [140], damage detection [75], [135], [69], and real time structure health monitoring [87], [83], [48], [50]. However, most of the aforementioned applications are restricted in the sense that they are focused on the problem of compressing efficiently the acquired signal (assumed to be complete) for circumventing the computational burden of compressing it locally at the sensor. Nevertheless, applying CS theory to the problem of missing data differs primarily in one respect; that is, missing data are not necessarily intentional. Unfortunately, this removes control over one important step of CS: the arrangement of the sampling matrix. CS relies on the choice of an appropriate sampling matrix. For instance, uniform random Fourier matrices obey the CS requirements for sparse reconstruction with high probability [12], [36]. Unfortunately, the missing data may not be uniformly distributed over the record; thus, regular or large gaps of missing data can lead to lower orthogonality between random columns of the sampling matrix. Further, even the papers that address the case of data losses such as in [143], focus primarily on deterministic signal reconstruction (e.g. in the time domain). Nevertheless, there are cases (e.g. system reliability assessment applications) where the main objective may not be signal reconstruction (in the time/space domains), but rather characterization and quantification of the underlying stochastic process/field statistics (i.e. Power Spectrum estimation).

Recently, Comerford et al. [25] utilized sparse signal reconstruction methods to develop stochastic process power spectrum estimation techniques subject to signals with missing data . The concept of the power spectrum has been indispensable for characterizing stochastic processes that exhibit frequency-dependent properties (e.g., [110], [19], [20]). Nevertheless, to estimate the power spectrum of a stochastic process, recorded realizations are often required, which may suffer from previously mentioned missing data problems. Note that power spectrum estimation methods that rely on the Discrete Fourier Transform (DFT) or on wavelet transforms for the non-stationary case, require full, uniformly sampled data sequences; hence the need for reconstruction. In this regard, many processes for which a power spectral model is of interest exhibit relative sparsity in the frequency domain, and thus, sparse reconstruction methods can be ideal. In [22], a CS based approach was developed for power spectrum estimation, in which multiple records were utilized to iteratively update a harmonic basis matrix, demonstrating significantly improved results over alternative methods.

In this chapter, $L_{1/2}$ norm minimization is proposed, set within a framework for power spectrum estimation subject to missing data. The framework utilizes a re-weighting scheme that makes the assumption of multiple process records being available for analysis. This can be construed as a caveat of the approach described herein but also the reason that it can be so incredibly effective in signal reconstruction from a spectral estimation standpoint. Further, it is noted that for both stationary and non-stationary processes for which only single records are available, windowing and down-sampling may be applied to emulate multiple process records. Results utilizing the $L_{1/2}$ norm are compared against an alternative L_1 norm set in the same basis re-weighting scheme for stationary, non-stationary and multi-dimensional stochastic process examples.

The following section comprises a brief background to identification of sparse solutions via L_p norm $(0 < p \leq 1)$ minimization schemes. Further, it provides an overview of the L_1 norm re-weighting procedure that utilizes multiple stochastic process records for power spectrum estimation described in detail in [22]. The re-weighting procedure is then utilized alongside $L_{1/2}$ norm minimization, further promoting sparsity. Both methods are then compared for varying numbers of available process records for stationary, nonstationary and multi-dimensional cases.

2.2 Sparse solutions via L_p norm minimization

The condition of sparsity requires that a signal can be defined in some known basis with far fewer coefficients than the number determined by the Shannon-Nyquist rate [31]. As an example, a discrete time signal $\mathbf{x}$ in one dimension can be viewed as an $N \times 1$ column vector. Given an orthogonal $N \times N$ basis matrix $\mathbf{A}$, in which the columns $\mathbf{A}_n$ are the basis functions, $\mathbf{x}$ can be represented in terms of this basis via a set of $N \times 1$ coefficients $\mathbf{y}$, i.e.,

$$\mathbf{x} = \sum_{n=1}^{N} \mathbf{A}_n y_n \tag{2.1}$$

The vector $\mathbf{x}$ is said to be K-sparse in the basis $\mathbf{A}$ if $\mathbf{y}$ has K non-zero entries and $K < N$, i.e.,

$$\mathbf{x} = \sum_{k=1}^{K} \mathbf{A}_{n_k} y_{n_k} \tag{2.2}$$

where n_k are the integer locations of the K non-zero entries in $\mathbf{y}$. Hence $\mathbf{y}$ is an $N \times 1$ column vector with only K non-zero elements. Therefore,

$$|\mathbf{y}|_{L_0} = K \tag{2.3}$$

where $|.|_{L_0}$ denotes the L_p norm defined as

$$|\mathbf{y}|_{L_p} = \left(\sum_n |y_n|^p \right)^{\frac{1}{p}} \tag{2.4}$$

Considering an under-sampled signal, transformation into a new basis (e.g., Fourier, wavelets etc.) leads to an under-determined system of equations, i.e.,

$$\mathbf{x} = \mathbf{B}\mathbf{y} \tag{2.5}$$

where $\mathbf{B}$ is an $M \times N$ reduced A matrix where $M < N$. The assumption that a signal is uniquely sparse in the given basis provides an objective to solving these equations. In general, if a unique sparsest solution of an under-determined system of equations exists, it is found when the L_0 norm is minimized. According to [15], this L_0 solution is said to be the exact reconstruction of the original signal with high probability if $M > CKlog(N)$ for some constant C, where as C increases, so does the probability of successful reconstruction. This L_0 optimization problem is non-convex with no known exact solution [12], [5]. However, a viable alternative exists in minimizing the L_1 norm instead. L_1 norm minimization promotes sparsity and in many cases will yield the same result as L_0 norm minimization [86]. Further, the problem becomes convex, and may be set in a convenient linear programming form, i.e.

$$\min |\mathbf{y}|_{L_1}, \quad \text{subject to} \quad \mathbf{x} = \mathbf{B}\mathbf{y} \tag{2.6}$$

Eq. (2.6) describes a basis pursuit optimization problem and can be easily solved via a gradient-based method, e.g. [124]. This notable feature led some of the authors to applying L_1 minimization in a CS framework for estimating the relatively narrow-band (evolutionary) power spectra of stationary and nonstationary stochastic processes based on available realizations with incomplete data [25], [22]. However, as minimizing the L_1 norm does not guarantee the sparsest solution, reconstruction can be improved, or accurately met with fewer sample data, when utilizing L_p norm minimization with $p < 1$. Although such problems appear to be non-convex, it was shown in [16] that even when finding a local minimum, exact reconstruction is possible with far fewer data than those required for L_1 reconstruction.

In fact, it was shown in [139] that $p = 1/2$ tends to yield the sparsest solution for $1/2 \leq p < 1$ and for $0 < p < 1/2$ the sparsity degree remains relatively unaffected. Hence, in this chapter, $L_{1/2}$ norm minimization is considered to be representative of the $p < 1$ cases for reconstruction of sparse signals. The herein utilized scheme for implementing the $L_{1/2}$ norm is based upon on a re-weighted least squares algorithm [16], [45]. In this regard, the L_1 minimization problem in Eq.

(2.6) becomes

$$\min |\mathbf{y}|_{1/2}^{1/2}, \quad \text{subject to} \quad \mathbf{x} = \mathbf{B}\mathbf{y} \tag{2.7}$$

To minimize Eq. (2.7), the Lagrangian $L(\mathbf{y}, \lambda)$ is introduced as

$$L(\mathbf{y}, \lambda) = \sum_n |y_n|^{\frac{1}{2}} + \lambda^T(\mathbf{B}\mathbf{y} - \mathbf{x}) \tag{2.8}$$

Setting the partial derivatives of Eq. (2.8) with respect to $\mathbf{y}$ and λ are equal to zero for

$$\mathbf{y} = \mathbf{Q}\mathbf{B}^T(\mathbf{B}\mathbf{Q}\mathbf{B}^T)^{-1}\mathbf{x} \tag{2.9}$$

$\mathbf{Q} = \text{diag}(|\mathbf{y}|^{\frac{3}{2}})$. Eq. (2.9) can be solved iteratively by computing $\mathbf{Q}$ from the solution of each previous iteration, i.e.,

$$\mathbf{y}_r = \mathbf{Q}_{r-1}\mathbf{B}^T(\mathbf{B}\mathbf{Q}_{r-1}\mathbf{B}^T)^{-1}\mathbf{x} \tag{2.10}$$

$$\mathbf{Q}_{r-1} = \text{diag}(|\mathbf{y}_{r-1}|^{\frac{3}{2}}) \tag{2.11}$$

Note that, this algorithm is equivalent to a weighted L_2 norm [45]

$$\min_{\mathbf{y}} \sum \omega_n y_n^2, \quad \text{subject to} \quad \mathbf{x} = \mathbf{B}\mathbf{y} \tag{2.12}$$

where $\omega_n = |y_{n,r-1}|^{-3/2}$. As the solution is sparse, the value of many y_i will tend toward zero. To avoid division by zero in ω_i as the algorithm converges to a solution, a decreasing parameter ϵ is introduced to regularize the optimization problem [17], i.e.,

$$\mathbf{Q}_{r-1} = \text{diag}\left(|\mathbf{y}_{r-1}|^2 + \epsilon_j \cdot (\text{E}[|\mathbf{y}_{s-1}|^2])^{\frac{3}{4}}\right) \tag{2.13}$$

$$\epsilon_j = \frac{\epsilon_{j-1}}{10} \tag{2.14}$$

where $\epsilon_0 = 1$ and for each ϵ_j, Eq. (2.10) is repeated until satisfying

$$\frac{\|\mathbf{y}_r - \mathbf{y}_{r-1}\|_2}{\|\mathbf{y}_{r-1}\|_2} < \frac{\sqrt{\epsilon_j}}{100} \tag{2.15}$$

Converging to the true $L_{1/2}$ solution can largely depend upon the initialization of $\mathbf{Q}$. Fortunately, in the case where multiple process records are used to estimate the power spectrum (a core assumption of the adaptive basis method presented in the next section), a satisfactory approximation of $\mathbf{y}$ can be realized on which to initialize the $L_{1/2}$ norm minimization algorithm. Essentially any standard spectrum estimation method that can process 'gappy' records, such as least-squares (L_2 norm),

can be used to produce an average estimation of the power spectrum across the ensemble, yielding suitable initialization coefficients for $\mathbf{Q}$. The proposed initialization of $\mathbf{Q}$ for both stationary and non-stationary cases is based on a least squares estimation of $\mathbf{y}$. Note that when utilizing multiple records, this initial estimation may also take advantage of the re-weighting procedure detailed in section 2.4.

The $L_{1/2}$ solution of Eq. (2.7) could be determined by the following steps

a) Initialize $\mathbf{Q}_0 = \mathbf{B}^T(\mathbf{B}\mathbf{B}^T)^{-1}\mathbf{x}$, when inner iteration index $r = 0$, and initialize $\epsilon_0 = 1$ when outer iteration index $j = 0$.

b) For each outer iteration j, calculate r^{th} iteration (inner) $\mathbf{y}_r$ with Eq. (2.10), and update $\mathbf{Q}$ wtih Eq. (2.13), until condition Eq. (2.15) is satisfied.

c) Update ϵ_j with Eq. (2.14).

d) Repeat b)-c), until ϵ_j become enough small.

Obviously, recorded signals are rarely ever truly sparse due to two aspects. First, even low levels of measurement noise will produce small coefficients across most bases. Further, the signals, in practice, are nearly sparse, which means most of spectral coefficients are not exactly zero, but small values near zero. Hence, a tolerance, ν, is included to deal with both above two aspects, and thus, Eq. (2.6) and Eq. (2.7) are re-cast in the form,

$$\min |\mathbf{y}|_{1/2}^{1/2}, \quad \text{subject to} \quad |\mathbf{B}\mathbf{y} - \mathbf{x}|_{L_2} \leq \nu \tag{2.16}$$

For the cases where either the signal is not sparse enough or the missing data are too extensive for $L_p(0 < p \leq 1)$ minimization to exactly reconstruct the original signal, it is important to note that there may still be significant advantages over a minimum L_2 solution. In spectral estimation, minimizing the L_2 norm (similar to zero-padding) is likely to spread the solution over many frequencies; this is because individually, large coefficients are heavily penalized. Minimizing the $L_p(0 < p \leq 1)$ norm however is far more likely to yield larger individual coefficients, having the effect of producing sharp, well-defined peaks at the key frequencies. Note that, the degree of data missing is relatively smaller than the degree of signal sparsity discussed in this chapter.

2.3 Stochastic process representation and spectral estimation

To utilize bases in which signals are assumed to be sparse in the context of power spectrum estimation, a mapping is required between the chosen basis, and a power spectrum model. Appropriate basis functions to be used in the context of the previous section are outlined here for both stationary and non-stationary stochastic processes.

2.3.1 Stationary case

Starting with a stationary model of a real-valued stochastic process, its power spectrum may be given as the ensemble average of the square of the absolute Fourier transform amplitudes of available discrete time realizations [80]; that is,

$$S_x(\omega_k) = \frac{2\Delta T}{N}\mathrm{E}\left[\left|\sum_{t=0}^{N-1} x_n e^{-2\pi i k n/N}\right|^2\right] \tag{2.17}$$

where N is the number of data points, t is the data point index in the record, k is the integer frequency for ω_k (i.e. $\omega_k = \dfrac{2\pi k}{T}$, where T is the total length in time of the record) and $\Delta T = T/N$ is the sampling time increment. Hence, the Fourier basis functions are utilized in this case.

2.3.2 Non-stationary case

A reliable spectral model providing frequency dependent information can be of significant importance in investigating the response of an engineering system to stochastic input. However, a time-invariant spectral model can only describe a stationary process, i.e. one in which the spectral content does not change over time. This assumption of stationarity often produces a poor approximation of the true process, as many important processes of interest are non-stationary in nature. For example, the frequency content of an earthquake induced excitation can change significantly over its duration, whereas wind systems may contain short infrequent bursts that do not conform to the otherwise stationarity of the rest of the process. Hence, in many cases, accounting for time-dependent properties of stochastic processes is critical in defining reliable spectral models [92], [71]. For these reasons, evolutionary power spectrum estimation of non-stationary processes will receive particular attention in the ensuing analysis.

For the case of non-stationary stochastic processes a time/frequency localized wavelet basis, as opposed to the Fourier decomposition of the signal is utilized. In this regard, Nason et al. [78] developed the wavelet based representation,

$$x(t) = \sum_j \sum_k \omega_{j,k}\psi_{j,k}(t)\xi_{j,k} \tag{2.18}$$

where $\psi_{j,k}(t)$ is the chosen family of wavelets and j and k represent the different scales and translation levels respectively; $\xi_{j,k}$ is a stochastic orthonormal increment sequence. This wavelet-based model relies on the theory of locally stationary processes (see [29]). Next, by utilizing the generalized harmonic wavelets [80], [81], defined in the time domain as,

$$\psi_{(m-n),k}(t) = \frac{e^{in\Delta\omega(t-k)} - e^{im\Delta\omega(t-k)}}{i(n-m)\Delta\omega(t-k)} \tag{2.19}$$

Eq. (2.18) becomes

$$x(t) = \sum_{(m,n)} \sum_{k} (\sqrt{S^X_{(m,n),k}(n-m)\Delta\omega})\psi_{(m,n),k}(t)\xi_{(m,n),k}(t) \tag{2.20}$$

Eq. (2.20) represents a localized process at scale (m, n) and translation (k) defined in the intervals $[m\Delta\omega, n\Delta\omega]$ and $\left[\frac{kT}{n-m}, \frac{(k+1)T}{n-m}\right]$, with $S^X_{(m,n),k}$ representing the spectrum $S_X(\omega, t)$ at scale (m, n) and translation (k); see also [117].

Regarding the problem of estimating the EPS of a non-stationary stochastic process based on available/measured realizations, a wavelet process based compatible estimation approach advocates that the EPS $S_X(\omega, t)$ of the process $X(t)$ is estimated by [117], [122]

$$S_X(\omega, t) = S^X_{(m,n),k} = \frac{\mathrm{E}\left[|W^G_{(m,n),k}[X]|^2\right]}{(n-m)\Delta\omega},\ m\Delta\omega \leq \omega \leq n\Delta\omega,\ \frac{kT}{n-m} \leq t \leq \frac{(k+1)T}{n-m} \tag{2.21}$$

where $W^G_{(m,n),k}$ is the generalized harmonic wavelet transform (GHWT) defined as

$$W^G_{(m,n),k} = \frac{n-m}{kT} \int_{-\infty}^{+\infty} f(t)\overline{\psi_{(m,n),k}(t)}dt \tag{2.22}$$

where the overbar denotes the complex conjugate.

Thus, the EPS can be estimated as the ensemble average of the square of the wavelet coefficients, whereas the wavelets of Eq. (2.19) serve as the basis functions.

2.4 Adaptive basis re-weighting procedure

The adaptive basis re-weighting procedure, first proposed in [22], has been shown to improve the stochastic process power spectrum estimate to a large extent. The rationale relates to exploiting the presence of the expectation operators in Eq. (2.17) and Eq. (2.21) for estimating power spectra. Given multiple process records, the objective is to estimate the power spectrum based on the mean square of their transform coefficients. This requires the core assumption that the individual records are produced by the same underlying stochastic process, and thus, are compatible with the same power spectrum. In this case, we would expect the individual record transforms to exhibit similarities. For instance, if the spectral power is estimated to be high at a specific frequency, then each individual record is more likely to have higher amplitude Fourier coefficients at that same frequency. When dealing with missing data, we can use this fact to skew the reconstruction optimization problem in the direction of the ensemble estimated power spectrum, in a similar way to the $L_{1/2}$ minimization presented previously.

The purpose of the re-weighting procedure is to iteratively update a weight matrix W to be

used in a least squares optimization, as was the case with **Q** in Eq. (2.11). However, rather than base **W** solely on the outcome of the least squares result, it is based on an ensemble mean. Once the iterations are complete, the final **W** is multiplied by the basis matrix to influence the result of the chosen L_p norm minimization. Hence, Eq. (2.6) and Eq. (2.7) become

$$\min |\mathbf{y}|_{1/2}^{1/2}, \text{ subject to } \quad \mathbf{x} = \mathbf{WBy} \tag{2.23}$$

The contribution of a single process record to the next iteration of the re-weighting matrix $\mathbf{W}_s$ is given by

$$\mathbf{y}_{k,s} = (\mathbf{BW}_{s-1})^T(\mathbf{BW}_{s-1}(\mathbf{BW}_{s-1})^T)^{-1}\mathbf{x} \tag{2.24}$$

where **B** is the reduced $M \times N$ matrix as in Eq. (2.5) and $\mathbf{y}_{k,s}$ is an $N \times 1$ least squares estimation of the k^{th} signal realization's basis coefficients, subject to the $(s-1)^{th}$ re-weighted basis matrix $\mathbf{W}_{s-1}$. Further, odd and even functions (e.g., sine and cosine) are paired when forming the **W** matrix and their combined magnitude is used for both individual weights. This is a necessary step as the power spectrum models given by Eq. (2.17) and Eq. (2.21) do not exhibit phase-dependent properties. For basis matrices composed of real functions, with odd and even functions of equal frequency adjacent to one another, the **W** matrix is constructed in the following way

$$\mathbf{W}_s = \text{diag}(\omega_{s,n=0,1,\ldots,N}) \tag{2.25}$$

where

$$\omega_{s,n} = \frac{\sum_R \left(\sqrt{y_{k,s,n_f}^2 + y_{k,s,n_f+1}^2}\right)}{R} + c \tag{2.26}$$

y_{k,s,n_f} are the scalar coefficients at positions n_f from the vector $\mathbf{y}_{k,s}$, where

$$n_f = \text{floor}(j/2) \tag{2.27}$$

where floor(.) maps a real number to the largest previous integer. In Eq.(2.26), R is the total number of process realizations in the ensemble, and c is a constant. Although in the case where absolute sparsity (which means most of the spectral coefficients are exactly zero) is inferred, it might be beneficial to allow weight coefficients to reduce to zero, this assumption is seldom true when dealing with real recorded processes. Therefore, to prevent weight coefficients approaching zero and forcing functions out of the optimization, a constant, positive bias is included. In the following numerical examples, this is set equal to the mean weight at each iteration.

The optimization is initialized with an $N \times N$ identity matrix (i.e., without weights). The procedure is terminated when the change in weights between iterations is considered to be very

small,

$$\frac{\|\mathbf{W}_s - \mathbf{W}_{s-1}\|_2}{\|\mathbf{W}_{s-1}\|_2} < \delta_{\mathbf{W}} \tag{2.28}$$

where δ_W is some small value, several orders of magnitude lower than the mean square of $\mathbf{W}$.

The procedure is summarized as following

a) Initialize $\mathbf{W}_0$ as the $M \times M$ identity matrix when iteration index $s = 0$.

b) For each realization, calculate $\mathbf{y}_{k,s}$ with Eq.(2.24). k is the realization index.

c) Calculate the s^{th} iteration $\mathbf{W}_s$ with Eq.(2.25-2.27).

d) Repeat step a)-c) until the condition Eq.(2.28) is satisfied, and obtain the final $\mathbf{W}$.

e) With the obtained $\mathbf{W}$, for each realization, calculate $\mathbf{y}$ with Eq.(2.23) by the $L_{1/2}$ solution steps described in section 2.2. And then estimate the power spectrum.

2.5 Numerical examples

The numerical examples are split into four parts. First, the ability of L_1 and $L_{1/2}$ norm minimization in estimating spectra are compared for a stationary sea wave process without utilizing the basis re-weighting procedure. This first example demonstrates the ability of the $L_{1/2}$ norm minimization in finding sparser solutions. For the remaining parts, the iterative re-weighting procedure is introduced and implemented in both L_1 and $L_{1/2}$ norm minimization procedures over three separate examples, considering stationary sea wave, non-stationary earthquake and two dimensional material property processes. For each of re-weighting examples, the reconstruction capabilities of L_1 and $L_{1/2}$ norms are assessed utilizing two different sizes of record ensemble; that is, 20 process records and 200 process records.

To assess the reconstruction efficacy in the above scenarios, time histories compatible with predefined power spectra are generated. These are produced via the techniques described in [110] and [71] for stationary and non-stationary processes, respectively. Specifically, for a stationary record, a power spectrum compatible realization is given by

$$x(t) = \sum_{j=0}^{N-1} \sqrt{4S_X(\omega_j)\Delta\omega}\sin(\omega_j t + \phi_j) \tag{2.29}$$

where ϕ_j are uniformly distributed random phase angles in the range $0 \leq \phi_j < 2\pi$ and N relates to the discretization of the frequency domain. For non-stationary processes, $S_X(\omega_j)$ in Eq. (2.29) is replaced with an evolutionary power spectrum $S_X(\omega_j, t)$.

Next, missing data are imposed to the simulated power spectrum compatible realizations. In the following examples, missing data are considered to occur at random locations drawn from a

uniform distribution of the time index i.e.,

$$x_0(t) = \begin{cases} x(t), & \rho(t) \geq m \\ \text{NaN}, & \rho(t) < m \end{cases} \tag{2.30}$$

where $x_0(t)$ is the realization with missing data, $x(t)$ is the original realization, ρ is a vector of N_0 equally spaced numbers from 0 to 1 arranged in random order, and m is the fraction of missing data. Through Eq. (2.30), the uniform distributed locations of missing data are selected and the corresponding data values are removed, which are denoted as NaN. For each realization, an independent uniform distribution of time index is applied. In this way, the incomplete samples with missing data are generated.

Power spectra may be estimated based on complete realizations of Eq. (2.29) using the methods outlined in section 2.3. They are then compared against those estimated from realizations with simulated missing data. Specifically, a normalized power spectrum error is calculated for stationary processes

$$\text{error} = \frac{\int_0^{\omega_u} |S_E(\omega) - S_T(\omega)| d\omega}{\int_0^{\omega_u} |S_T(\omega)| d\omega} \tag{2.31}$$

and for non-stationary processes

$$\text{error} = \frac{\int_0^{t_u} \int_0^{\omega_u} |S_E(\omega) - S_T(\omega)| d\omega dt}{\int_0^{t_u} \int_0^{\omega_u} |S_T(\omega)| d\omega dt} \tag{2.32}$$

It is important to note that the error is calculated from two spectral estimates (with missing data and without missing data), and does not utilize the original power spectrum. This is because the objective of this work is not to assess the accuracy of the underlying spectrum estimation method (in this case Fourier or GHW based methods which have already been studied extensively in this context [122], [115], [62]), but to investigate, specifically, the effect of the missing data upon spectral estimation. Further, due to the random nature of the generated process records and arrangement of missing data, the calculated error is a random variable for any given case. Hence, statistics are determined for the error as well, by considering an ensemble of power spectrum estimates obtained via repetitions of the same experiment.

2.5.1 Stationary sea wave spectrum without re-weighting

As previously mentioned, the first example is presented without utilizing the basis re-weighting procedure to demonstrate the un-biased difference between L_1 and $L_{1/2}$ solutions. The fact that $L_{1/2}$ is shown to out-perform L_1 indicates that it could be a more appropriate choice when estimating spectra from single process records (where the basis re-weighting procedure may not be

applicable). Note that in this example, **Q** in Eq. (2.10) is initialized using a least squares estimation of **y**,

$$\mathbf{Q}_0 = \text{diag}(\mathbf{q}_0) \tag{2.33}$$

where

$$\mathbf{q}_0 = \mathbf{B}^T(\mathbf{B}\mathbf{B}^T)^{-1}\mathbf{x} \tag{2.34}$$

In Eq. (2.34), **B** is the reduced $M \times N$ basis matrix and **x** is the time-history record after data have been removed. The JONSWAP sea wave spectrum of Eq. (2.35) [51] is used to produce stationary process time histories,

$$S(\omega) = \frac{ag^2}{\omega^5} e^{\frac{5}{4}(\omega_\rho/\omega)^4} \gamma^r;\ r = e^{-\left(\frac{\omega-\omega_\rho}{2\sigma\omega_\rho}\right)^2} \tag{2.35}$$

where $\alpha = 0.03$, $\omega_\rho = 0.05$, $\gamma = 3.3$ and $\sigma = \begin{cases} 0.07, & \omega \leq \omega_\rho \\ 0.09, & \omega > \omega_\rho \end{cases}$.

Figures 2.1 and 2.2 show the target spectra along with the reconstructed spectra for L_1 norm and $L_{1/2}$ norm minimization averaged over 20 samples and 200 samples, respectively. For these examples, spectra were reconstructed after 75% of the data were removed via Eq. 30. While in both figures, the L_1 and $L_{1/2}$ norms succeed in determining spectra that match moderately well with the target, a trend emerges when comparing the calculated errors for spectral estimates produced from 20 and 200 samples, which are shown as normalized histograms in Figure 2.3. Note that for all four cases (L_1 and $L_{1/2}$ norm with 20 and 200 samples), the results were repeated 500 times to produce these histograms due to the fact that any single error result is not representative of the full set. In both cases, the $L_{1/2}$ solution leads to spectral estimates with lower error than the L_1 solution. However, it is clear from Figure 2.3 that this difference becomes more prominent as the number of samples increases. It should also be noted that even for the 20 sample case (in which the histograms intersect), for each sample set, the $L_{1/2}$ norm solution produced a lower error than the L_1 norm solution.

2.5.2 Stationary sea wave spectrum with basis re-weighting

The following example is similar to the previous one, with the exception that when solving the L_p norm minimization problems, the weighted Fourier basis is used instead of the original orthonormal one. The same weight matrix is used for both L_1 and $L_{1/2}$ norm problems, calculated again, based on 20 and 200 process records. For the $L_{1/2}$ norm minimization algorithm, Q is this time initialized

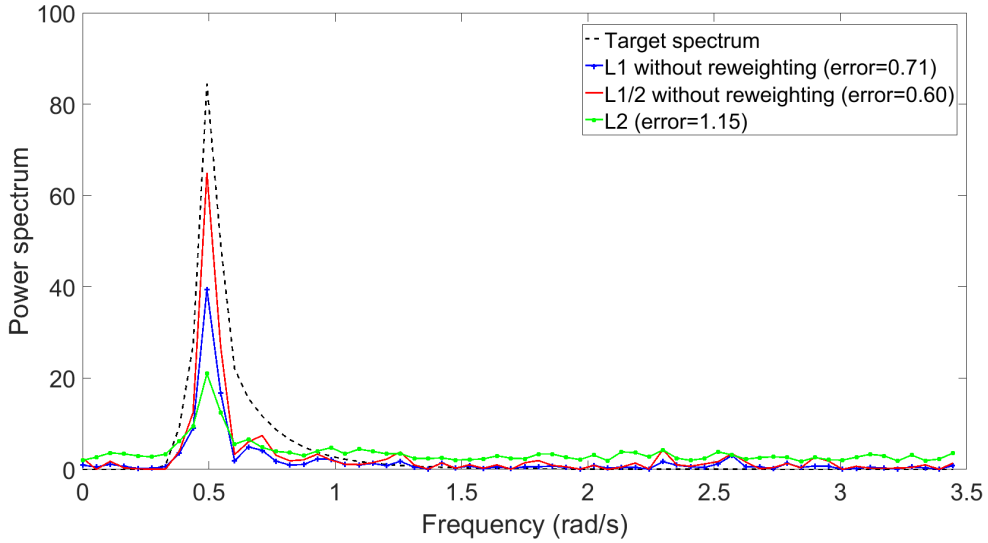

Figure 2.1: JONSWAP stationary power spectrum estimates of Eq.(2.35) from 20 samples without re-weighting (75% missing data)

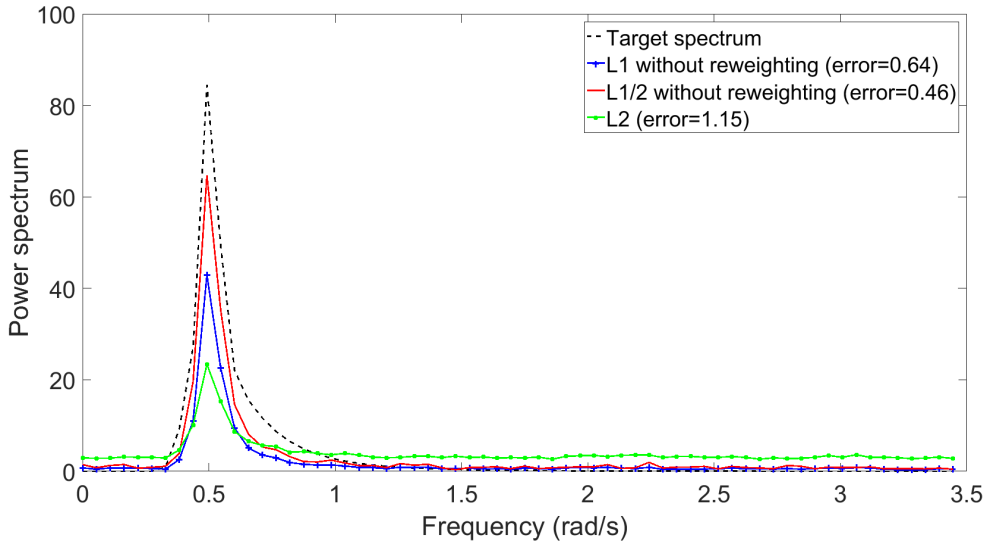

Figure 2.2: JONSWAP stationary power spectrum estimates of Eq.(2.35) from 200 samples without re-weighting (75% missing data)

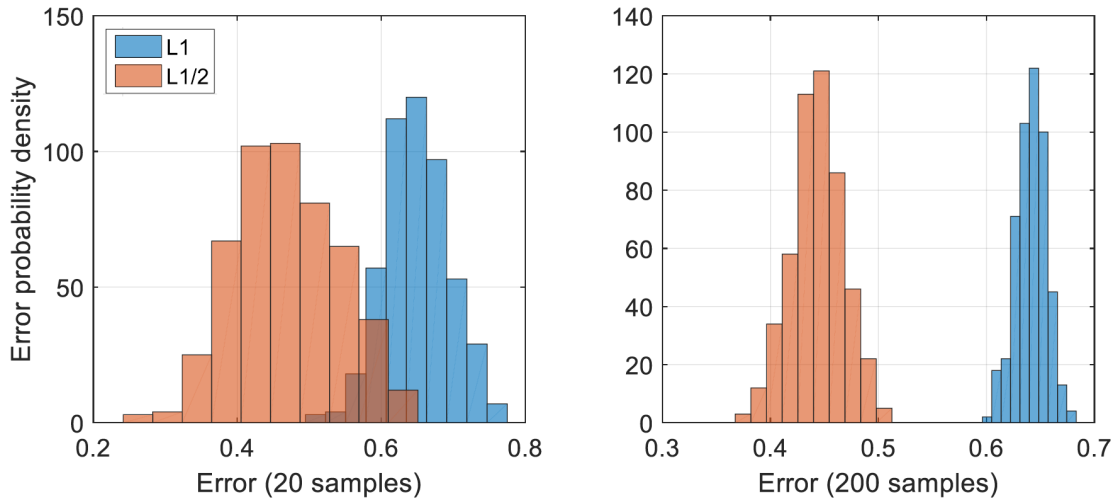

Figure 2.3: Distribution of error over 500 repeated estimations of Eq.(2.35) without re-weighting for 20 and 200 samples

after taking account of the final weight matrix,

$$\mathbf{Q}_0 = \text{diag}(\mathbf{q}_0) \tag{2.36}$$

where

$$\mathbf{q}_0 = (\mathbf{WB})^T(\mathbf{WB}(\mathbf{WB})^T)^{-1}\mathbf{x} \tag{2.37}$$

Figures 2.4 and 2.5 show the target spectra along with the reconstructed spectra for L_1 and $L_{1/2}$ norm minimization averaged over 20 samples and 200 samples, respectively. Again, 75% of the data were removed based on Eq. (2.30). The errors with reference to the target spectrum estimates are shown as histograms for 500 test runs in Figure 2.6 for 20 and 200 time histories. As with the non re-weighted case, the distribution of error changes with number of samples used to estimate the spectrum. However, when comparing Figure 2.6 to Figure 2.3, it is clear that the re-weighting procedure has had a significant effect. Firstly, the mean error for both cases has decreased dramatically, this is also apparent when comparing the plotted spectra in the non re-weighted case (Figures 2.1 & 2.2) to the re-weighted case (Figures 2.4 & 2.5). Secondly, the L_1 norm solution has also improved relative to the $L_{1/2}$ solution. In fact, for 20 samples, the L_1 norm solution provided a superior spectral estimate in $> 70\%$ of trials. However, in the 200 sample case, despite the slight overlap in the histograms (Figure 6, right), for each individual trial, the $L_{1/2}$ norm solution provided the lowest error.

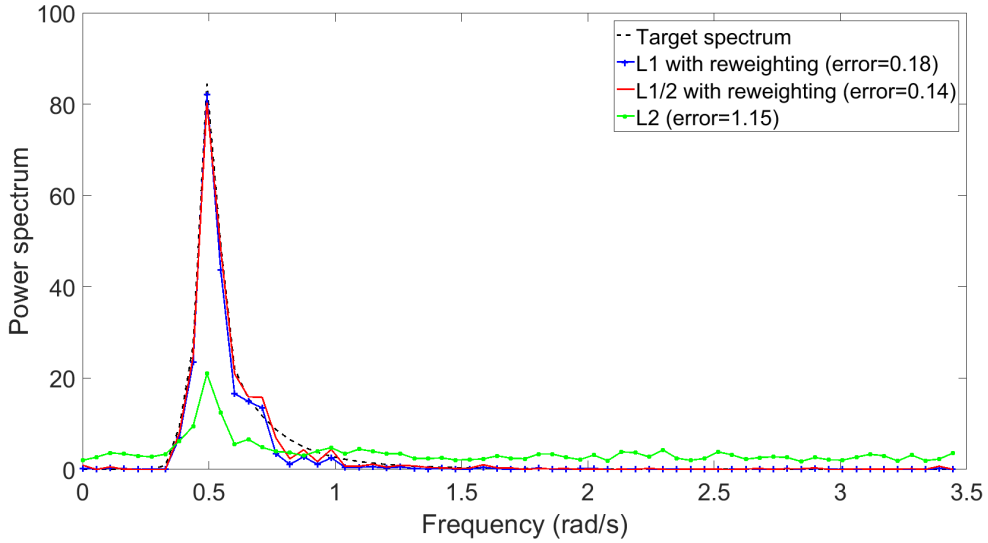

Figure 2.4: JONSWAP stationary power spectrum estimates of Eq.(2.35) from 20 samples with re-weighting (75% missing data)

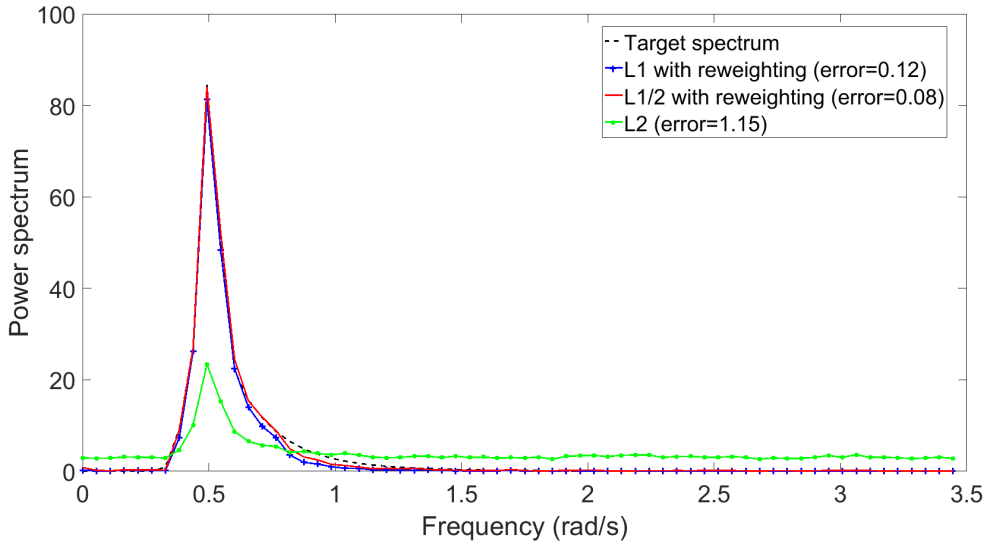

Figure 2.5: JONSWAP stationary power spectrum estimates of Eq.(2.35) from 200 samples with re-weighting (75% missing data)

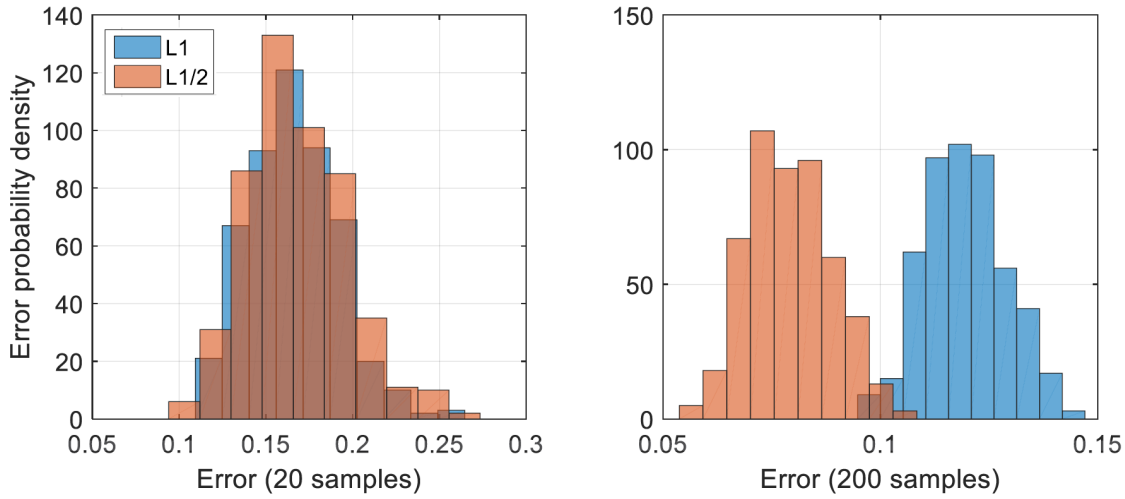

Figure 2.6: Distribution of error over 500 repeated estimations of Eq.(2.35) with re-weighting for 20 and 200 samples

2.5.3 Non-stationary earthquake spectrum with basis re-weighting

For the non-stationary case, the following time-modulated Clough-Penzien earthquake EPS model [21] is used to generate process realizations i.e.,

$$S_X(\omega, t) = a(t) S_{X,2}(\omega) \tag{2.38}$$

where

$$a(t) = 4(e^{-0.3t} - e^{-0.6t}) \tag{2.39}$$

and

$$S_{X,2}(\omega) = S_0 \frac{\omega^4}{(\omega^2 - \omega_f^2)^2 + 4\zeta_f^2\omega_f^2\omega^2} \frac{\omega_g^4 + 4\zeta_g^2\omega_g^2\omega^2}{(\omega^2 - \omega_g^2)^2 + 4\zeta_g^2\omega_g^2\omega^2} \tag{2.40}$$

where $S_0 = 0.06$, $\zeta_f = 0.6$, $\omega_f = 1$, $\zeta_g = 0.4$ and $\omega_g = 10$. The results are produced given the same parameters as the previous stationary case with basis re-weighting, except with a GHW source basis. A wavelet bandwidth of $(n - m = 8)$ is used which offers a satisfactory trade-off between time and frequency resolutions. Figures 2.7, 2.8, 2.9 and 2.10 show the estimated spectrum with no missing data, and with 75% missing data (L_2, L_1 and $L_{1/2}$ norm cases), respectively, for 20 realizations only. For ease of comparison, figures 2.11 and 2.12 show all three estimated spectra compared at a single time instant $(t = 1s)$ for both 20 and 200 realizations respectively.

As with the stationary case, the reconstructed spectra compare well with the target with as few as 20 realizations, with a small but noticeable increase in accuracy for 200 realizations. Figure 2.13 shows error histograms for the non-stationary case. Again, when more samples are used the $L_{1/2}$ norm solution improves compared to the L_1 norm solution (as before, for 200 samples, all of

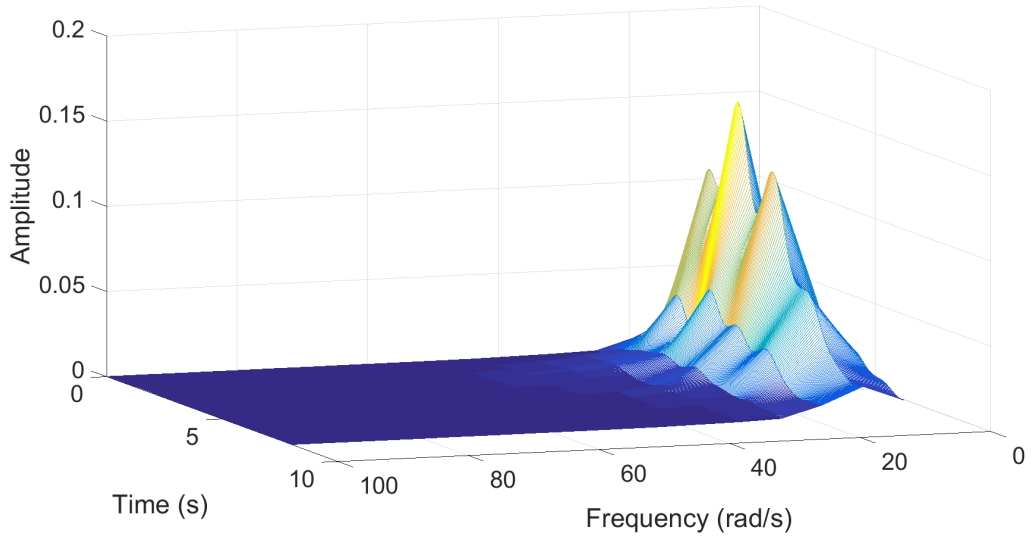

Figure 2.7: Clough-Penzien evolutionary power spectrum estimate of Eq.(2.38) from 20 samples (no missing data)

the individual $L_{1/2}$ trials exhibit a lower error), though for the 20 sample case there is almost no difference.

2.5.4 Two-dimensional stochastic field spectrum with basis re-weighting

Two-dimensional random fields are typically utilized for modeling material properties (e.g. [130]). While the signal of interest is a two-dimensional field, it can be decomposed by rows or columns into a one-dimensional vector. The two-dimensional Fourier decomposition provides a two-dimensional basis matrix for each frequency up to the Nyquist rate. These matrices are also decomposed into one-dimensional vectors to produce a single square basis matrix as in the one-dimensional case. Thus, the problem is treated as in the one-dimensional case.

Further, to generate realizations, a two-dimensional generalization of Eq. (2.29) is utilized [111], i.e.,

$$g(x_1,x_2)=\sqrt{2}\sum_{n_1}^{N_1-1}\sum_{n_2}^{N_2-1}[A_{n_1n_2}\cos(\kappa_{1n_1}x_1+\kappa_{2n_2}x_1+\phi^{(1)}_{n_1n_2})+\bar{A}_{n_1n_2}\cos(\kappa_{1n_1}x_1+\kappa_{2n_2}x_1+\phi^{(2)}_{n_1n_2})] \tag{2.41}$$

where

$$A_{n_1n_2}=\sqrt{2S_g(\kappa_{1n_1},\kappa_{2n_2})\Delta\kappa_1\Delta\kappa_2} \tag{2.42}$$

$$\bar{A}_{n_1n_2}=\sqrt{2S_g(\kappa_{1n_1},-\kappa_{2n_2})\Delta\kappa_1\Delta\kappa_2} \tag{2.43}$$

and x_j and κ_j are the two-dimensional space and wave number domains respectively.

Note that records generated via Eq. (2.41) tend to exhibit a Gaussian distribution [111], [110],

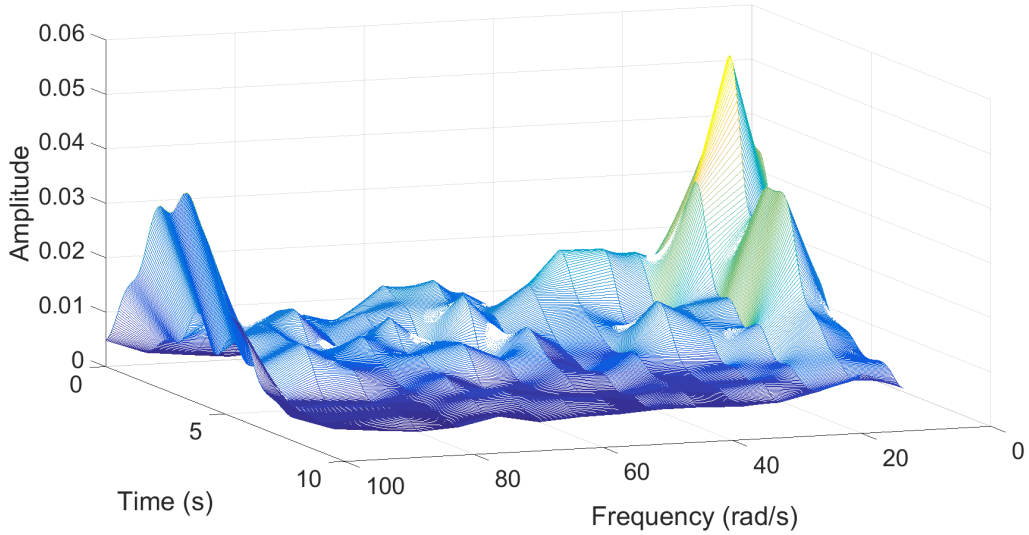

Figure 2.8: Clough-Penzien evolutionary power spectrum estimate of Eq.(2.38) from 20 samples (75% missing data, L_2 norm reconstruction, $error = 1.1$)

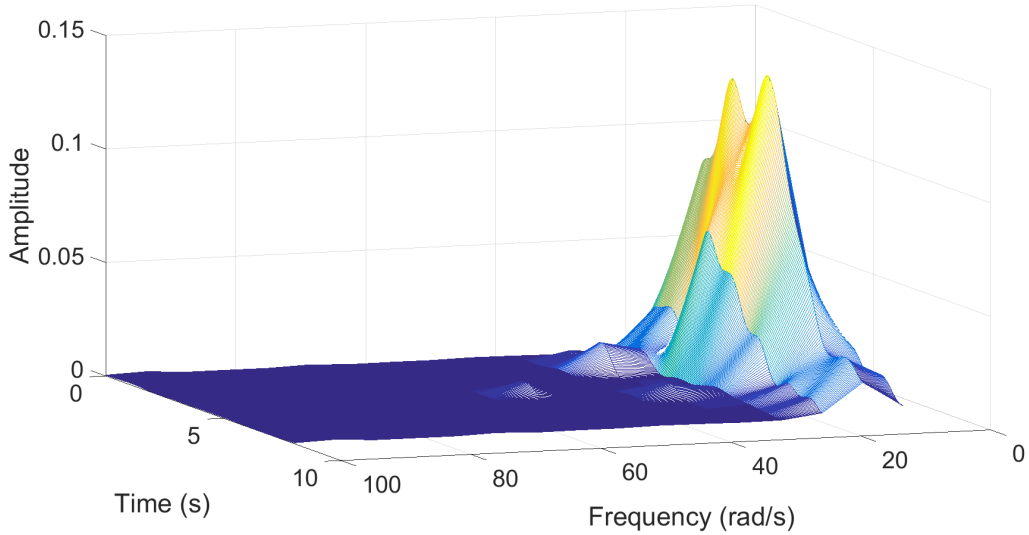

Figure 2.9: Clough-Penzien evolutionary power spectrum estimate of Eq.(2.38) from 20 samples with re-weighting (75% missing data, L_1 norm reconstruction, $error = 0.26$)

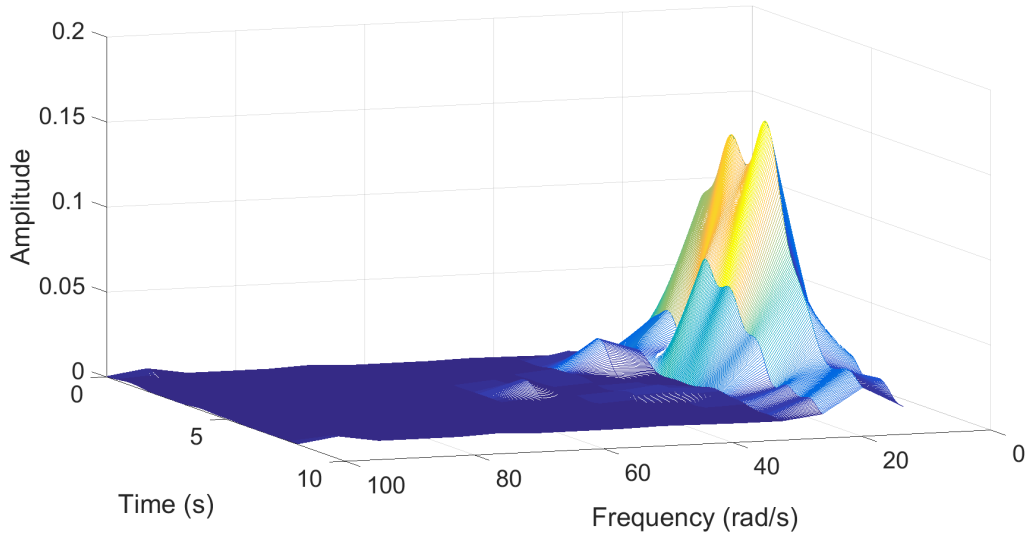

Figure 2.10: Clough-Penzien evolutionary power spectrum estimate of Eq.(2.38) from 20 samples with re-weighting (75% missing data, $L_{1/2}$ norm reconstruction, $error = 0.26$)

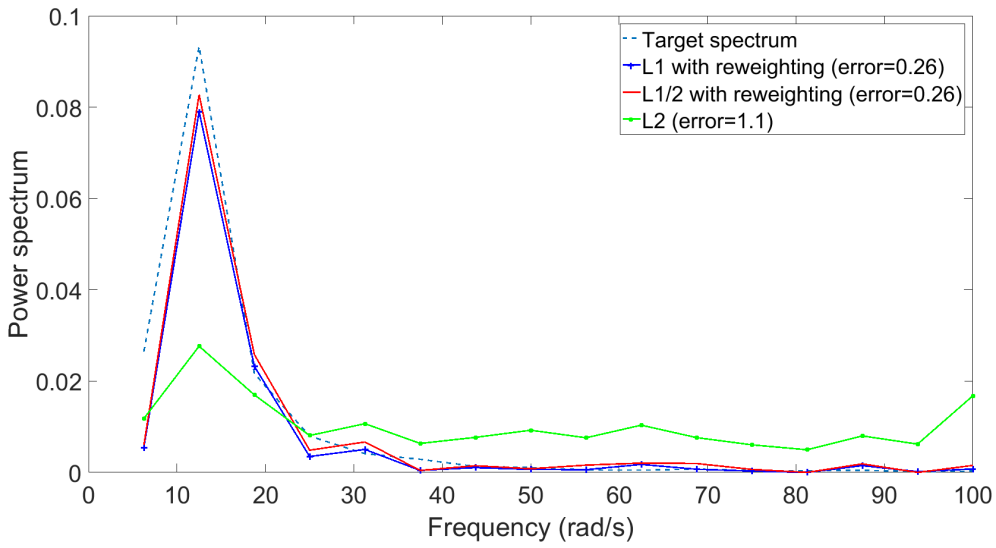

Figure 2.11: Clough-Penzien evolutionary power spectrum estimate of Eq.(2.38) from 20 samples with re-weighting at $t = 1s$ (75% missing data)

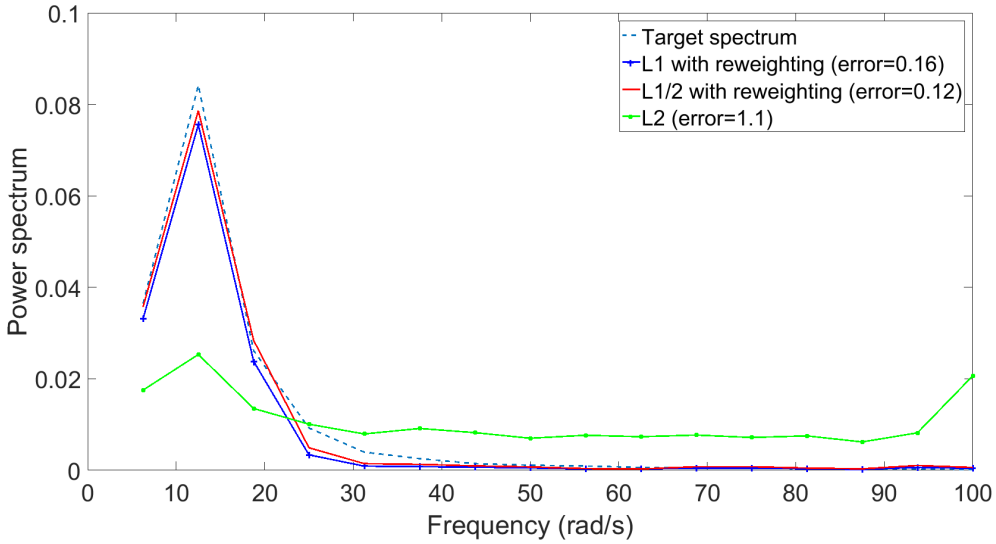

Figure 2.12: Clough-Penzien evolutionary power spectrum estimate of Eq.(2.38) from 200 samples with re-weighting at $t = 1s$ (75% missing data)

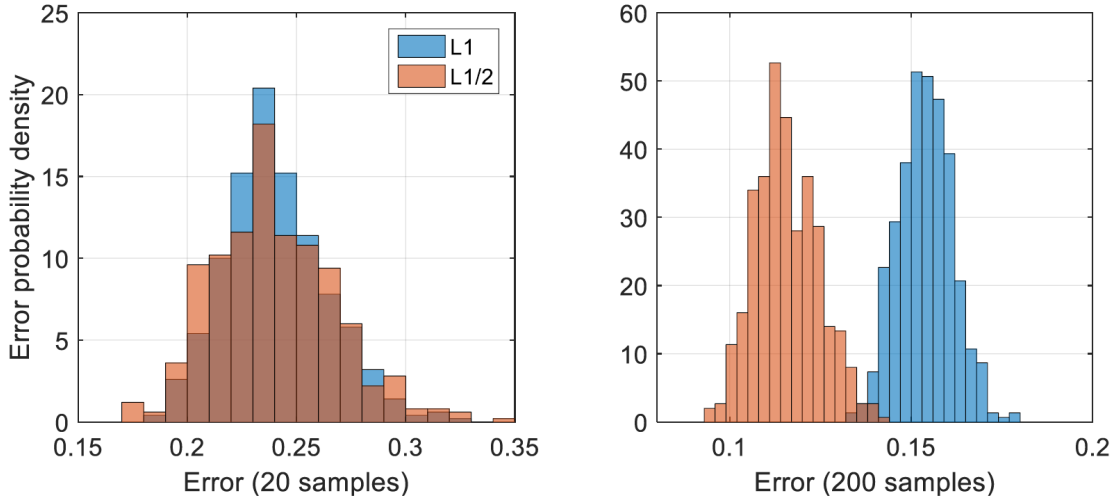

Figure 2.13: Distribution of error over 500 repeated estimations of Eq.(2.38) with re-weighting for 20 and 200 samples

whereas a wide range of techniques exist for producing realizations compatible with a given power spectrum and a non-Gaussian probability density function e.g., [47], [8], [109], [33]. For instance, following [47], a Gaussian field, denoted by $g(x_1, x_2)$ may be transformed into a non-Gaussian field, $f(x_1, x_2)$ by way of the transformation

$$f(x_1, x_2) = F_f^{-1}(F_g(g(x_1, x_2))) \tag{2.44}$$

where F_g is the Gaussian cumulative distribution function and F_f^{-1} is the inverse cumulative distribution for the desired non-Gaussian target field $f(x_1, x_2)$.

Next, following [130], the material modulus of elasticity is modelled as a homogeneous stochastic field with a power spectrum and a cumulative distribution function given by

$$S(\kappa_1, \kappa_2) = \frac{2}{\pi} e^{-2(\kappa_1^2 + \kappa_1^2)} \tag{2.45}$$

$$F_f(f(x_1, x_2)) = \frac{f(x_1, x_2) - a_l}{a_u - a_l} \tag{2.46}$$

respectively, where $a_u = 0.99$ and $a_l = -0.99$. 80% of the data are removed at uniformly distributed random locations and reconstructed using re-weighted L_1 and $L_{1/2}$ norm minimization for 20 and 200 samples. The target spectrum with no missing data and with reconstruction via $L_{1/2}$ norm minimization are shown in Figures 2.14 and 2.16, respectively (both refer to the 200 samples case), compared with the L_2 norm minimization in Figure 2.15. As with the previous examples, histograms showing the distribution of error for repeated trials are shown (Figure 2.17) providing greater insight into the reconstruction effectiveness. The results here are similar to those for the re-weighted stationary case. In particular, L_1 norm minimization is superior at lower sample numbers, with $L_{1/2}$ norm improving at a higher rate with increasing sample numbers. Again for 200 samples, the $L_{1/2}$ norm solution appears to be always superior.

2.6 Summary

In this chapter, a general L_p norm $(0 < p \leq 1)$ minimization approach has been proposed for estimating stochastic process power spectra subject to realizations with missing data. For comparisons, three different examples are considered including the stationary, nonstationary process and 2 dimensional field. In particular, focusing on the L_1 and $L_{1/2}$ norms, it has been shown that the approach can be significantly enhanced by an adaptive basis re-weighting scheme, while it can satisfactorily estimate the power spectra of stationary, non-stationary, and multi-dimensional processes. It is shown that there are clear advantages to utilizing $L_{1/2}$ norm over L_1 norm minimization in signal reconstruction for power spectrum estimation. In addition, where multiple realizations are available for basis re-weighting, $L_{1/2}$ norm is shown to provide more accurate

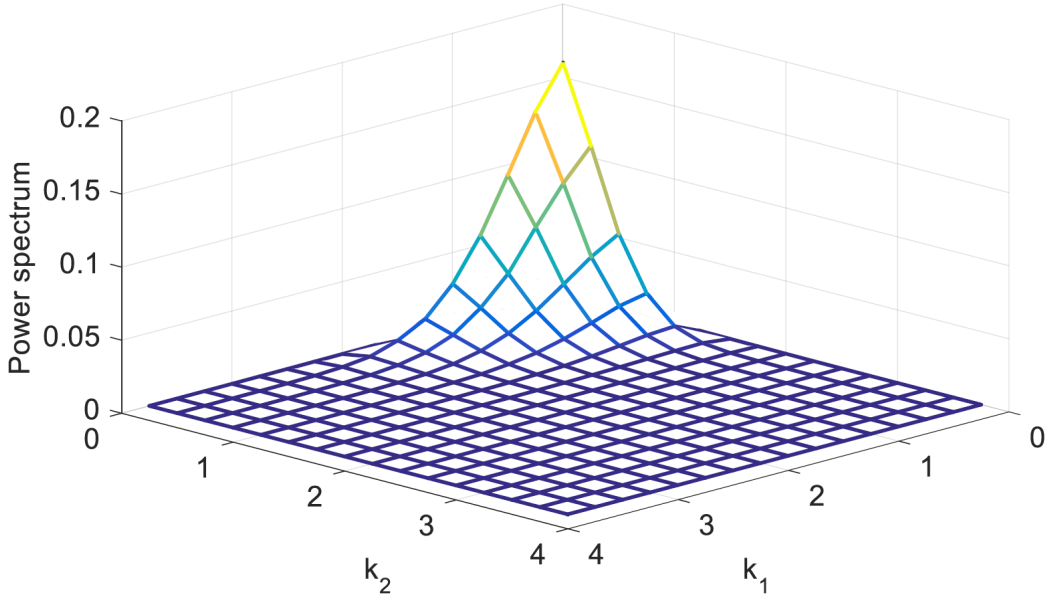

Figure 2.14: Two-dimensional non-Gaussian power spectrum estimate of Eq.(2.45) from 200 samples (no missing data)

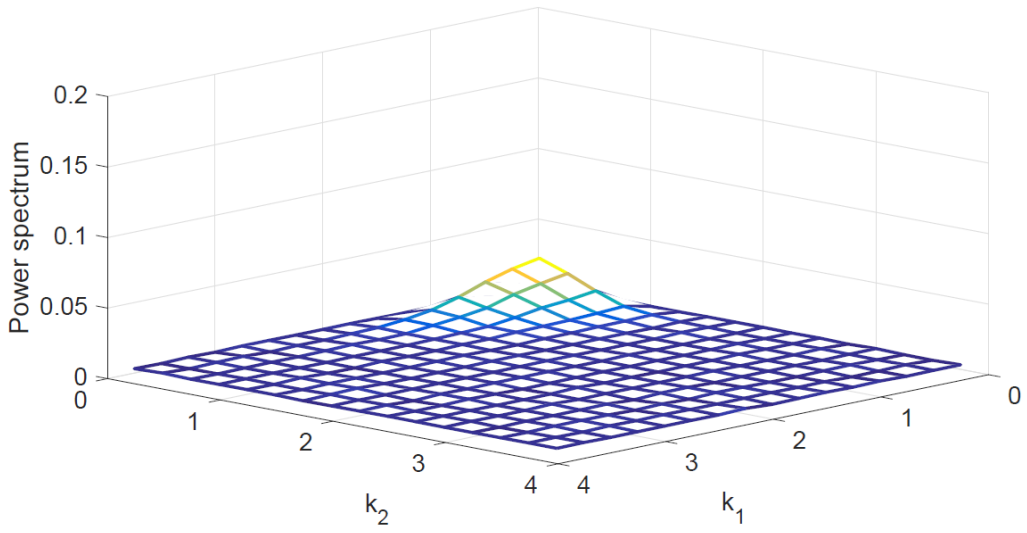

Figure 2.15: Two-dimensional non-Gaussian power spectrum estimate of Eq.(2.45) from 200 samples (80% missing data, L_2 norm reconstruction, $error = 1.2$)

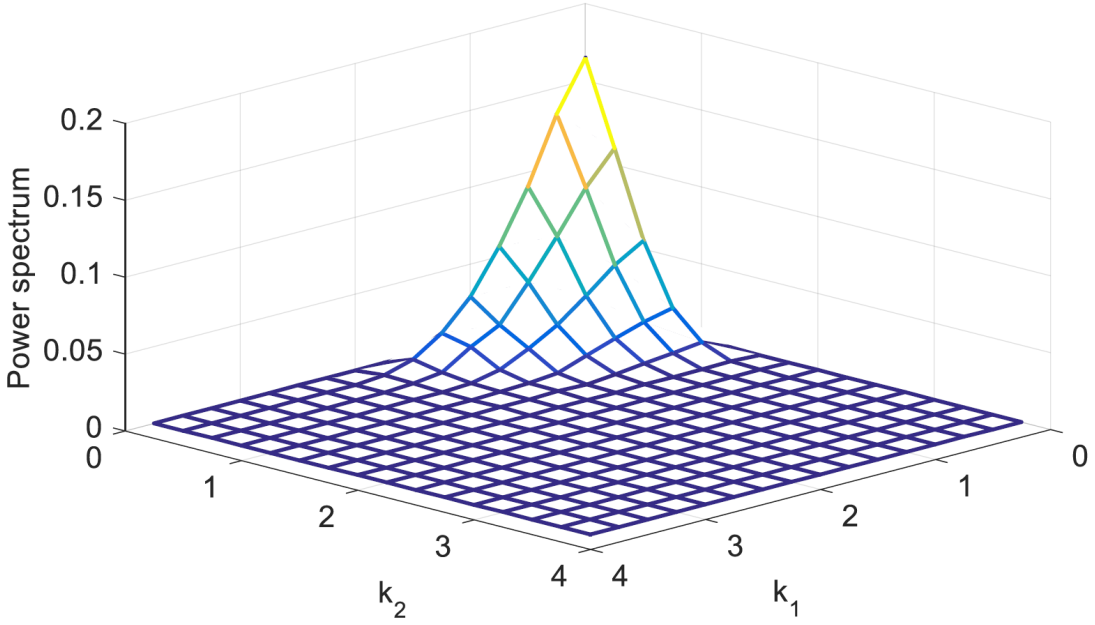

Figure 2.16: Two-dimensional non-Gaussian power spectrum estimate of Eq.(2.45) from 200 samples with re-weighting (80% missing data, $L_{1/2}$ norm reconstruction, $error = 0.07$)

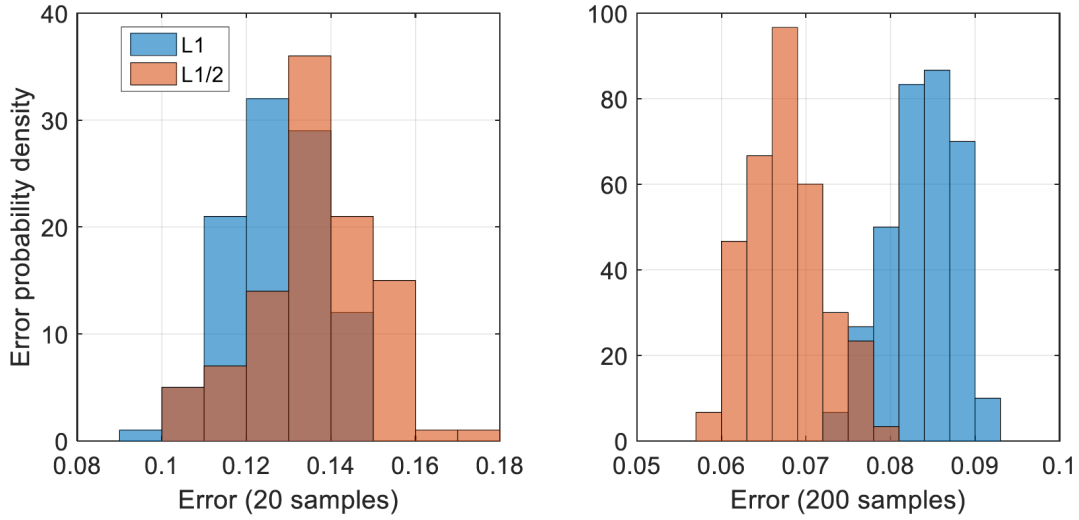

Figure 2.17: Distribution of error over 100 repeated estimations of Eq.(2.45) with re-weighting for 20 and 200 samples

spectrum estimations when large sample sizes are utilized. L_1 norm minimization has been shown to exhibit a greater magnitude of improvement after re-weighting when compared to $L_{1/2}$. Nevertheless, despite the re-weighting, the $L_{1/2}$ solution still succeeds in producing sparser spectral estimates.

Chapter 3

Uncertainty quantification of power spectrum and spectral moments estimates subject to missing data

3.1 Preliminary remarks

In research fields such as stochastic structural dynamics, stochastic processes are most often described by statistical quantities such as the power spectrum. In this regard, several approaches exist in the literature for stochastic process power spectrum estimation. For instance, a Fourier basis is typically utilized in the spectral estimation of stationary processes [80]. Further, similar to the stationary case, the evolutionary power spectrum related to non-stationary processes can be estimated by employing wavelet (e.g. [115]; [62]) or chirplet bases [90] among other alternatives; see also [93] for a detailed presentation of joint time-frequency analysis techniques.

It is noted that the above spectral estimation approaches often require a large number of complete data samples for attaining a predefined adequate degree of accuracy. However, missing data in measurements is frequently an unavoidable situation. In fact, missing data are possible in almost any situation where data are collected and stored. Indicative reasons in engineering dynamics measurement applications include failure and/or restricted use of equipment, as well as data corruption and cost/bandwidth limitations.Thus, standard spectral analysis techniques that inherently assume the existence of full sets of data, such as those based on Fourier, wavelet and chirplet transforms, cannot be used in a straightforward manner.

To address this challenge, a number of signal reconstruction techniques subject to missing / incomplete data (e.g. Lomb-Scargle periodogram, iterative deconvolution method CLEAN, ARMA-model based techniques, etc) have been developed with various degrees of accuracy; see [136] for a review. Indicatively, [25] developed recently a compressive sensing approach (e.g. [37]) based on L_1 norm minimization for stationary and non-stationary stochastic process/field (evolutionary) power spectrum estimation subject to highly incomplete data. The approach has been shown to be particularly advantageous for cases where multiple records / realizations compatible with a stochastic process are available. In such cases, a reweighting procedure can be introduced to

improve the result to a large degree [22]. Further, an artificial neural network based approach was also developed recently having the advantage that no prior knowledge of the underlying process is required [24].

Although all of the above methodologies can, depending on the setting, potentially provide a relatively accurate stochastic process power spectrum estimate, they will also propagate inaccuracies from missing data predictions in the time domain through to the final spectral estimates. Most of the aforementioned techniques estimate the power spectrum by reconstructing missing parts of the data, and based on these reconstructed full data, standard spectral analysis methods are applied. Nevertheless, reconstructing the available records, and thus, deterministically estimating/predicting missing values, rarely accounts for the inherent uncertainty associated with the missing data. Hence, there is merit in developing a methodology for quantifying the uncertainty in a given spectral estimate as a result of the uncertainty related to the missing data in the time/space domain.

In this manner, to quantify the uncertainty of spectral estimates subject to missing data, a stochastic model accounting for the uncertainty in the missing data in the time/space domain can be considered based on any available prior knowledge (e.g. an appropriately estimated probability density function (PDF)). Further, the uncertainty in the missing data can be propagated and the PDF for each individual power spectrum point can be determined in the frequency domain. In this regard, [23] proposed a methodology and determined a closed form expression for the power spectrum estimate PDF under the assumption that the (missing data) variables in the time domain are independent Gaussian random variables. Note, however, that this approach does not consider the correlation between the missing points, and thus, can be largely unrepresentative, for instance, of a signal with harmonic features.

In this chapter, the approach developed in [23] is extended to account for the correlation between the missing data. Although determining the exact correlation between points is practically a quite challenging task, an estimate can be obtained by relying on existing available data and employing various modeling schemes such as Kriging [125]. Further, an additional significant contribution of the herein proposed methodology is that it is generalized to evaluate not only the power spectrum points PDFs, but also the PDFs of the corresponding spectral moments. Clearly, this is of considerable importance to various engineering dynamics applications such as to structural system reliability assessment, where the survival probability (or equivalently, the first-passage time) can be estimated approximately based on knowledge of spectral moments [134]. Several numerical examples are included and compared against pertinent Monte Carlo simulations for demonstrating the validity of the approach.

3.2 Mathematical formulation

3.2.1 Stochastic process power spectrum estimate uncertainty quantification under missing data

Consider a zero mean stationary process represented as ([27]; [91])

$$f(t) = \int_{-\infty}^{+\infty} A(\omega) e^{i\omega t} dZ(\omega), \tag{3.1}$$

where $A(\omega)$ is a deterministic function and $dZ(\omega)$ is a zero mean orthonormal increment stochastic process. The two-sided power spectrum $S_f(\omega)$ of process $f(t)$ is then defined as $S_f(\omega) = |A(\omega)|^2$. In general, stochastic process realizations compatible with a given spectrum can be generated by a spectral representation methodology [110] as Eq.(2.29). The realizations generated by Eq.(2.29) exhibit the property of ergodicity [110]; hence, the power spectrum $S_f(\omega)$ of the underlying process can be estimated by utilizing a single realization only. In this regard, and employing the discrete Fourier transform (DFT) yields Eq.(2.17). In the following, the condition $N \longrightarrow \infty$ is omitted, for convenience, under the assumption that the length is long enough to provide with an accurate spectrum estimate. The data points are divided into 2 parts: the known points x_α and missing points x_β, where α and β are indices of the known and unknown points, respectively; thus, Eq.(2.17) can be further cast in the form

$$S_f(\omega_k) = \frac{T}{2\pi N^2} |M_1 + M_2 - i(M_3 + M_4)|^2 = \frac{T}{2\pi N^2} [(M_1 + M_2)^2 + (M_3 + M_4)^2] \tag{3.2}$$

where $M_1 = \sum_\alpha x_\alpha \cos\left(\frac{2\pi k\alpha}{N}\right)$, $M_2 = \sum_\beta x_\beta \cos\left(\frac{2\pi k\beta}{N}\right)$, $M_3 = \sum_\alpha x_\alpha \sin\left(\frac{2\pi k\alpha}{N}\right)$, and $M_4 = \sum_\alpha x_\alpha \sin\left(\frac{2\pi k\alpha}{N}\right)$. Next, $S_f(\omega_k)$ is rewritten into the simpler form

$$S_f(\omega_k) = (c_1 + \mathbf{a}'\mathbf{X}_\beta)^2 + (c_2 + \mathbf{b}'\mathbf{X}_\beta)^2 \tag{3.3}$$

where

$$c_1 = \sqrt{\frac{T}{2\pi N^2}} \sum_\alpha x_\alpha \cos\left(\frac{2\pi k\alpha}{N}\right) \tag{3.4}$$

$$c_2 = \sqrt{\frac{T}{2\pi N^2}} \sum_\alpha x_\alpha \sin\left(\frac{2\pi k\alpha}{N}\right) \tag{3.5}$$

$$\mathbf{a} = \sqrt{\frac{T}{2\pi N^2}} \left(\cos\left(\frac{2\pi k\beta_1}{N}\right), \cos\left(\frac{2\pi k\beta_2}{N}\right), ..., \cos\left(\frac{2\pi k\beta_u}{N}\right)\right)^T \tag{3.6}$$

$$\mathbf{b} = \sqrt{\frac{T}{2\pi N^2}} \left(\sin\left(\frac{2\pi k \beta_1}{N}\right), \sin\left(\frac{2\pi k \beta_2}{N}\right), ..., \sin\left(\frac{2\pi k \beta_u}{N}\right) \right)^T \tag{3.7}$$

and

$$\mathbf{X}_\beta = (x_{\beta 1}, x_{\beta 2}, ..., x_{\beta u})^T \tag{3.8}$$

where u is the number of missing points.

By virtue of the central limit theorem [7], it is reasonable in many cases to make the approximation that missing points follow a multi-variate Gaussian PDF. In this regard, the various statistical quantities such as the mean and variance for each missing point as well as the correlation between missing points are taken into consideration. In the ensuing analysis, it is assumed that the mean vector $\boldsymbol{\mu}$ and correlation matrix $\boldsymbol{\Sigma}$ of the missing data following a Gaussian distribution, i.e. $\mathbf{X}_\beta \sim N(\boldsymbol{\mu}, \boldsymbol{\Sigma})$, are obtained by some available estimation scheme, such as the Kriging model; see following section for more details.

Next, Eq.(3.3) is rearranged (see also [85]) as a function of two variables in the form

$$S_f(\omega_k) = (c_1 + \mathbf{a}^T \mathbf{X}_\beta)^2 + (c_2 + \mathbf{b}^T \mathbf{X}_\beta)^2 = X_1^2 + X_2^2 \tag{3.9}$$

It is readily seen that $X_1 = c_1 + \mathbf{a}^T \mathbf{X}_\beta \sim N(c_1 + \mathbf{a}^T \boldsymbol{\mu}, \mathbf{a}^T \boldsymbol{\Sigma} \mathbf{a})$ and $X_2 = c_2 + \mathbf{b}^T \mathbf{X}_\beta \sim N(c_2 + \mathbf{b}^T \boldsymbol{\mu}, \mathbf{b}^T \boldsymbol{\Sigma} \mathbf{b})$. Because both X_1 and X_2 are related to the same set of random variables $\mathbf{X}_\beta$, it is obvious that they exhibit some degree of correlation. In this regard, the correlation matrix $\mathbf{C}_{X_1 X_2}$ of joint Gaussian variables $\mathbf{X} = (X_1, X_2)^T$ is given by

$$\mathbf{C}_{X_1 X_2} = \begin{pmatrix} \mathbf{a}^T \boldsymbol{\Sigma} \mathbf{a} & \sum_i \sum_j a_i b_j (\Sigma_{ij} + \mu_1 \mu_2) - \mathbf{b}^T \boldsymbol{\mu} \mathbf{a}^T \boldsymbol{\mu} \\ \sum_i \sum_j a_i b_j (\Sigma_{ij} + \mu_1 \mu_2) - \mathbf{b}^T \boldsymbol{\mu} \mathbf{a}^T \boldsymbol{\mu} & \mathbf{b}^T \boldsymbol{\Sigma} \mathbf{b} \end{pmatrix} \tag{3.10}$$

and the mean vector of joint Gaussian variables X_1 and X_2 takes the form

$$\boldsymbol{\mu}_{X_1 X_2} = (c_1 + \mu_1, c_2 + \mu_2)^T \tag{3.11}$$

where $\mu_1 = c_1 + \mathbf{a}^T \boldsymbol{\mu}, \mu_2 = c_2 + \mathbf{b}^T \boldsymbol{\mu}$.

Further, to determine the PDF of variable $S_f(\omega_k)$ in Eq.(3.9), the celebrated input-output PDF relationship [85] is applied, and the cumulative distribution function (CDF) of $S_f(\omega_k)$ is defined as

$$F(S_f) = P(S_f \leq s) = P[(X_1, X_2) \in D_z] = \iint_{(X_1, X_2) \in D_z} f_{X_1, X_2}(X_1, X_2) dX_1 dX_2 \tag{3.12}$$

where $f_{X_1,X_2}(X_1, X_2)$ is the distribution function of variables X_1 and X_2, and the PDF of $S_f(\omega_k)$ is given by

$$f_s(s) = \frac{dF(S_f)}{ds} \tag{3.13}$$

Thus, taking into account Eqs. (3.9-3.13), an analytical expression for the power spectrum PDF at a given frequency ω_k is derived in the form

$$\begin{aligned} p_{S_f(\omega_k)}(s) =& \frac{d}{ds} \iint_{X_1^2+X_2^2 \leq s} \frac{1}{2\pi\sqrt{|\mathbf{C}_{X_1X_2}|}} \\ & exp[-\frac{1}{2}(\mathbf{X} - \boldsymbol{\mu}_{X_1X_2})^T C_{X_1X_2}^{-1}(\mathbf{X} - \boldsymbol{\mu}_{X_1X_2})]dX_1dX_2 \end{aligned} \tag{3.14}$$

In this section an approach has been developed for quantifying the uncertainty in a stochastic process power spectrum estimate subject to missing data. Specifically, a closed form analytical expression has been derived in Eq.(3.14) for the power spectrum estimate PDF corresponding to a given frequency. In comparison with the methodology in [23], which adopts the assumption that missing data in a given realization are independent and identically distributed Gaussian random variables, the rather strict assumption of independence is abandoned herein. In this manner, the correlation between the missing data is taken into account in estimating the power spectrum PDF.

3.2.2 Kriging model for estimating correlations between missing data

Clearly, the approach developed in the previous section relies on prior knowledge of the correlation between the missing data. Among the various available techniques in the literature for estimating data correlation relationships a Kriging based scheme (e.g. [125]; [43] and [58]) is considered in the ensuing analysis.

Specifically, let $f(t)$ be a sample of a stationary stochastic process with a power spectrum $S_f(\omega)$. Given the n known points $t_k, k = 1, 2, ..., n$, an estimate of $f(t_j)$ at the missing point t_j, can be obtained as a weighted linear combination of the available known points [125], i.e.,

$$f(t_j) = \sum_{k=1}^{n} \chi_k f(t_k) + z(t) \tag{3.15}$$

where χ_k is the weight of each known point, and $z(t)$ is a stationary Gaussian process with zero mean and covariance

$$C = \text{cov}(z(t), z(t^*)) = \gamma(|t - t^*|) = \sigma_z^2 R(|t - t^*|) \tag{3.16}$$

where σ_z^2 is the constant variance of the process and R is the correlation function. Several types of

correlation functions, such as exponential, linear and Gaussian, have been proposed in the literature [60]. Herein, a correlation function of exponential form is adopted, i.e.

$$\gamma(h) = \sigma_z^2 e^{-\theta_1 h} \cos(\theta_2 h)(1 + \theta_1 h) \tag{3.17}$$

where $h = |t - t^*|$ is the interval between two time instants, and θ_1, θ_2 are constant values to be determined. Next, σ_z^2, θ_1 and θ_2 are obtained by

$$\min_{\sigma_z^2, \theta_1, \theta_2} |\gamma(h) - \gamma_e(h)|_2 \tag{3.18}$$

where $\gamma_e(h) = \dfrac{1}{n} \sum_{k=1}^{n} [f(t_k + h) f(t_k)]$, and $f(t_k + h), f(t_k)$ are the known points.

Further, utilizing the Kriging model of Eq.(3.15) the estimate error variance is given by

$$V = Var[f^*(t_j) - f(t_j)] = 2 \sum_{k=1}^{n} \chi_k \gamma(|t_k - t_j|) - \sum_{k=1}^{n} \sum_{v=1}^{n} \chi_k \chi_v \gamma(|t_k - t_v|) - \sigma_z^2 \tag{3.19}$$

Next, to minimize the error variance V, a Lagrange multipliers approach is applied yielding the equations

$$\begin{cases} \sum_{k=1}^{n} \chi_k \gamma(|t_k - t_v|) + \kappa = \gamma(|t_k - t_j|), (j = 1, ..., n) \\ \sum_{k=1}^{n} \chi_k = 1 \end{cases} \tag{3.20}$$

to be solved for the weights χ_k and Lagrange multiplier κ . Further, an estimate of the missing point is given by Eq.(3.15). Then, the covariance matrix $\mathbf{C}$ of the sample could be easily obtained through Eq.(3.16).

Note that, denoting the time history vector $\mathbf{x}$ as $\mathbf{x} = (\mathbf{x}_\beta, \mathbf{x}_\alpha)$, the covariance matrix $\mathbf{C}$ can be expressed as $\mathbf{C} = \begin{pmatrix} \mathbf{C}_{\beta\beta} & \mathbf{C}_{\beta\alpha} \\ \mathbf{C}_{\alpha\beta} & \mathbf{C}_{\alpha\alpha} \end{pmatrix}$, where $\mathbf{C}_{\beta\beta}$ is the matrix whose rows and columns correspond to the missing points $\mathbf{x}_\beta$, while $\mathbf{C}_{\alpha\alpha}$ corresponds to the known points $\mathbf{x}_\alpha$. In this regard, the conditional covariance matrix $\mathbf{\Sigma}$ of the missing points is calculated as [85]

$$\mathbf{\Sigma} = \mathbf{C}\{\mathbf{x}_\beta | \mathbf{x}_\alpha\} = \mathbf{C}_{\beta\beta} - \mathbf{C}_{\beta\alpha} \mathbf{C}_{\alpha\alpha}^{-1} \mathbf{C}_{\alpha\beta} \tag{3.21}$$

and the mean value can be obtained through Eq.(3.15). Overall, adopting a Kriging modeling approach in this section, the mean and covariance of missing data are estimated, and can be used as an input to the approach developed in the previous section.

3.2.3 Stochastic process spectral moment estimate uncertainty quantification under missing data

For stationary random processes, the spectral moments are defined as

$$\lambda_m = \int_{-\infty}^{+\infty} \omega^m S(\omega) d\omega \tag{3.22}$$

where $S(\omega)$ is the two-sided power spectrum (e.g. [73]). Considering next the case of a zero mean process, the zero spectral moment λ_0 is equal to the mean square $E[X^2]$ of the process X (also equal to the squared standard deviation σ_X^2 in this case), and the second spectral moment λ_2 is the mean square $E[\dot{X}^2]$ of the derivative process X. In a similar manner as the moments of a random variable are used to describe certain features of the related PDF, spectral moments are indispensable in a variety of applications such as determining approximately the survival probability (or equivalently, the first-passage time) and assessing the reliability of structural systems (e.g. [133]; [134]; [73]).

Further, Eq.(3.22) can be recast into a discrete form in the frequency domain, i.e.

$$\lambda_m = \sum_k \omega_k^m S(\omega_k) \Delta\omega \tag{3.23}$$

Clearly, based on Eq.(3.23) the spectral moment can be viewed as a linear combination of individual power spectrum points. Note that although the PDFs of the power spectrum points $S(\omega_k)$ can be obtained by the methodology developed in the previous sections, a straightforward determination of the PDF of the spectral moment λ_m can be quite daunting due to the following reasons. First, the various power spectrum points $S(\omega_k)$ do not, in general, follow the same PDF for different frequency values ω_k. Second, the variables $S(\omega_k)$ exhibit correlation as they are defined by utilizing the same set of random variables.

Next, to address these challenges, a methodology based on characteristic functions is proposed. The characteristic function of a random variable is defined as [85]

$$\Phi_X(\omega) = \mathrm{E}[e^{i\omega x}] = \int_{-\infty}^{+\infty} f_X(x) e^{i\omega x} dx \tag{3.24}$$

where $f_X(x)$ is the probability density function of X. Clearly, the characteristic function and the PDF of a random variable form a Fourier transform pair. Further, the spectral moment Eq.(3.23) can be construed as a quadratic transformation of missing points $\mathbf{X}_\beta$. The correlated variables $\mathbf{X}_\beta \sim N(\boldsymbol{\mu}, \boldsymbol{\Sigma})$, where $\boldsymbol{\Sigma}$ can be cast into the Cholesky-like factorization form $\boldsymbol{\Sigma} = \mathbf{A}\mathbf{A}^T$ ($\mathbf{A}$ being a lower triangular matrix), are replaced by a new set of independent standard Gaussian

variables $\mathbf{X}_g \sim N(\mathbf{0}, \mathbf{I})$ as

$$\mathbf{X}_\beta = \boldsymbol{\mu} + \mathbf{A}\mathbf{X}_g \tag{3.25}$$

Next, employing Eqs.(3.23-3.25), Eq.(3.3) can be cast in the matrix form

$$S_f(\omega_k) = (c_{1,k} + \mathbf{a}_k^T\boldsymbol{\mu} + \mathbf{a}_k^T\mathbf{X}_g)^2 + (c_{2,k} + \mathbf{b}_k^T\boldsymbol{\mu} + \mathbf{b}_k^T\mathbf{X}_g)^2 = \mathbf{X}_{gn}^T\mathbf{B}_k\mathbf{X}_{gn} \tag{3.26}$$

where

$$\mathbf{X}_{gn} = (\mathbf{X}_g^T, 1)^T = (x_{g1}, x_{g2}, ..., x_{gu}, 1)^T \tag{3.27}$$

and

$$\mathbf{B}_{k,vj} = \begin{cases} a_{k,v}a_{k,v} + b_{k,v}b_{k,v}, & v, j \leq u \\ (c_{1,k} + \mathbf{a}_k^T\boldsymbol{\mu})a_{k,v} + (c_{2,k} + \mathbf{b}_k^T\boldsymbol{\mu})b_{k,v}, & j = u+1, v \neq u+1 \\ (c_{1,k} + \mathbf{a}_k^T\boldsymbol{\mu})a_{k,j} + (c_2 + \mathbf{b}_k^T\boldsymbol{\mu})b_{k,j}, & v = u+1, j \neq u+1 \\ (c_{1,k} + \mathbf{a}_k^T\boldsymbol{\mu})^2 + (c_2 + \mathbf{b}_k^T\boldsymbol{\mu})^2, & v = j = u+1 \end{cases} \tag{3.28}$$

$c_{1,k}, c_{2,k}, \mathbf{a}_k, \mathbf{b}_k$ are defined by Eq.(3.4-3.7).

Combining Eqs.(3.23) and (3.27), the spectral moments are given, alternatively, in the form

$$\lambda_m = \mathbf{X}_{gn}^T(\sum_k \omega_k^m \Delta\omega \mathbf{B}_k)\mathbf{X}_{gn} \tag{3.29}$$

whereas utilizing Eq.(3.29) the characteristic function of the spectral moments becomes [85]

$$\Phi_{\lambda_m}(\omega) = E[e^{i\omega\lambda_m}] = \int_{-\infty}^{+\infty} (2\pi)^{-\frac{u}{2}} exp(-\frac{1}{2}[\mathbf{X}_g^T\mathbf{X}_g - i\omega\mathbf{X}_{gn}^T(\sum_k \omega_k^m \Delta\omega \mathbf{B}_k)\mathbf{X}_{gn}])d\mathbf{X}_g \tag{3.30}$$

Note that, the evaluation of Eq.(3.30) can be simplified based on the following steps. Specifically,

a) Let

$$Y = \frac{1}{2}[\mathbf{X}_g^T\mathbf{X}_g - i\omega\mathbf{X}_{gn}^T(\sum_k \omega_k^m \Delta\omega \mathbf{B}_k)\mathbf{X}_{gn}] \tag{3.31}$$

Eq.(3.31) can be divided into two parts, i.e., $Y = Y_1 + Y_2$. The first includes the second order terms, i.e. $Y_1 = \sum_{k,j} c_{kj}x_{gk}x_{gj}$,while the second includes the first order terms plus the constant term, i.e. $Y_2 = \sum_k c_k x_{gk} + c_{cons}$. Thus, Eq.(3.30) can be rewritten as

$$\Phi_{\lambda_m}(\omega) = E[e^{i\omega\lambda_m}] = \int_{-\infty}^{+\infty} (2\pi)^{-\frac{u}{2}} exp(-Y_1 - Y_2)dx_g \tag{3.32}$$

b) Similar to Eq.(3.29), Y_1 can be expressed as $Y_1 = \mathbf{X}_g^T \mathbf{B}_{Y_1} \mathbf{X}_g$ where $\mathbf{B}_{Y_1}$ is given by

$$\mathbf{B}_{Y_1} = \mathbf{A}_{Y_1}^T \mathbf{A}_{Y_1} \tag{3.33}$$

In Eq.(3.33) $\mathbf{A}_{Y_1}$ is an upper triangular matrix, and $\mathbf{A}_{Y_1}^T$ is the non-conjugate transpose of $\mathbf{A}_{Y_1}$. The factorization in Eq.(3.33) is numerically implemented via a Cholesky factorization kind algorithm [44] with the note that the diagonal elements in $\mathbf{B}_{Y_1}$ are complex values.

c) After obtaining the upper triangular matrix $\mathbf{A}_{Y_1}$, Y may be expressed in a similar form to Y_1 (after accounting for first order terms and the constant); thus simplifying the solution of the integral in Eq.(3.32). Hence

$$Y = (\mathbf{A}_Y \mathbf{X}_{gn})^T (\mathbf{A}_Y \mathbf{X}_{gn}) + c_Y \tag{3.34}$$

where $\mathbf{A}_Y = (\mathbf{A}_{Y_1}, \mathbf{a}_{u\times 1})$, and $\mathbf{a}_{u\times 1}$ are the coefficients to account for the first order terms $\sum_k X_{gk}$ in Y_2 (with u being the number of missing data); and c_Y is a constant. A worked 2-variable example is shown in detail in Appendix A.

d) Finally, substituting Eq.(3.34) into Eq.(3.30), the integral in Eq.(3.30) may be simplified significantly to a function of B_{Y_1}, and the constant term c_Y in the form

$$\Phi_{\lambda_m}(\omega) = \mathrm{E}[e^{i\omega\lambda_m}] = 2^{-\frac{u}{2}} (\det(\mathbf{B}_{Y_1}))^{-\frac{1}{2}} e^{-c_Y} \tag{3.35}$$

whereas the spectral moments PDFs are estimated via the inverse Fourier transform of Eq.(3.30), i.e.

$$p_{\lambda_i}(s) = \frac{1}{2\pi} \int_{-\infty}^{+\infty} \Phi_{\lambda_i}(\omega) e^{i\omega s} d\omega \tag{3.36}$$

In this section an efficient approach has been developed for quantifying the uncertainty in the spectral moments estimates of an underlying stochastic process based on available realizations with missing data. Specifically, a closed form expression has been derived in Eq.(3.30) for the spectral moment characteristic function. The rather daunting brute force numerical evaluation of the integral appearing in the derived expression has been conveniently circumvented via a "Cholesky" kind decomposition of the integrand function. Clearly, the development in this section is of considerable importance (as illustrated in the following section) to various engineering dynamics applications such as to structural system reliability assessment [134].

3.2.4 Survival probability estimate uncertainty quantification under missing data

A persistent challenge in the field of stochastic dynamics has been the determination of the system survival probability, i.e. the probability that the structural system response will stay below a certain threshold over a given period of time. Many research efforts for addressing the aforementioned challenge exist in the literature ranging from semi-analytical to purely numerical approaches (e.g. [118]; [11]; [2]). One of the first semi-analytical approximate approaches proposed by Vanmarke [134] that relies on the knowledge of the system response spectral moments [133] is considered next.

Specifically, consider a linear single-degree-of-freedom (SDOF) oscillator, whose motion is governed by the stochastic differential equation

$$\ddot{x} + 2\zeta_0\omega_0\dot{x} + \omega_0^2 x = w(t) \tag{3.37}$$

where x is the response displacement, a dot over a variable denotes differentiation with respect to time t; ζ_0 is the ratio of critical damping; ω_0 is the oscillator natural frequency and $w(t)$ represents a Gaussian, zero-mean stationary stochastic process possessing a broad-band power spectrum $S(\omega)$. Focusing next on the stationary response of the oscillator, the response displacement and velocity power spectra are given by [80]

$$S_X(\omega) = |H(\omega)|^2 S(\omega) \tag{3.38}$$

and

$$S_{\dot{X}}(\omega) = \omega^2 S_X(\omega) = \omega^2 |H(\omega)|^2 S(\omega) \tag{3.39}$$

respectively; and the frequency response function $H(\omega)$ is given by

$$H(\omega) = \frac{1}{\omega_0^2 - \omega^2 + 2i\zeta_0\omega_0\omega} \tag{3.40}$$

According to [134] and [28], the time-dependent survival probability $P_B(t)$ of a linear oscillator given a barrier level B can be approximated by

$$P_B(t) = \text{exp}\left[-\frac{1}{\pi}\sqrt{\frac{\lambda_{X,2}}{\lambda_{X,0}}}t \cdot \text{exp}(-\frac{B^2}{2\lambda_{X,0}})\right] \tag{3.41}$$

where $\lambda_{X,m}$ is the m-th order spectral moment of the displacement x. Note that for the specific case of the linear oscillator of Eq.(3.37), and considering a low value for the damping ratio, i.e. $\zeta_0 \leq 0.05$, its response exhibits a narrow-band feature in the frequency domain due to the form of the frequency response function (see Eq.(3.38)). In particular, it can be seen that $|H(\omega)|^2$ is a function with a sharp peak around the oscillator natural frequency $\omega = \omega_0$, and decays quickly

for $\omega \neq \omega_0$. Thus, it is reasonable to assume that the response of the linear oscillator exhibits a pseudo-harmonic behavior [113], and the response displacement and velocity can be represented, respectively, as

$$x = A\cos(\omega_0 t + \varphi) \tag{3.42}$$

and

$$\dot{x} = -A\omega_0 \sin(\omega_0 t + \varphi) \tag{3.43}$$

In Eq.(3.42), A and φ represent the response amplitude and phase processes, respectively; see also [113] and [64] for more details. Considering next Eqs.(3.42-3.43), the independence of A with φ and taking into account that $\mathrm{E}(\cos^2(\omega_0 t + \varphi)) = \mathrm{E}(\sin^2(\omega_0 t + \varphi))$ yields

$$\mathrm{E}(\dot{x}^2) = \omega_0^2 \mathrm{E}(x^2) \tag{3.44}$$

or in other words

$$\lambda_{X,2} = \omega_0^2 \lambda_{X,0} \tag{3.45}$$

Substituting Eq.(3.45) into Eq.(3.41) yields an approximate expression for the oscillator survival probability that depends only on $\lambda_{X,0}$, i.e.

$$P_B(t) = \exp[-\frac{\omega_0}{\pi} t \cdot \exp(-\frac{B^2}{2\lambda_{X,0}})] \tag{3.46}$$

In Eq.(3.46), the analytical expression for the PDF of $\lambda_{X,0}$ in the case of missing data can be derived by the methodology described in the previous sections. After determining the PDF $p_{\lambda_{X,0}}$, the system survival probability characteristic function can be obtained as

$$\Phi_{P_B}(\omega_k) = \mathrm{E}[e^{i\omega_k P_B}] = \int_{-\infty}^{+\infty} e^{i\omega_k P_B} p_{\lambda_{X,0}} d\lambda_{X,0} \tag{3.47}$$

whereas, an inverse Fourier transform can applied to Eq.(3.47) for numerically evaluating the survival probability PDF.

3.3 Numerical examples

3.3.1 Excitation records with missing data

To demonstrate the validity of the developed uncertainty quantification approach, stationary stochastic process time histories compatible with the Kanai-Tajimi-like earthquake engineering power

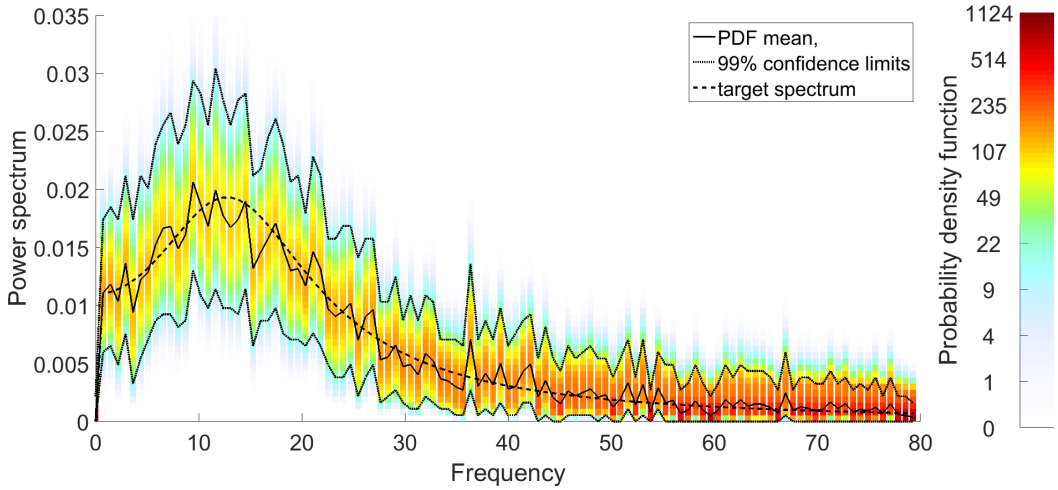

Figure 3.1: Power spectrum probability densities with 10% missing data replaced by correlated Gaussian random variables

spectrum of the form

$$S(\omega) = S_0 \frac{\omega_g^4 + 4\zeta_g^2 \omega_g^2 \omega^2}{(\omega_g^2 - \omega^2)^2 + 4\zeta_g^2 \omega_g^2 \omega^2} \tag{3.48}$$

where $\omega_g = 5\pi$ rad/s and $\zeta_g = 0.63$ and $S(0) = 0$, are generated via Eq.(2.29). To compare with the method described in [23], a factor $S_0 = 0.011$ is introduced to make the standard deviation equal to 1. Next, uniformly randomly distributed missing data are artificially induced. The width of missing data gaps is also uniformly randomly distributed and the locations of the missing data are different for each realisation.

Figure 3.1 shows the estimated power spectrum PDFs and confidence ranges determined via the herein developed approach for 10% missing data, and the pertinent Monte Carlo simulation is applied with the mean and variance obtained by Kriging model. For comparison purposes Figure 3.2 is the result of applying the methodology in [23], where correlations between missing data are not taken into consideration and the missing points follow independent identical Gaussian distributions $\mathbf{X}_\beta \sim N(\mathbf{0}, \mathbf{I})$, the pertinent Monte Carlo simulation is applied with $\mathbf{X}_\beta \sim N(\mathbf{0}, \mathbf{I})$. Compared with Figure 3.2, the method developed herein provides with a smaller range, and the mean spectrum fits the original spectrum better. Figure 3.3 shows the PDFs corresponding to frequencies 10.9 and 30.5 rad/s with 10% missing data replaced both by correlated and by independent identically distributed Gaussian random variables. The vertical lines correspond to the spectral values without missing data. Figure 3.4 shows the spectral moment λ_0 of the excitation spectrum, compared with pertinent Monte Carlo simulations. It can be readily seen that in all cases accounting for the correlation of the missing data, as estimated via the Kriging model, yields spectral estimates PDFs that are much closer to the true value.

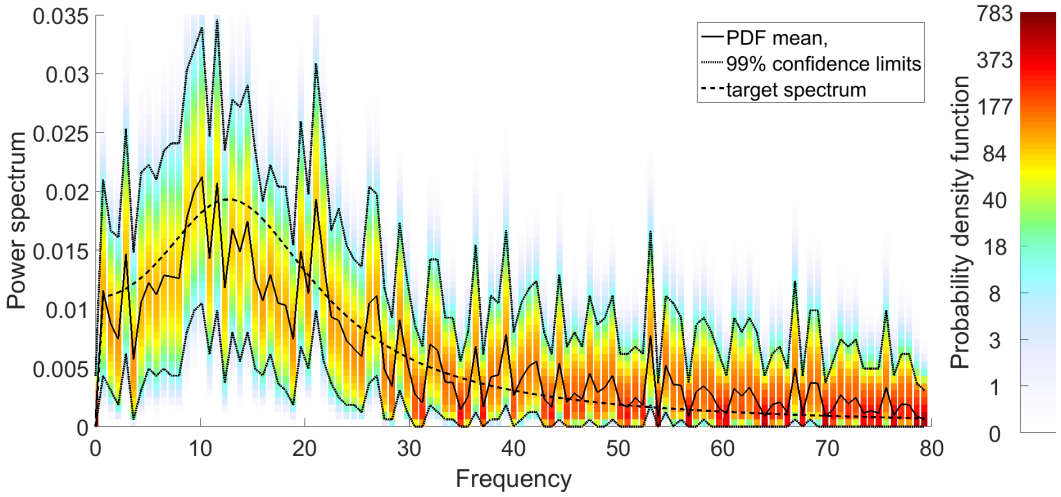

Figure 3.2: Power spectrum probability densities with 10% missing data replaced by independent identically distributed Gaussian random variables

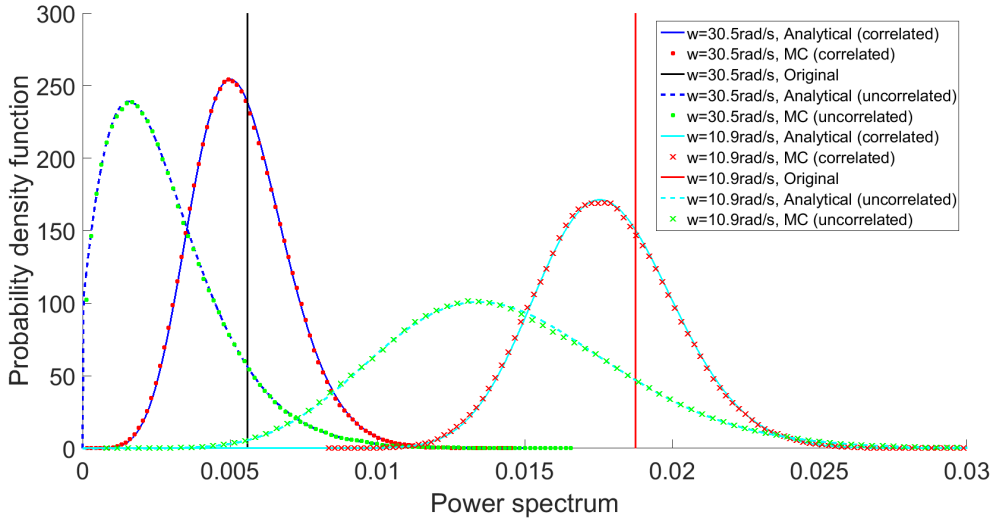

Figure 3.3: PDFs at 10.9 and 30.5 rad/s with 10% missing data replaced by both correlated and independent identically distributed Gaussian random variables. The vertical line shows the spectral value without missing data

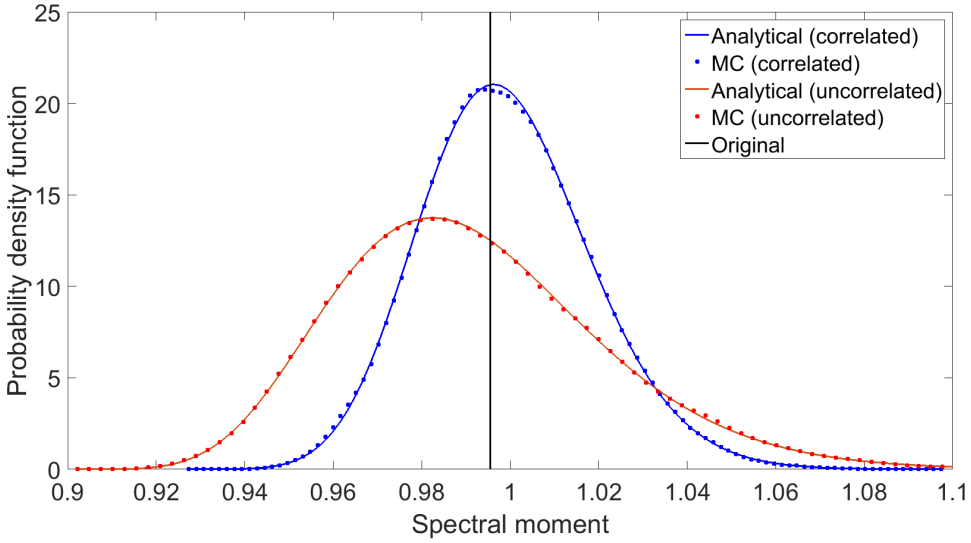

Figure 3.4: PDF of spectral moment λ_0 with 10% missing data replaced by both correlated and independent identically distributed Gaussian random variables. The vertical line shows the spectral moment λ_0 value without missing data

3.3.2 Structural response records with missing data

In the second example, consider a linear oscillator with $\omega_0 = 10.9$ rad/s, and $\zeta_0 = 0.05$. Further, the missing data are introduced into the stationary records of the oscillator response, which are generated by utilizing the same excitation spectrum as in the first example, and by numerically solving the equation of motion. Similarly, the artificially induced missing data in the response records are uniformly randomly distributed.

Figure 3.5 shows the power spectrum PDF and confidence ranges of the oscillator response with 70% missing data determined by the herein developed methodology. For comparison purposes Figure 3.7 is the result of applying the methodology in [23], where correlations between missing data are not taken into consideration and the missing points follow independent identical Gaussian distributions. As anticipated, it can be readily seen that neglecting the correlation structure in the missing data has a bigger negative effect when considering narrow-band signals (see Figures 3.1 and 3.2) rather than broad-band ones (see Figures 3.5 and 3.6). In fact, for the highly correlated oscillator response process disregarding the correlation structure yields an almost constant power spectrum estimate value. Figure 3.7 shows the PDF of the response spectral moment λ_0, compared with pertinent Monte Carlo simulations. In Figure 3.8 the PDF of the oscillator survival probability Eq.(3.46) with 70% missing data and a barrier level $D = 0.05$ is plotted and compared with pertinent Monte Carlo simulations of Eq.(3.41).

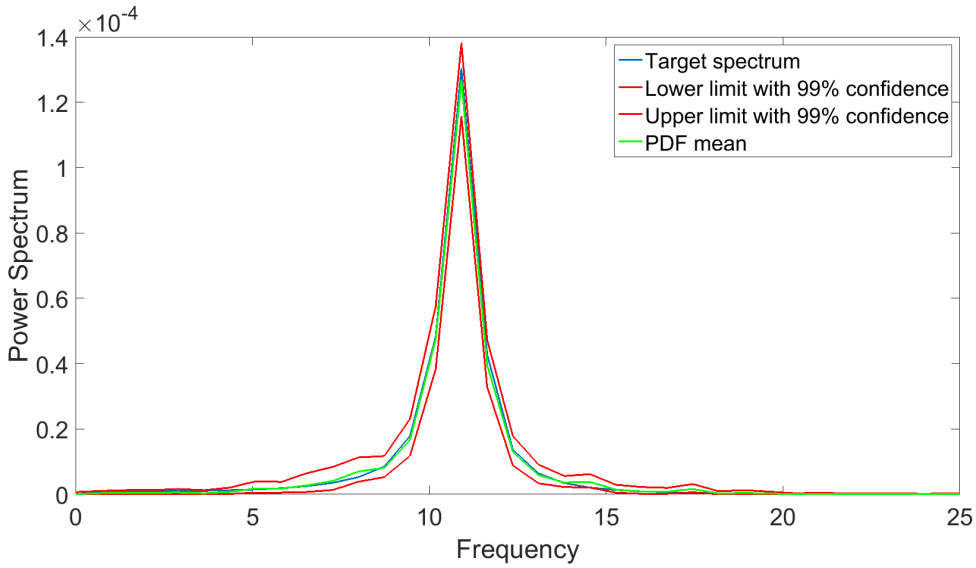

Figure 3.5: Oscillator response power spectrum PDF with 70% missing data replaced by correlated Gaussian random variables

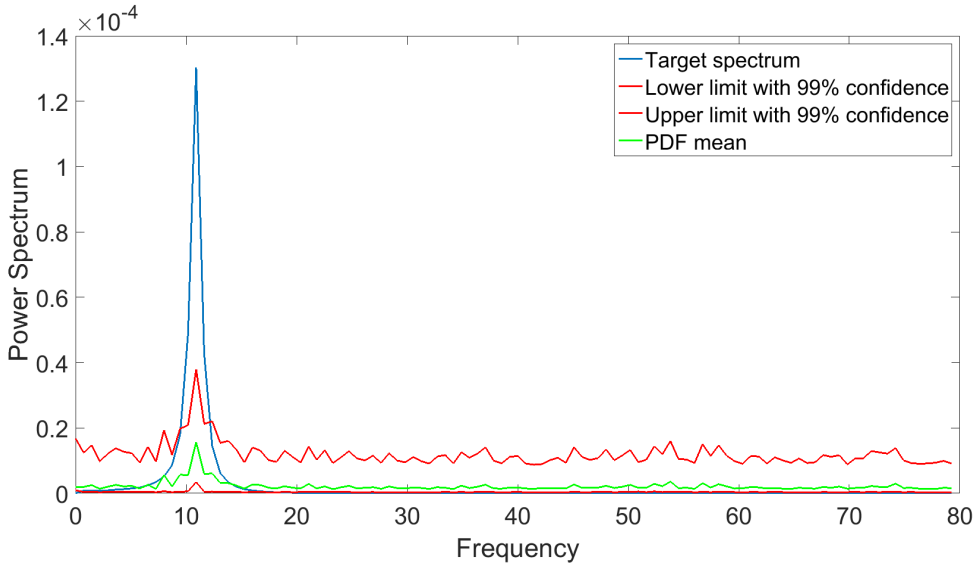

Figure 3.6: Oscillator response power spectrum PDF with 70% missing data replaced by independent identically distributed Gaussian random variables

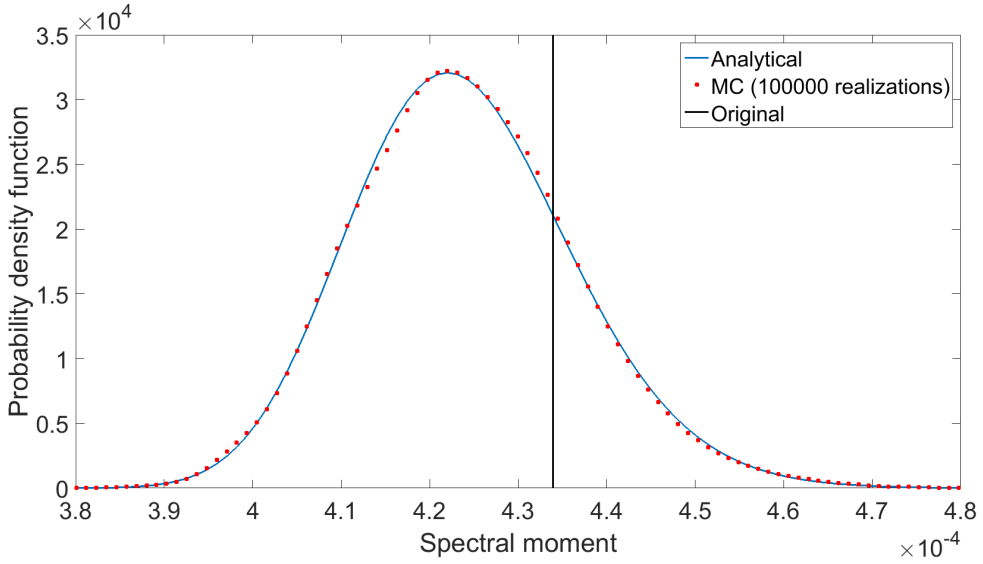

Figure 3.7: PDF of response spectral moment λ_0 with 70% missing data

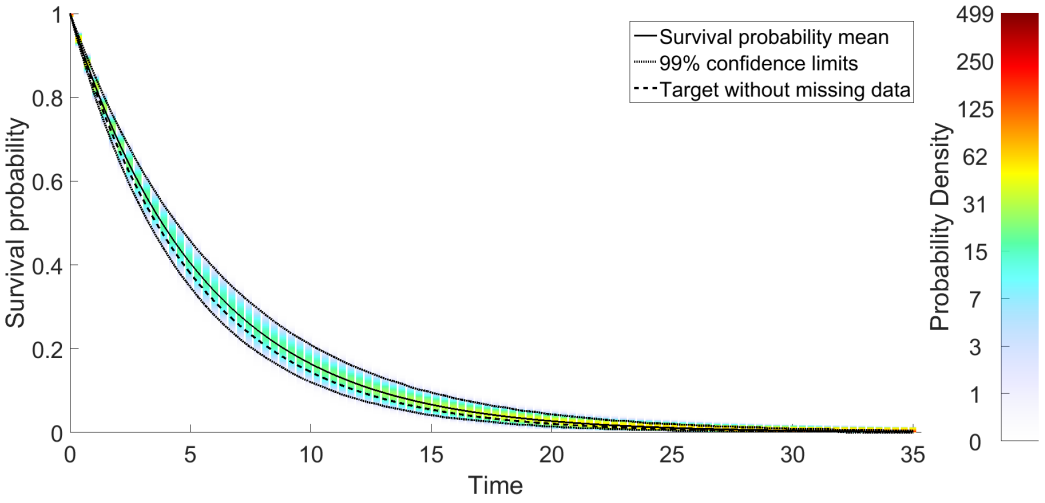

Figure 3.8: Survival probability of oscillator response with 70% missing data and barrier $B = 0.05$ via Eq.(3.46); comparisons with pertinent Monte Carlo simulations of Eq.(3.41)

3.4 Summary

In this chapter, an analytical approach for quantifying the uncertainty in stochastic process power spectrum estimates based on samples with missing data has been developed. In this method, the correlations between the missing data are considered by employing a Kriging model, and a closed form expression has been derived for the power spectrum estimate PDF at each frequency. Next, the approach has been extended for determining the PDF of spectral moments estimates and spectral moments based survival probability assessment as well.

Chapter 4

Uncertainty propagation: Wiener path integral based nonlinear oscillator stochastic response and survival probability determination

4.1 Preliminary remarks

The previous two chapters discuss the excitation estimation problem, in this chapter, the system response problem can be considered accordingly. Although Monte Carlo simulation could deal with a large amount of stochastic problems in engineering field, its computational cost are very high to obtain a reliable results even with the advanced Monte Carlo simulations (eg. [11], [3], [2], [106]), especially in the case for large scale complex systems or when the quantity of interest has a relatively small probability of occurrence. To deal with this issue, among the analytical methods, one of the promising frameworks relates to the concept of the Wiener path integral (WPI). In this regard, note that although the WPI has strongly impacted the field of theoretical physics, the engineering community has ignored its potential as a powerful uncertainty quantification tool. The concept of path integral was introduced by Wiener [138] and was reinvented in a different form by Feynman [40] to reformulate quantum mechanics. A more detailed treatment of path integrals, especially of their applications in physics, can be found in a number of books such as the one by Chaichian and Demichev [14]. Recently, Kougioumtzoglou and Spanos [64] developed an approximate analytical WPI technique based on a variational formulation and on the concepts of stochastic averaging/linearization for addressing certain stochastic engineering dynamics problems. In this regard, relying on the concept of the most probable trajectory an approximate expression was derived for the non-stationary response probability density function (PDF). Further, the aforementioned technique was extended by Kougioumtzoglou and Spanos [67] to treat multi-degree-of-freedom (MDOF) systems and hysteretic nonlinearities. In [34] the technique was further enhanced and generalized to treat linear and nonlinear systems endowed with fractional derivatives terms (e.g. [84]).

The aforementioned WPI technique should not be confused with alternative numerical schemes (commonly referred to as numerical path integral schemes [137], [77], [35]) which constitute, in essence, a discrete version of the Chapman-Kolmogorov (C-K) equation (e.g. [89], [66], [68]). Note that these schemes can be computationally demanding potentially; this is due to the fact that the solution needs to be advanced in short time steps, while multi-dimensional numerical integration needs to be performed at every time step as well.

In this chapter, a variational formulation based WPI technique is developed together with a stochastic averaging/linearization treatment of the problem of determining response and reliability statistics of nonlinear oscillators subject to stochastic excitation. Specifically, first the nonlinear oscillator is cast into an equivalent linear time-variant oscillator. Next, relying on the concept of the most probable trajectory and considering a small time interval an approximate closed-form expression is derived for the oscillator joint transition PDF. Further, the joint transition PDF is used in conjunction with a discrete version of the C-K equation to propagate the solution in short time steps. In this manner, not only the non-stationary response PDF, but also the survival probability and first-passage PDF of the nonlinear oscillator are determined. In comparison with existing numerical path integral schemes, a significant advantage of the proposed WPI technique is that closed-form analytical expressions are derived for the involved multi-dimensional integrals; thus, the computational cost is kept at a minimum level. Numerical examples include the hardening Duffing and the bilinear hysteretic oscillators. Further, pertinent Monte Carlo simulations are included to demonstrate the reliability of the developed technique. Different from [64] where the analytical WPI is applied focussing on the response amplitude envelope, the proposed method in this chapter concentrates on determining the response displacement and velocity, and the reliability based on the displacement.

4.2 Mathematical Formulation

4.2.1 Stochastic averaging treatment

The basic elements of an approximate analytical technique developed in [63] are reviewed in this section for completeness. Consider a nonlinear single-degree-of-freedom (SDOF) oscillator whose motion is governed by the stochastic differential equation (SDE)

$$\ddot{x}_n(t) + \beta \dot{x}_n(t) + z(t, x_n, \dot{x}_n) = w(t) \tag{4.1}$$

where a dot over a variable denotes differentiation with respect to time t; x_n , $\dot{x}_n$, and $\ddot{x}_n$ denote the response displacement, velocity and acceleration, respectively; $z(t, x_n, \dot{x}_n)$ is the restoring force which can be either hysteretic or depend only on the instantaneous values of x_n and $\dot{x}_n$; β is a linear damping coefficient so that $\beta = 2\zeta_0\omega_0$; ζ_0 is the ratio of critical damping; ω_0 is the natural

frequency corresponding to the linear oscillator (i.e. $z(t, x_n, \dot{x}_n) = \omega_0^2 x_n$); and $w(t)$ represents a Gaussian zero-mean white noise process with a power spectrum value equal to S_0 .

Focusing next on lightly damped systems (i.e. $\zeta_0 \ll 1$), it can be argued (e.g. [119]) that the response x of the oscillator of Eq.(4.1) exhibits a pseudo-harmonic behavior described by the equations

$$x_n(t) = A(t)\cos[\omega(A)t + \phi(t)] \tag{4.2}$$

and

$$\dot{x}_n(t) = -\omega(A)A(t)\sin[\omega(A)t + \phi(t)] \tag{4.3}$$

In Eqs.(4.2-4.3), ϕ and A represent a slowly varying with time phase and a slowly varying with time response amplitude, respectively. Manipulating Eqs.(4.2-4.3) yields the following expression for the oscillator response amplitude; that is,

$$A(t) = \sqrt{x^2(t) + \frac{\dot{x}^2(t)}{\omega^2(A)}} \tag{4.4}$$

Further, relying primarily on the assumption of light damping a combination of deterministic and stochastic averaging is performed in this section for approximating the second-order SDE Eq.(4.1) by a first-order (Ito) SDE governing the response amplitude process A. A more detailed presentation/discussion of the assumptions involved and the corresponding assumed pseudo-harmonic behavior of the response process can be found in references such as [119], [99], [142]. Applying next a stochastic averaging/linearization procedure [63], [100], a linearized version of Eq.(4.1) becomes

$$\ddot{x}(t) + \beta(A)\dot{x}(t) + \omega^2(A)x(t) = w(t) \tag{4.5}$$

where

$$\beta(A) = \beta + \frac{-\frac{1}{\pi}\int_0^{2\pi} \sin\Psi \cdot z(t, A\cos\Psi, -\omega(A)A\sin\Psi)d\Psi}{A\omega(A)} \tag{4.6}$$

and

$$\omega^2(A) = \frac{\frac{1}{\pi}\int_0^{2\pi} \cos\Psi \cdot z(t, A\cos\Psi, -\omega(A)A\sin\Psi)d\Psi}{A} \tag{4.7}$$

Further, assuming that denotes the non-stationary oscillator response amplitude PDF, equivalent time-varying damping and stiffness elements can be defined by taking expectations on Eqs.(4.6-4.7); that is,

$$\beta_{eq}(t) = \mathrm{E}[\beta(A)] = \int_0^{+\infty} \beta(A)p(A,t)dA \tag{4.8}$$

and

$$\omega_{eq}^2(t) = \mathrm{E}[\omega^2(A)] = \int_0^{+\infty} \omega^2(A)p(A,t)dA \tag{4.9}$$

respectively. Note that due to the definition of the equivalent linear elements of Eqs.(4.8-4.9), it

can be argued that they inherently are slowly varying functions with respect to time. Considering next Eqs.(4.8-4.9), the equivalent linear system of Eq.(4.5) can be cast in the form

$$\ddot{x}(t) + \beta_{eq}(t)\dot{x}(t) + \omega_{eq}^2(t)x(t) = w(t) \tag{4.10}$$

It can be readily seen that the linear time-variant oscillator of Eq.(4.10) is an alternative to Eq.(4.5) linearized version of Eq.(4.1). Further, based on a stochastic averaging approach Eq.(4.10) can be cast in a first-order Ito SDE governing the evolution in time of the amplitude ; see [118], [63], [119], [99] for a more detailed presentation. Related to this SDE is the Fokker-Planck (F-P) partial differential equation

$$\begin{aligned}\frac{\partial}{\partial t}p(A_2,t_2|A_1,t_1) = &-\frac{\partial}{\partial A}[K_1(A,t)p(A_2,t_2|A_1,t_1)] \\ &+\frac{1}{2}\frac{\partial^2}{\partial A^2}[K_2^2(A,t)p(A_2,t_2|A_1,t_1)]\end{aligned} \tag{4.11}$$

where

$$K_1(A,t) = -\frac{1}{2}\beta_{eq}(t)A + \frac{\pi S_0}{2A\omega_{eq}^2(t)} \tag{4.12}$$

and

$$K_2(A,t) = \sqrt{\frac{\pi S_0}{\omega_{eq}^2(t)}} \tag{4.13}$$

Eq.(4.11) governs the transition PDF of the response amplitude . In reference [63] (see also [66]) it has been shown that Eq.(4.11) is satisfied by a solution of the form

$$p(A,t) = \frac{A}{c(t)}\exp\left(-\frac{A^2}{2c(t)}\right) \tag{4.14}$$

for $p(A_2,t_2|A_1=0,t_1=0) = p(A,t)$. In Eq.(4.14), $c(t)$ accounts for the variance of the transient oscillator response process x. Specifically, substituting Eq.(4.14) into the associated F-P Eq.(4.11) and assuming that the oscillator is initially at rest (i.e. $p(A,t=0) = \delta(A)$, where δ is the Dirac delta function), yields

$$\dot{c}(t) = -\beta_{eq}(c(t))c(t) + \frac{\pi S_0}{\omega_{eq}^2(c(t))} \tag{4.15}$$

Note that the representation of Eq.(4.15) is suitable not only for the herein considered white noise excitation process, but also for non-stationary stochastic excitations of arbitrary evolutionary power spectrum forms (e.g. [118], [63]). Eq.(4.15) constitutes a simple first-order ordinary differential equation (ODE) which can be solved efficiently by standard numerical schemes, such as the Runge-Kutta. Once solved, the nonlinear oscillator (Eq.(4.1)) non-stationary response variance is obtained, and the time-varying equivalent linear damping and stiffness elements are determined

via Eqs.(4.8) and (4.9), respectively.

4.2.2 Wiener path integral formulation

According to the WPI technique (e.g. [14]) the joint transition PDF $p(x_m, \dot{x}_m, t_m|x_{m-1}, \dot{x}_{m-1}, t_{m-1})$ of the oscillator response going from a state $(x_{m-1}, \dot{x}_{m-1}, t_{m-1})$ at $t = t_{m-1}$ to a new state $(x_m, \dot{x}_m, t_m)$ at $t = t_m$, with $t_m > t_{m-1}$ can be expressed as a functional integral over the space of all possible paths $c\{x_m, \dot{x}_m, t_m|x_{m-1}, \dot{x}_{m-1}, t_{m-1}\}$ of the form

$$p(x_m, \dot{x}_m, t_m|x_{m-1}, \dot{x}_{m-1}, t_{m-1}) = \int_{\{x_{m-1}, \dot{x}_{m-1}, t_{m-1}\}}^{\{x_m, \dot{x}_m, t_m\}} W[x(t)][dx(t)] \tag{4.16}$$

The WPI of Eq.(4.16) possesses a probability distribution on the path space as its integrand, which is denoted by $W[x(t)]$ and is called probability density functional. Note that the probability density functional for the white noise process $w(t)$ is given by (e.g. [14], [128])

$$W[x(t)] = C\text{exp}\left(-\int_{t_{m-1}}^{t_m} \frac{1}{2}\frac{w^2(t)}{2\pi S_0}dt\right) \tag{4.17}$$

where C is a normalization coefficient. Following next the approach proposed in [67], Eq. (4.10) is substituted into Eq. (4.17) and the probability density functional $W[w(t)]$ for $w(t)$ is interpreted as the probability density functional $W[x(t)]$ for $x(t)$. This yields

$$W[x(t)] = C\text{exp}\left(-\int_{t_{m-1}}^{t_m} \frac{1}{2}\frac{[\ddot{x}(t) + \beta_{eq,m}(t)\dot{x}(t) + \omega_{eq,m}^2(t)x(t)]^2}{2\pi S_0}dt\right) \tag{4.18}$$

In Eq.(4.18) and in the ensuing analysis it is assumed that the time interval $[t_{m-1}, t_m]$ is relatively small, i.e., $t_m - t_{m-1} \to 0$; thus, $\beta_{eq}(t) = \beta_{eq}(t_m) = \beta_{eq,m}$ and $\omega_{eq}^2(t) = \omega_{eq}^2(t_m) = \omega_{eq,m}^2$ for $t \in [t_{m-1}, t_m]$. Further, note that even if the probability density functional is constructed, the analytical solution of the WPI of Eq.(4.16) is a rather challenging task. To address this challenge a variational formulation is invoked in the following for determining the transition PDF $p(x_m, \dot{x}_m, t_m|x_{m-1}, \dot{x}_{m-1}, t_{m-1})$ in an approximate manner; see [14], [64], [67] for a more detailed presentation. In this regard, for the oscillator of Eq.(4.10) and for $t_m - t_{m-1} \to 0$, a Lagrangian function is defined as

$$L(x, \dot{x}, \ddot{x}) = \frac{1}{2}\frac{(\ddot{x} + \beta_{eq,m}\dot{x} + \omega_{eq,m}^2 x)^2}{2\pi S_0} \tag{4.19}$$

Next, focusing on Eq.(4.19), the largest contribution to the WPI comes from the trajectory for which the integral in the exponential becomes as small as possible. Variational calculus rules (e.g.

[38]) dictate that this trajectory with fixed end points is subject to the condition

$$\delta \int_{t_{m-1}}^{t_m} L(x_c, \dot{x}_c, \ddot{x}_c) dt = 0 \tag{4.20}$$

where x_c is the most probable path, namely the most probable trajectory connecting points $(x_{m-1}, \dot{x}_{m-1}, t_{m-1})$ and $(x_m, \dot{x}_m, t_m)$. Eq.(4.20) yields a corresponding Euler-Lagrange equation of the form

$$\frac{\partial L}{\partial x_c} - \frac{\partial}{\partial t}\frac{\partial L}{\partial \dot{x}_c} + \frac{\partial^2}{\partial t^2}\frac{\partial L}{\partial \ddot{x}_c} = 0 \tag{4.21}$$

in conjunction with the boundary conditions

$$\begin{aligned} &x_c(t_{m-1}) = x_{m-1}, \quad \dot{x}_c(t_{m-1}) = \dot{x}_{m-1}, \\ &x_c(t_m) = x_m, \qquad \dot{x}_c(t_m) = \dot{x}_m \end{aligned} \tag{4.22}$$

Solving the boundary value problem of Eq.(4.21) together with Eq.(4.22) yields a closed form expression for the transition PDF $p(x_m, \dot{x}_m, t_m | x_{m-1}, \dot{x}_{m-1}, t_{m-1})$; that is,

$$p(x_m, \dot{x}_m, t_m | x_{m-1}, \dot{x}_{m-1}, t_{m-1}) = G_{con} exp\left(- \int_{t_{m-1}}^{t_m} L(x_c, \dot{x}_c, \ddot{x}_c) dt \right) \tag{4.23}$$

where G_{con} is a normalization coefficient. Clearly, the primary approximation of the technique relates to the fact that only the most probable path x_c is considered in the evaluation of the functional integral of Eq.(4.16) instead of all the possible paths $\{x_m, \dot{x}_m, t_m | x_{m-1}, \dot{x}_{m-1}, t_{m-1}\}$. It can be argued that the concept of the most probable path can be viewed as something equivalent to the fact that the most probable value of a random variable is the one corresponding to the maximum value of the PDF. Substituting next Eq.(4.19) into (4.21) yields

$$\frac{d^4 x_c}{dt^4} + 2(1 - 2\zeta_{eq,m}^2)\omega_{eq,m}^2 \frac{d^2 x_c}{dt^2} + \omega_{eq,m}^4 x_c = 0 \tag{4.24}$$

where $\beta_{eq,m} = 2\zeta_{eq,m}\omega_{eq,m}$. Eq.(4.24) is a fourth-order linear ODE which can be readily solved analytically to obtain

$$x_c(t) = G_1 exp(\lambda_{c,1} t) + G_2 exp(\lambda_{c,2} t) + G_3 exp(\lambda_{c,3} t) + G_4 exp(\lambda_{c,4} t) \tag{4.25}$$

where

$$\begin{aligned}
\lambda_{c,1} &= (\zeta_{eq,m} + i\sqrt{1-\zeta_{eq,m}^2})\omega_{eq,m} \\
\lambda_{c,2} &= (\zeta_{eq,m} - i\sqrt{1-\zeta_{eq,m}^2})\omega_{eq,m} \\
\lambda_{c,3} &= (-\zeta_{eq,m} + i\sqrt{1-\zeta_{eq,m}^2})\omega_{eq,m} \\
\lambda_{c,4} &= (-\zeta_{eq,m} - i\sqrt{1-\zeta_{eq,m}^2})\omega_{eq,m}
\end{aligned} \tag{4.26}$$

and G_1, G_2, G_3, G_4 are complex constants to be determined by utilizing the boundary conditions of Eq.(4.22). For simplification, Eq.(4.25) is recast into a real form as

$$\begin{aligned}
x_c(t) =& C_1 exp(\zeta_{eq,m}\omega_{eq,m}t)cos(\omega_{eq,m}t) + C_2 exp(\zeta_{eq,m}\omega_{eq,m}t)sin(\omega_{eq,m}t) \\
&+ C_3 exp(-\zeta_{eq,m}\omega_{eq,m}t)cos(\omega_{eq,m}t) + C_4 exp(-\zeta_{eq,m}\omega_{eq,m}t)sin(\omega_{eq,m}t)
\end{aligned} \tag{4.27}$$

where C_1, C_2, C_3, C_4 are real constants. In this regard, analytical expressions for C_1, C_2, C_3, C_4 have been obtained by utilizing the symbolic toolbox of $MATLAB$; these are provided in the Appendix B. Further, Eqs.(4.25-4.26) are substituted into Eq.(4.23). Next, relying on the assumption that $t_m - t_{m-1} \to 0$, a Taylor series expansion is employed for the most probable path (Eq.(4.25)) around point $t = t_m$ yielding a closed-form expression for the transition PDF of the form

$$\begin{aligned}
p(x_m, \dot{x}_m, t_m | x_{m-1}, \dot{x}_{m-1}, t_{m-1}) =& \frac{n_{4,m} n_{7,m}}{\pi} \\
&\cdot exp\{-[(n_{1,m}x_{m-1} + n_{2,m}\dot{x}_{m-1} + n_{3,m}x_m + n_{4,m}\dot{x}_m)^2 \\
&+ (n_{5,m}x_{m-1} + n_{6,m}\dot{x}_{m-1} + n_{7,m}x_m)^2]\}
\end{aligned} \tag{4.28}$$

where the analytical expressions of the constants $n_{1,m}$, $n_{2,m}$, $n_{3,m}$, $n_{4,m}$, $n_{5,m}$, $n_{6,m}$, $n_{7,m}$ are provided in the Appendix B. Equivalently, using a vectorial notation Eq.(4.28) can be cast into the Gaussian PDF form

$$\begin{aligned}
&p(x_m, \dot{x}_m, t_m | x_{m-1}, \dot{x}_{m-1}, t_{m-1}) = \\
&\qquad (2\pi)^{-1} |\boldsymbol{\Sigma}_t|^{-\frac{1}{2}} \exp\left[-\frac{1}{2}(\mathbf{X}_t - \boldsymbol{\mu}_t)^T \boldsymbol{\Sigma}_t^{-1} (\mathbf{X}_t - \boldsymbol{\mu}_t)\right]
\end{aligned} \tag{4.29}$$

where

$$\begin{aligned}
\mathbf{X}_t &= (x_m, \dot{x}_m)^T, \boldsymbol{\mu}_t = (\mu_{x,t}, \mu_{\dot{x},t})^T \\
\boldsymbol{\Sigma}_t &= \begin{pmatrix} \sigma_{x,t}^2 & \rho_t \sigma_{x,t}\sigma_{\dot{x},t} \\ \rho_t \sigma_{x,t}\sigma_{\dot{x},t} & \sigma_{\dot{x},t}^2 \end{pmatrix}
\end{aligned} \tag{4.30}$$

$$\mu_{x,t} = -\left(\frac{n_{5,m}}{n_{7,m}} x_{m-1} + \frac{n_{6,m}}{n_{7,m}} \dot{x}_{m-1}\right) \tag{4.31}$$

$$\mu_{\dot{x},t} = \left(\frac{n_{3,m}n_{5,m}}{n_{4,m}n_{7,m}} - \frac{n_{1,m}}{n_{4,m}}\right) x_{m-1} + \left(\frac{n_{3,m}n_{6,m}}{n_{4,m}n_{7,m}} - \frac{n_{2,m}}{n_{4,m}}\right) \dot{x}_{m-1} \tag{4.32}$$

$$\sigma_{x,t} = \frac{1}{\sqrt{2} n_{7,m}} \tag{4.33}$$

$$\sigma_{\dot{x},t} = \frac{\sqrt{n_{3,m}^2 + n_{7,m}^2}}{\sqrt{2} n_{7,m} n_{4,m}} \tag{4.34}$$

and

$$\rho_m = -\frac{n_{3,m}}{\sqrt{n_{3,m}^2 + n_{7,m}^2}} \tag{4.35}$$

Obviously, the joint transition PDF of Eq.(4.28) is Gaussian as anticipated given that the system of Eq.(4.10) is linear. Further, note that in comparison with alternative approximate expressions of the transition PDF based on a stochastic averaging treatment [112], the herein determined transition PDF of Eq.(4.29) based on the WPI technique takes into account the correlation of the processes via the correlation coefficient . This is important for the accuracy of the response analysis especially during the transient phase where the oscillator response displacement and velocity are correlated (e.g. [100]). Further, invoking the Markov property of the response process , the C-K equation

$$\begin{aligned} p(x_{m+1}, \dot{x}_{m+1}, t_{m+1} | x_{m-1}, \dot{x}_{m-1}, t_{m-1}) = \\ \int_{-\infty}^{+\infty} \int_{-\infty}^{+\infty} p(x_{m+1}, \dot{x}_{m+1}, t_{m+1} | x_m, \dot{x}_m, t_m) \\ p(x_m, \dot{x}_m, t_m | x_{m-1}, \dot{x}_{m-1}, t_{m-1}) dx_m d\dot{x}_m \end{aligned} \tag{4.36}$$

holds true. Note that the Gaussian form for the short-time transition PDF is in agreement with the concept of time-local Gaussian processes introduced by Dekker [32]. In this regard, it was shown that even for a nonlinear system, subject to the condition $t_m - t_{m-1} \to 0$, a Gaussian form for the transition PDF together with the Chapman-Kolmogorov Eq.(4.36) can lead, in an exact manner, to the corresponding F-P equation. In fact, the discretized version of the C-K equation in conjunction with a Gaussian form of the transition PDF has been the core of several numerical path integral solution schemes that have been developed recently (e.g. [77], [35], [89], [66], [68], [56]). These schemes have proven to be highly accurate. Nevertheless, they appear to be computationally demanding, mainly due to the fact that high-dimensional numerical integration needs to be performed for every time step.

To circumvent this challenge, for the quite general system considered herein, i.e. the nonlinear oscillator of Eq.(4.1), the aforementioned numerical integration is circumvented by analytically

evaluating the involved integrals; thus, the joint transition and non-stationary response PDF of the oscillator can be obtained at minimum computational cost. Specifically, starting from an initial state $(x_0, \dot{x}_0, t_0)$ with short-time transition PDFs $p(x_1, \dot{x}_1, t_1|x_0, \dot{x}_0, t_0)$ and $p(x_2, \dot{x}_2, t_2$ $|x_1, \dot{x}_1, t_1)$ of the form of Eq.(4.28) (or, alternatively, Eq.(4.29)) and utilizing the C-K Eq.(4.36), analytical evaluation of the involved convolution integral yields the transition PDF $p(x_2, \dot{x}_2, t_2|x_0, \dot{x}_0, t_0)$ of the form

$$\begin{aligned} p(x_2, \dot{x}_2, t_2|x_0, \dot{x}_0, t_0) =& \frac{k_{4,2}k_{7,2}}{\pi}\text{exp}\{-[(k_{1,2}x_0 + k_{2,2}\dot{x}_0 + k_{3,2}x_2 + k_{4,2}\dot{x}_2)^2 \\ &+ (k_{5,2}x_0 + k_{6,2}\dot{x}_0 + k_{7,2}x_2)^2]\} \end{aligned} \tag{4.37}$$

The analytical expressions of the constants $k_{1,m}$, $k_{2,m}$, $k_{3,m}$, $k_{4,m}$, $k_{5,m}$, $k_{6,m}$, $k_{7,m}$ can be found in the Appendix B. Obviously, in this manner the non-stationary joint response PDF of the original nonlinear oscillator can be advanced in short time steps at essentially zero computational cost. Specifically, for a given time instant $t = t_{m-1}$, the transition PDF $p(x_{m-1}, \dot{x}_{m-1}, t_{m-1}|x_0, \dot{x}_0, t_0)$ has an expression similar to Eq.(4.37); that is,

$$\begin{aligned} p(x_{m-1}, \dot{x}_{m-1}, t_{m-1}|x_0, \dot{x}_0, t_0) =& \frac{k_{4,m-1}k_{7,m-1}}{\pi}\text{exp}\{-[(k_{1,m-1}x_0 + k_{2,m-1}\dot{x}_0 \\ &+ k_{3,m-1}x_{m-1} + k_{4,m-1}\dot{x}_{m-1})^2 + (k_{5,m-1}x_0 + k_{6,m-1}\dot{x}_0 + k_{7,m-1}x_{m-1})^2]\} \end{aligned} \tag{4.38}$$

Utilizing the short-time transition PDF form of Eq.(4.28), the C-K equation

$$\begin{aligned} p(x_m, \dot{x}_m, t_m|x_0, \dot{x}_0, t_0) =& \\ &\int_{-\infty}^{+\infty}\int_{-\infty}^{+\infty} p(x_m, \dot{x}_m, t_m|x_{m-1}, \dot{x}_{m-1}, t_{m-1}) \\ &p(x_{m-1}, \dot{x}_{m-1}, t_{m-1}|x_0, \dot{x}_0, t_0)dx_{m-1}d\dot{x}_{m-1} \end{aligned} \tag{4.39}$$

can be used to determine the transition PDF at time $t = t_m$; that is, analytical evaluation of the integral of Eq.(4.39) yields

$$\begin{aligned} p(x_m, \dot{x}_m, t_m|x_0, \dot{x}_0, t_0) =& \frac{k_{4,m}k_{7,m}}{\pi}\text{exp}\{-[(k_{1,m}x_0 + k_{2,m}\dot{x}_0 + k_{3,m}x_m \\ &+ k_{4,m}\dot{x}_m)^2 + (k_{5,m}x_0 + k_{6,m}\dot{x}_0 + k_{7,m}x_m)^2]\} \end{aligned} \tag{4.40}$$

Equivalently, using a vectorial notation Eq.(4.40) can be cast into the Gaussian PDF form

$$p(x_m, \dot{x}_m, t_m | x_0, \dot{x}_0, t_0) = \\ (2\pi)^{-1} |\mathbf{\Sigma}_m|^{-\frac{1}{2}} \exp\left[-\frac{1}{2}(\mathbf{X}_m - \boldsymbol{\mu}_m)^T \mathbf{\Sigma}_m^{-1} (\mathbf{X}_m - \boldsymbol{\mu}_m)\right] \tag{4.41}$$

where

$$\mathbf{X}_m = (x_m, \dot{x}_m)^T, \boldsymbol{\mu}_m = (\mu_{x,m}, \mu_{\dot{x},m})^T$$
$$\mathbf{\Sigma}_m = \begin{pmatrix} \sigma_{x,m}^2 & \rho_m \sigma_{x,m} \sigma_{\dot{x},m} \\ \rho_m \sigma_{x,m} \sigma_{\dot{x},m} & \sigma_{\dot{x},m}^2 \end{pmatrix} \tag{4.42}$$

$$\mu_{x,m} = -\left(\frac{k_{5,m}}{k_{7,m}} x_0 + \frac{k_{6,m}}{k_{7,m}} \dot{x}_0\right) \tag{4.43}$$

$$\mu_{\dot{x},m} = \left(\frac{k_{3,m} k_{5,m}}{k_{4,m} k_{7,m}} - \frac{k_{1,m}}{k_{4,m}}\right) x_0 + \left(\frac{k_{3,m} k_{6,m}}{k_{4,m} k_{7,m}} - \frac{k_{2,m}}{k_{4,m}}\right) \dot{x}_0 \tag{4.44}$$

$$\sigma_{x,m} = \frac{1}{\sqrt{2} k_{7,m}} \tag{4.45}$$

$$\sigma_{\dot{x},m} = \frac{\sqrt{k_{3,m}^2 + k_{7,m}^2}}{\sqrt{2} k_{7,m} k_{4,m}} \tag{4.46}$$

and

$$\rho_m = -\frac{k_{3,m}}{\sqrt{k_{3,m}^2 + k_{7,m}^2}} \tag{4.47}$$

Considering the case $x_0 = \dot{x}_0 = 0$ and integrating with respect to $\dot{x}_m$ yields the oscillator transient response displacement PDF $p(x_m, t_m)$ of the form

$$p(x_m, t_m) = \frac{1}{\sqrt{2\pi} \sigma_{x,m}} \exp\left(-\frac{x_m^2}{2\sigma_{x,m}^2}\right) \tag{4.48}$$

4.2.3 Nonlinear oscillator survival probability determination

The WPI technique developed in section 4.2.2, besides determining the nonlinear oscillator transition and non-stationary response PDFs efficiently, can be used for determining the oscillator reliability/first-passage statistics as well without additional significant computational effort. In this regard, an approximate analytical technique is developed in this section for determining the survival probability $P_B(t)$ of the nonlinear oscillator of Eq.(4.1). This is defined as the probability that the system response displacement x stays within the bounded interval $[-B, B]$ over the time

interval $[t_0, T]$; that is,

$$P_B(T) = \text{Prob}\{-B < x(t) < B; t_0 < t < T | x(t_0) = x_0, \dot{x}(t_0) = \dot{x}_0\} \tag{4.49}$$

In general, it is rather challenging to calculate the survival probability exactly as it has been defined in Eq.(4.49) with its state in continuous time; see also [118], [99]. Thus, in the following the survival probability is calculated numerically by adopting the discretization in time introduced in section 4.2.2. In this regard, Eq.(4.49) becomes

$$P_B(T = t_m) = \text{Prob}\{-B < x(t_m) < B; m = 1, ..., M | x(t_0) = x_0, \dot{x}(t_0) = \dot{x}_0\} \tag{4.50}$$

where $t_m = t_0 + m\triangle t, m = 1, ..., M$ and $\triangle t = (T - t_0)/M$. Note that Eq.(4.50) can approximate the survival probability as closely as desired by appropriately choosing $\triangle t$. Further, it can be readily shown that the corresponding first-passage PDF $p_B(T)$ can be determined as

$$p_B(T) = -\frac{dP_B(T)}{dT} \tag{4.51}$$

Taking into account the discretization of Eq.(4.50), the survival probability $P_B(T)$ is obviously given by the equation

$$P_B(T = t_m) = \prod_{m=1}^{M} F_m \tag{4.52}$$

where F_m denotes the probability that $x(t)$ stays within the range $[-B, B]$ in the time interval $[t_{m-1}, t_m]$, given that no crossings have occurred prior to time t_{m-1} . Next, invoking the Markov property for the process $x(t)$ and utilizing the standard definition of conditional probability yields

$$F_m = \frac{\text{Prob}[|x(t_m)| < B \cap |x(t_{m-1})| < B]}{\text{Prob}[|x(t_{m-1})| < B]} = \frac{Q_{m-1,m}}{H_{m-1}} \tag{4.53}$$

where

$$H_{m-1} = \int_{-B}^{B} p(x_{m-1}, t_{m-1}) dx_{m-1} \tag{4.54}$$

and

$$Q_{m-1,m} = \int_{-B}^{B} \int_{-B}^{B} p(x_{m-1}, t_{m-1}; x_m, t_m) dx_{m-1} dx_m \tag{4.55}$$

Note that the probabilities H_{m-1} and $Q_{m-1,m}$ can be readily determined via the technique developed in section 4.2.2. Specifically, H_{m-1} can be evaluated by utilizing Eq.(4.54). Further, taking into account the Markov property for the response process, the joint response PDF $p(x_{m-1}, \dot{x}_{m-1}, t_{m-1};$

$x_m, \dot{x}_m, t_m)$ is expressed as

$$p(x_{m-1}, \dot{x}_{m-1}, t_{m-1}; x_m, \dot{x}_m, t_m) = \\ p(x_{m-1}, \dot{x}_{m-1}, t_{m-1}) p(x_m, \dot{x}_m, t_m | x_{m-1}, \dot{x}_{m-1}, t_{m-1}) \tag{4.56}$$

Considering Eq.(4.56) $Q_{m-1,m}$ becomes

$$Q_{m-1,m} = \int_{-\infty}^{+\infty} \int_{-B}^{B} \int_{-\infty}^{+\infty} \int_{-B}^{B} p(x_{m-1}, \dot{x}_{m-1}, t_{m-1}) \\ p(x_m, \dot{x}_m, t_m | x_{m-1}, \dot{x}_{m-1}, t_{m-1}) dx_{m-1} d\dot{x}_{m-1} dx_m d\dot{x}_m \tag{4.57}$$

where $p(x_{m-1}, \dot{x}_{m-1}, t_{m-1})$ is given by Eq.(4.40) and $p(x_m, \dot{x}_m, t_m | x_{m-1}, \dot{x}_{m-1}, t_{m-1})$ is given by Eq.(4.28).

4.2.4 Mechanization of the WPI based technique

The mechanization of the developed technique involves the following steps:

a) Numerical solution (e.g. standard Runge-Kutta integration scheme) of the first-order ODE (Eq.(4.15)) to determine the system response variance $c(t)$.

b) Determination of the equivalent linear time-dependent damping $\beta_{eq}(t)$ and stiffness $\omega_{eq}(t)$ elements via Eqs.(4.8) and (4.9), respectively.

c) Determination of the oscillator short-time joint transition PDF in the form of Eq.(4.28) by utilizing the analytical expressions of the constants $n_{1,m}$, $n_{2,m}$, $n_{3,m}$, $n_{4,m}$, $n_{5,m}$, $n_{6,m}$, $n_{7,m}$ (see Appendix B).

d) Determination of the oscillator non-stationary joint response PDF in the form of Eq.(4.40) in short time steps by utilizing the analytical expressions of the constants $k_{1,m}$, $k_{2,m}$, $k_{3,m}$, $k_{4,m}$, $k_{5,m}$, $k_{6,m}$, $k_{7,m}$ (see Appendix B).

Note that steps a) to d) constitute an efficient scheme for determining approximately the non-linear oscillator joint transition PDF and the oscillator non-stationary joint response PDF. Further, these steps can be used as a basis for determining the nonlinear oscillator reliability statistics; that is,

e) Determination of parameters H_{m-1} and $Q_{m-1,m}$ via Eqs.(4.54) and (4.57), respectively.

f) Determination of the survival probability $P_B(T)$ via Eq.(4.52) and of the corresponding first-passage PDF $p_B(T)$ via Eq.(4.51).

In comparison with alternative, albeit more versatile, numerical path integral schemes for determining first-passage PDFs (e.g. [56]), the herein developed technique appears significantly more efficient computationally. This is due to the fact that the computationally demanding task of numerically integrating for every time step the high-dimensional convolution integrals involved in the C-K equation has been circumvented. In this regard, the computational cost is kept at a minimum level since it is restricted, in essence, to the numerical integration of Eq.(4.15) via standard schemes (e.g. Runge-Kutta), and to the numerical integration involved in Eqs.(4.54) and (4.57).

4.3 Numerical Examples

The Duffing hardening and the bilinear hysteretic oscillators are considered in this section to demonstrate the reliability of the technique. For this purpose, the non-stationary response PDFs, the survival probabilities and the first-passage PDFs obtained via the developed approximate analytical WPI technique are compared with response PDF, survival probability, and first-passage PDF estimates obtained via pertinent Monte Carlo simulations (10000 realizations). A standard fourth-order Runge-Kutta numerical integration scheme is employed for solving the nonlinear oscillator differential equation of motion (Eq.(4.1)), whereas the barrier level B is expressed as a fraction λ_f of the corresponding linear oscillator stationary response standard deviation, i.e., $B = \lambda_f \sigma$ where $\sigma^2 = \dfrac{\pi S_0}{2\zeta_0 \omega_0^3}$ (e.g. [100]). Further, the value $\triangle t = t_m - t_{m-1} = 0.1s$ is chosen for the time discretization of the WPI technique, whereas the initial distributions chosen for the response displacement and velocity PDFs are the Dirac delta function, i.e. $p(x(t_0, t_0 = 0)) = \delta(x_0)$, and $p(\dot{x}(t_0, t_0 = 0)) = \delta(\dot{x}_0)$, assuming the system is initially at rest. In the ensuing analysis a 7^{th} order Taylor series expansion is chosen for determining the coefficients $n_{1,m}$, $n_{2,m}$, $n_{3,m}$, $n_{4,m}$, $n_{5,m}$, $n_{6,m}$, $n_{7,m}$ in Eq.(4.28).

4.3.1 Duffing nonlinear (hardening) oscillator

A Duffing oscillator is considered, which has been used in some engineering areas, such as energy harvester [46]. Thus, its equation of motion is described by

$$\ddot{x}(t) + \beta_0 \dot{x}(t) + \omega_0^2 x(t) + \varepsilon \omega_0^2 x^3(t) = w(t) \tag{4.58}$$

where the parameter $\varepsilon > 0$ represents the magnitude of the nonlinearity. Further, the nonlinear restoring function $z(t, x, \dot{x})$ of Eq.(4.1) becomes

$$z(t, x, \dot{x}) = \omega_0^2 x(t) + \varepsilon \omega_0^2 x^3(t) \tag{4.59}$$

Substituting Eq.(4.59) into Eqs.(4.6) and (4.7), yields

$$\beta(A) = \beta_0 \tag{4.60}$$

and

$$\omega^2(A) = \omega_0^2 \left(1 + \frac{3}{4}\varepsilon A^2\right) \tag{4.61}$$

Next, substituting Eqs.(4.60) and (4.61) into Eqs.(4.8) and (4.9), and considering Eq.(4.14) yields

$$\beta_{eq}(c(t)) = \beta_0 \tag{4.62}$$

and

$$\omega_{eq}^2(c(t)) = \omega_0^2 \left(1 + \frac{3}{2}\varepsilon c(t)\right) \tag{4.63}$$

For comparison, the classical statistical linearization method [100] can also be used to obtain the equivalent stiffness for duffiing oscillator as following

$$\omega_{eq}^2(c(t)) = \omega_0^2 \left(1 + 3\varepsilon c(t)\right) \tag{4.64}$$

In Fig.(4.1) the non-stationary response variance $c(t)$ determined by solving Eq.(4.15) is plotted for a Duffing oscillator with parameters values $S_0 = 0.0637$, $\omega_0^2 = 1$, $\beta_0 = 0.2$, $\varepsilon = 0.2$ (Case 1), and $S_0 = 0.0637$, $\omega_0^2 = 1$, $\beta_0 = 0.2$, $\varepsilon = 1$ (Case 2). It can be readily seen that the degree of nonlinearity is significant, especially for Case 2 where the stationary response variance ($\lim_{t \to +\infty} c(t)$) is approximately half of that of a corresponding linear oscillator (i.e. $(\lim_{t \to +\infty} c(t)) = \sigma^2 = 1$). From Fig.(4.1), both the path integral method and statistical linearization approach approximately match the Monte Carlo simulation at an acceptable degree. The differences occur due to fact that both the path integral method and statistical linearization approach are the approximations of real response. The main difference between the WPI method and MC is due to the linearization approximation of no-linearity. In Fig.(4.2) the time-varying equivalent linear natural frequency $\omega_{eq}(t)$ determined via Eq.(4.9) is plotted for Case 1 and Case 2.

Further, in Figs.(4.3) and (4.4) the non-stationary response displacement PDF is plotted for various time instants for Case 1 and Case 2, respectively. It is seen that the approximate WPI tech-

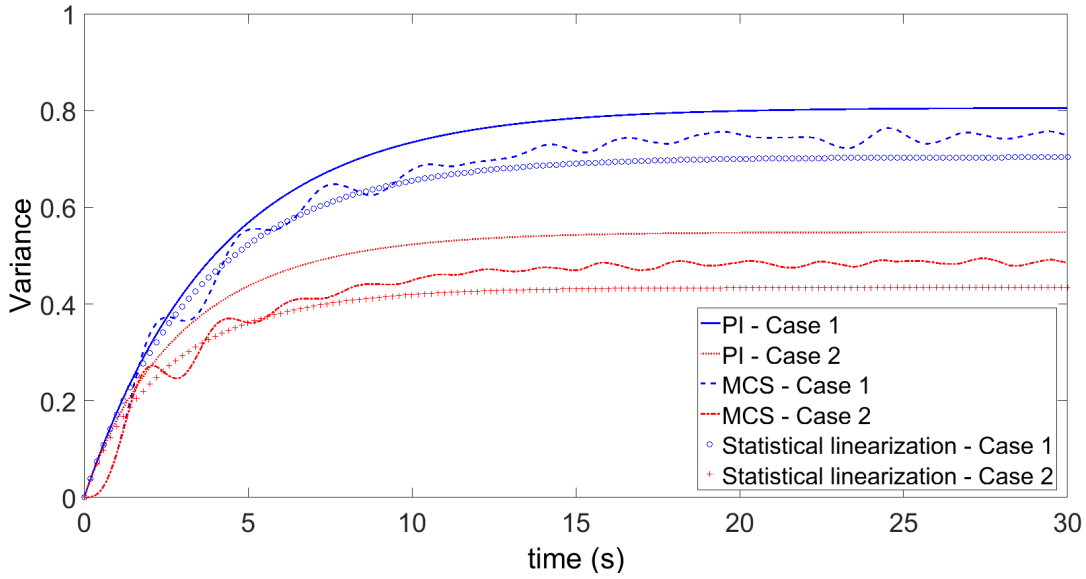

Figure 4.1: Transient response variance $c(t)$ of a Duffing oscillator under white noise excitation with parameters values $S_0 = 0.0637$, $\omega_0^2 = 1$, $\beta_0 = 0.2$, $\varepsilon = 0.2$ (Case 1), and $S_0 = 0.0637$, $\omega_0^2 = 1$, $\beta_0 = 0.2$, $\varepsilon = 1$ (Case 2); comparison with pertinent Monte Carlo simulations (10000 realizations).

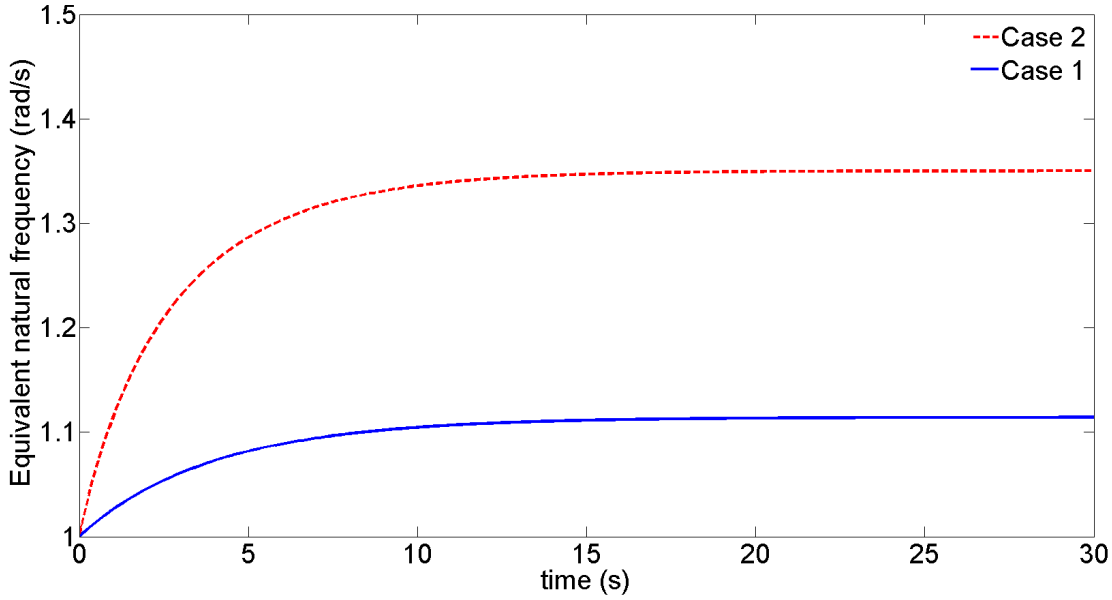

Figure 4.2: Time-varying equivalent linear natural frequency $\omega_{eq}(t)$ for a Duffing oscillator under white noise excitation with parameters values $S_0 = 0.0637$, $\omega_0^2 = 1$, $\beta_0 = 0.2$, $\varepsilon = 0.2$ (Case 1), and $S_0 = 0.0637$, $\omega_0^2 = 1$, $\beta_0 = 0.2$, $\varepsilon = 1$ (Case 2).

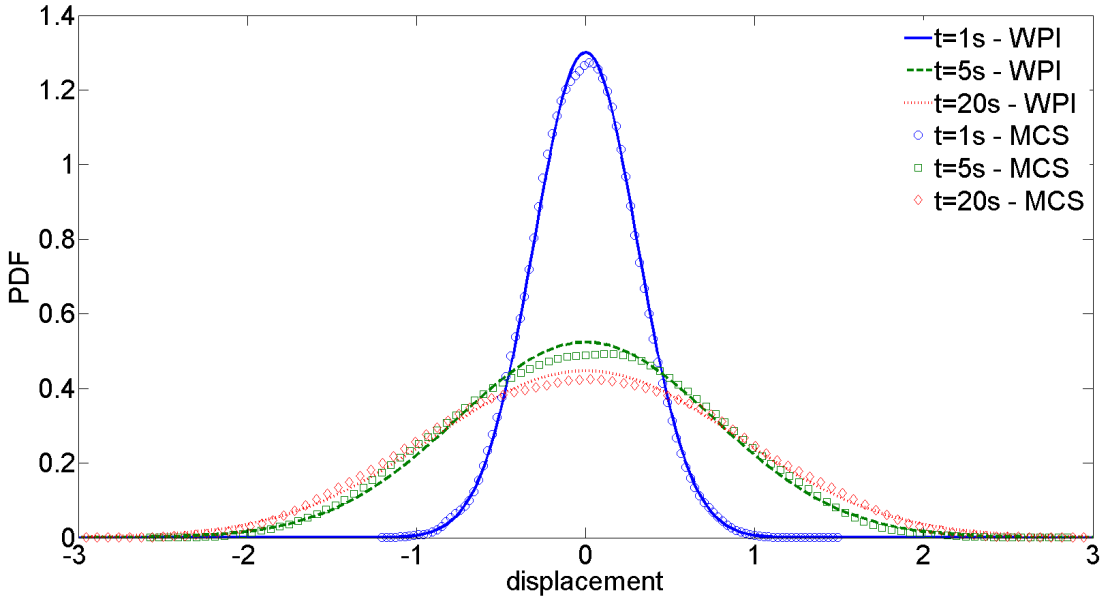

Figure 4.3: Response displacement PDF for a Duffing oscillator under white noise excitation with parameters values $S_0 = 0.0637$, $\omega_0^2 = 1$, $\beta_0 = 0.2$, $\varepsilon = 0.2$ (Case 1) for various time instants; comparison with pertinent Monte Carlo simulations (10000 realizations).

nique exhibits acceptable satisfactory accuracy when compared with MCS based estimates, even for the a higher nonlinearity case (Case 2). The difference between WPI and MC comes from the fact that in WPI, the Gaussian distribution assumption is made. Finally, in Figs.(4.5) and (4.6), the survival probability and the corresponding first-passage PDF for Case 1 for various barrier levels are plotted, respectively. Similarly, in Figs.(4.7) and (4.8), the survival probability and corresponding first-passage PDF for Case 2 for various barrier levels are plotted, respectively. Comparisons with pertinent MCS (10000 realizations) are included as well demonstrating a satisfactory agreement. It is noted that the irregular/non-smooth shape of the WPI based first-passage PDFs is due to the differentiation of the survival probability (Eq.(4.51)). In this regard, the survival probability Eq.(4.52) is assumed to have constant values over the time intervals resulting in a non-smooth representation. Obviously, the level of non-smoothness increases when differentiation takes place. In addition, it can be expected that WPI matches MC result better, when the nonlinearity decreases.

4.3.2 Bilinear hysteretic oscillator

A bilinear hysteretic oscillator is considered next, which has been widely studied in conjunction with earthquake engineering applications (eg. [18], [116], [57], [13]). In this regard, its equation

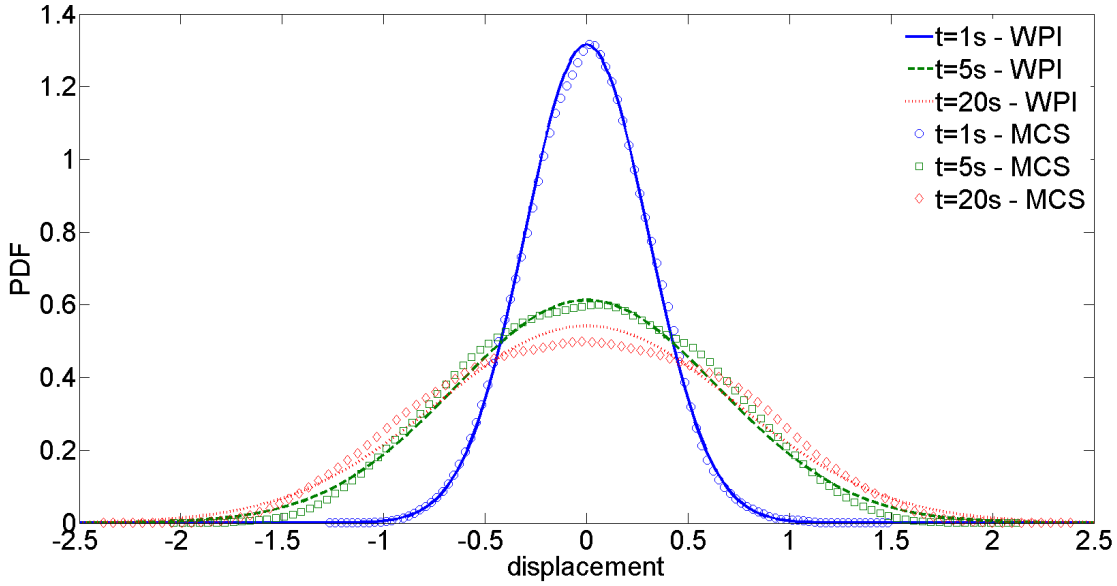

Figure 4.4: Response displacement PDF for a Duffing oscillator under white noise excitation with parameters values $S_0 = 0.0637$, $\omega_0^2 = 1$, $\beta_0 = 0.2$, $\varepsilon = 1$ (Case 2) for various time instants; comparison with pertinent Monte Carlo simulations (10000 realizations).

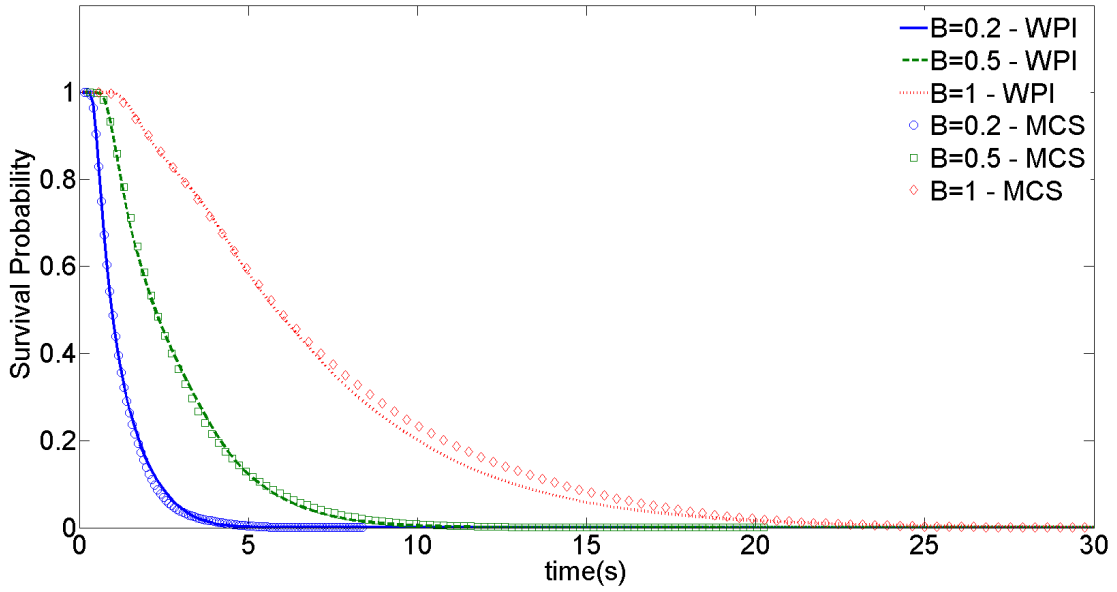

Figure 4.5: Survival probability for a Duffing oscillator under white noise excitation with parameters values $S_0 = 0.0637$, $\omega_0^2 = 1$, $\beta_0 = 0.2$, $\varepsilon = 0.2$ (Case 1) for various barrier levels; comparison with pertinent Monte Carlo simulations (10000 realizations).

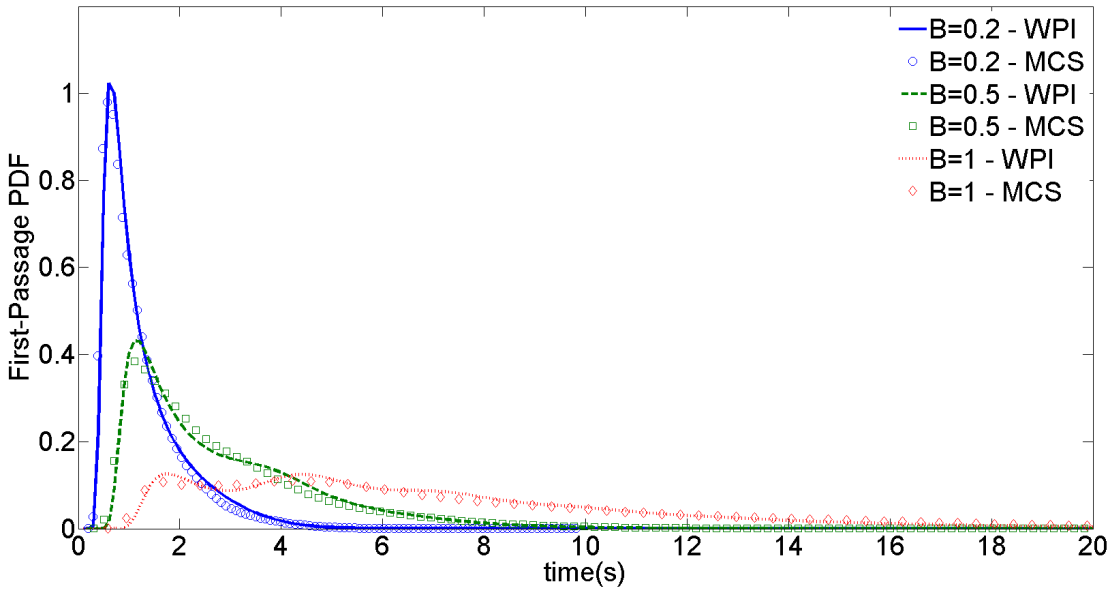

Figure 4.6: First passage PDF for a Duffing oscillator under white noise excitation with parameters values $S_0 = 0.0637$, $\omega_0^2 = 1$, $\beta_0 = 0.2$, $\varepsilon = 0.2$ (Case 1) for various barrier levels; comparison with pertinent Monte Carlo simulations (10000 realizations).

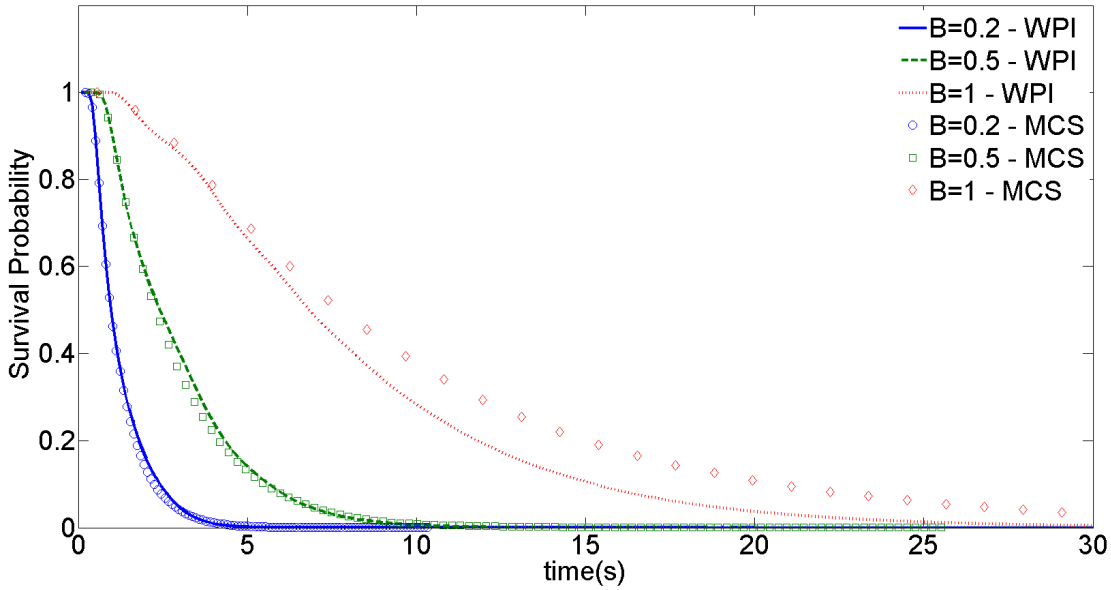

Figure 4.7: Survival probability for a Duffing oscillator under white noise excitation with parameters values $S_0 = 0.0637$, $\omega_0^2 = 1$, $\beta_0 = 0.2$, $\varepsilon = 1$ (Case 2) for various barrier levels; comparison with pertinent Monte Carlo simulations (10000 realizations).

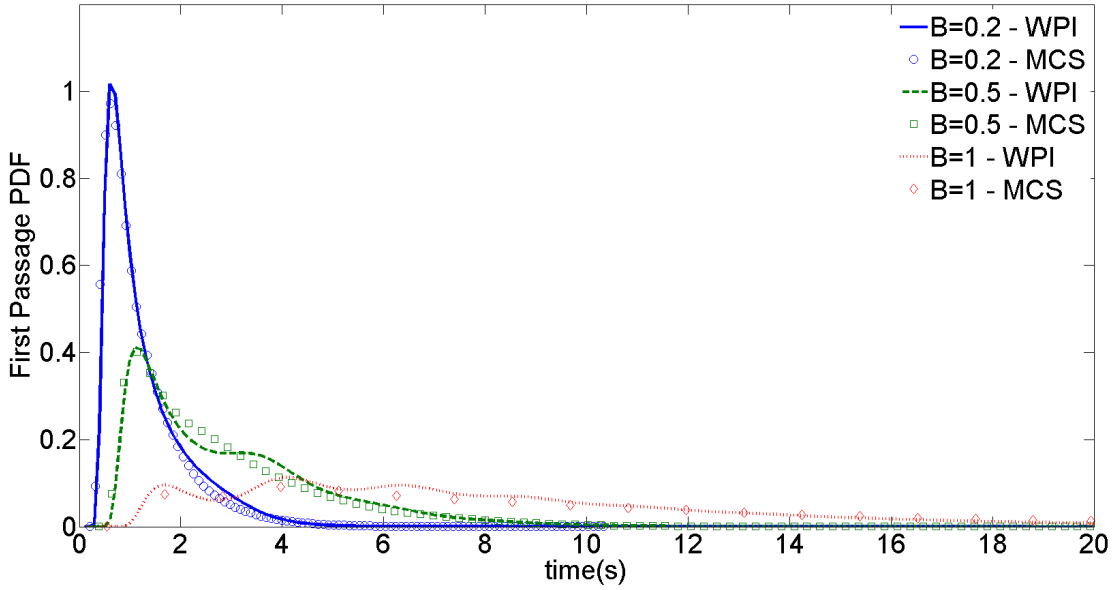

Figure 4.8: First passage PDF for a Duffing oscillator under white noise excitation with parameters values $S_0 = 0.0637$, $\omega_0^2 = 1$, $\beta_0 = 0.2$, $\varepsilon = 1$ (Case 2) for various barrier levels; comparison with pertinent Monte Carlo simulations (10000 realizations).

of motion takes the form

$$\ddot{x}(t) + \beta_0 \dot{x}(t) + a\omega_0^2 x(t) + (1-a)\omega_0^2 x_y u(t) = w(t) \tag{4.65}$$

where a denotes the post-elastic-to-elastic stiffness ratio, x_y is the yield displacement of the system; and $u(t)$ is an additional variable controlling the evolution of the plastic behaviour in the structure via the differential equation

$$x_y \dot{u}(t) = \dot{x}(t)[1 - H_u(\dot{x}(t))H_u(u(t)-1) - H_u(-\dot{x}(t))H_u(-u(t)-1)] \tag{4.66}$$

In Eq.(4.66) $H_u(x)$ represents the Heaviside function defined as

$$H_u(x) = \begin{cases} 1, & x \geq 0 \\ 0, & x < 0 \end{cases} \tag{4.67}$$

Further, the nonlinear restoring function $z(x, \dot{x}, \ddot{x})$ of Eq.(4.1) becomes

$$z(x, \dot{x}, \ddot{x}) = a\omega_0^2 x(t) + (1-a)\omega_0^2 x_y u(t) \tag{4.68}$$

Taking into account Eqs.(4.6) and (4.7) as well as (4.68), the equivalent linear damping and stiffness elements take the form

$$\beta(A) = \beta_0 + \frac{(1-a)\omega_0^2}{A\omega(A)} S_h(A) \tag{4.69}$$

and

$$\omega^2(A) = \omega_0^2 \left[a + (1-a)\frac{C_h(A)}{A} \right] \tag{4.70}$$

where $C_h(A)$ and $S_h(A)$ are given via the expressions [100], [13]

$$C_h(A) = \begin{cases} \frac{A}{\pi}[A - 0.5\sin(2\Lambda)] & , A > x_y \\ A & , A \leq x_y \end{cases} \tag{4.71}$$

and

$$S_h(A) = \begin{cases} \frac{4x_y}{\pi}\left(1 - \frac{x_y}{A}\right) & , A > x_y \\ 0 & , A \leq x_y \end{cases} \tag{4.72}$$

where

$$\cos(\Lambda) = 1 - \frac{2x_y}{A} \tag{4.73}$$

Further, substituting Eqs. (4.69)-(4.73) into Eqs. (4.8) and (4.9), and considering Eq.(4.14), yields

$$\begin{aligned} \beta_{eq}(c(t)) =& \beta_0 + \frac{4x_y(1-a)\omega_0^2}{\pi c(t)} \\ & \cdot \int_{x_y}^{+\infty} \frac{1}{\omega_0\sqrt{a + (1-a)\frac{\Lambda - 0.5\sin(2\Lambda)}{\pi}}} (1 - \frac{x_y}{A}) \text{exp}\left(-\frac{A^2}{2c(t)}\right) dA \end{aligned} \tag{4.74}$$

and

$$\begin{aligned} \omega_{eq}^2(c(t)) =& \omega_0^2 \{a + (1-a)[1 - \text{exp}\left(-\frac{x_y^2}{2c(t)}\right) \\ & + \frac{1}{\pi c(t)} \int_{x_y}^{+\infty} (\Lambda - 0.5\sin(2\Lambda))A \cdot \text{exp}\left(-\frac{A^2}{2c(t)}\right) dA]\} \end{aligned} \tag{4.75}$$

In Fig. 4.9 the non-stationary response variance $c(t)$ determined by solving Eq.(4.15) is plotted for a bilinear hysteretic oscillator with parameters values $S_0 = 0.0637$, $a = 0.6$, $\beta_0 = 0.1$, $\omega_0 = 1$, $x_y = 1$. In Figs. 4.10 and 4.11 the time-varying equivalent linear natural frequency $\omega_{eq}(t)$ of Eq.(4.9) and damping $\beta_{eq}(t)$ of Eq.(4.8) are plotted, respectively. Further, in Fig. 4.12

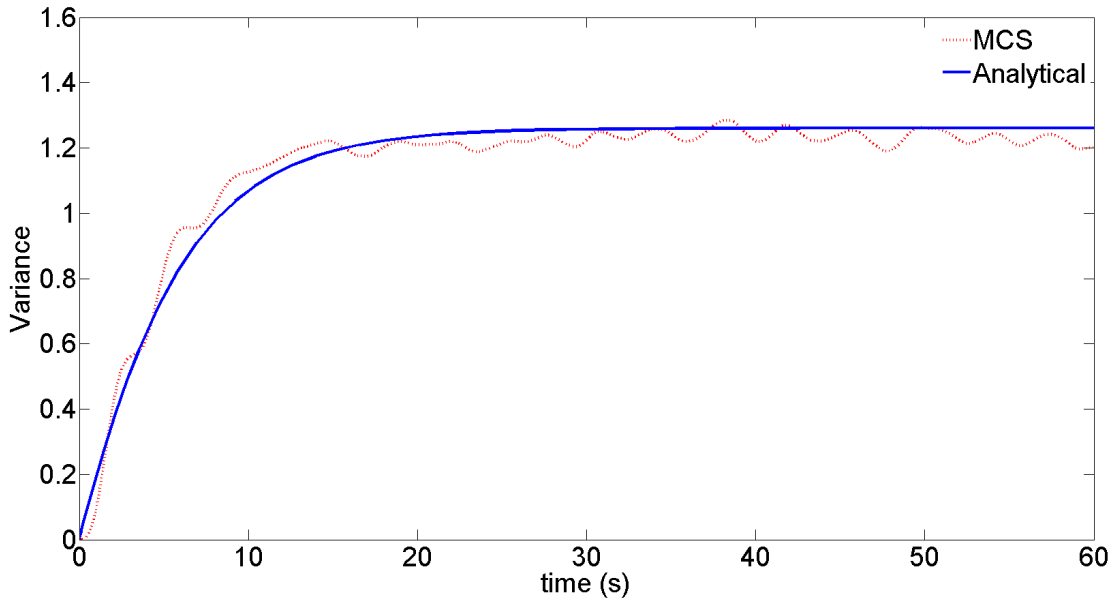

Figure 4.9: Transient response variance $c(t)$ of a bilinear hysteretic oscillator under white noise excitation with parameters values $S_0 = 0.0637$, $a = 0.6$, $\beta_0 = 0.1$, $\omega_0 = 1$, $x_y = 1$; comparison with pertinent Monte Carlo simulations (10000 realizations).

the non-stationary response displacement PDF is plotted for various time instants. Comparisons with pertinent MCS data (10000 realizations) demonstrate a satisfactory level of accuracy. Finally, in Figs. 4.13 and 4.14, the survival probability and corresponding first-passage PDF for various barrier levels are plotted, respectively. Comparisons with pertinent MCS (10000 realizations) are included as well demonstrating a quite satisfactory agreement. It can be expected that WPI matches MC result better, when the barrier level decreases. This is due to the fact that the analytical method considers the response satisfying Gaussian distribution, which is an approximation of real response distribution.

4.4 Summary

In chapter 4, a WPI based technique for determining the non-stationary response PDF, the survival probability and the first-passage PDF of nonlinear/hysteretic oscillators subject to stochastic excitation has been developed. Specifically, based on a stochastic averaging/linearization treatment of the problem, the nonlinear oscillator has been cast into an equivalent linear time-variant oscillator. Further, relying on a variational formulation and on the concept of the most probable path, a closed-form analytical expression has been derived for the oscillator short-time transition PDF and the oscillator transient joint response PDF has been derived. And the survival probability and the first-passage PDF of the nonlinear oscillator is obtained through the transit probability. In compari-

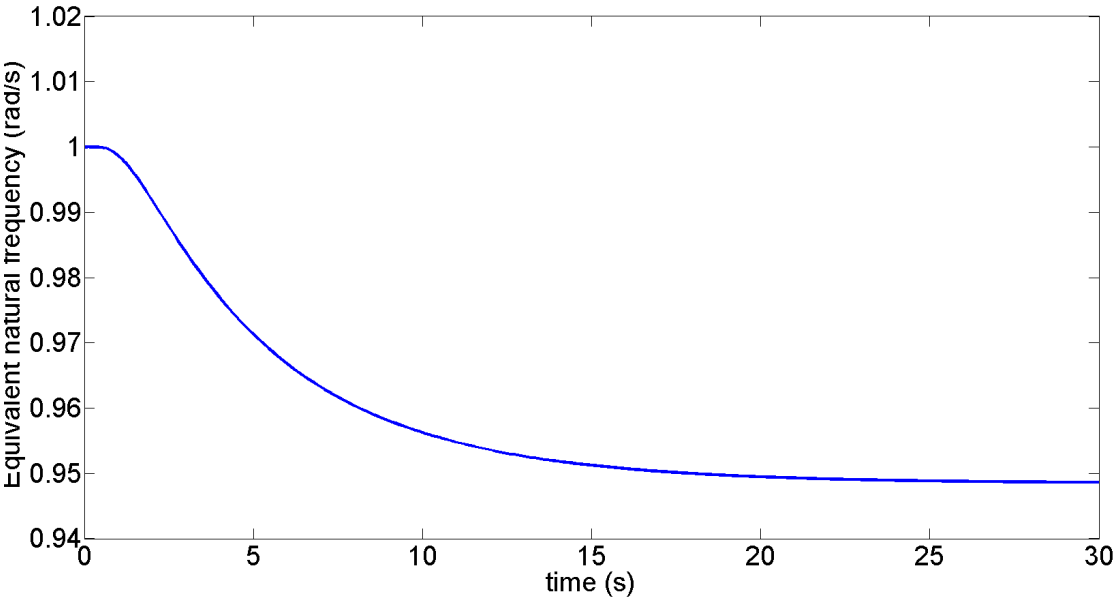

Figure 4.10: Time-varying equivalent linear natural frequency $\omega_{eq}(t)$ for a bilinear hysteretic oscillator under white noise excitation with parameters values $S_0 = 0.0637$, $a = 0.6$, $\beta_0 = 0.1$, $\omega_0 = 1$, $x_y = 1$.

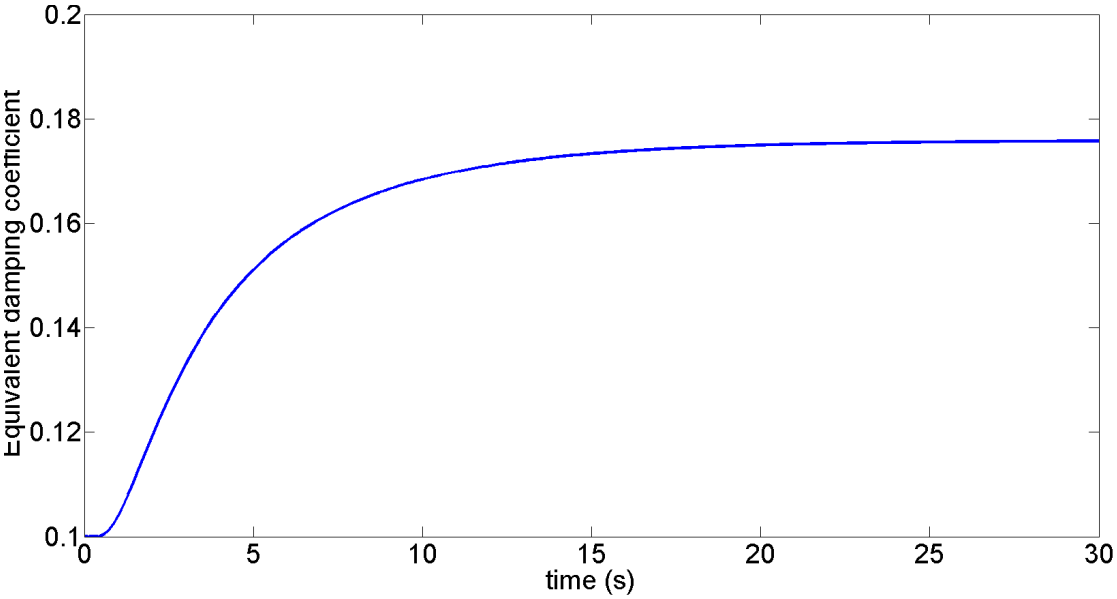

Figure 4.11: Time-varying equivalent linear damping $\beta_{eq}(t)$ for a bilinear hysteretic oscillator under white noise excitation with parameters values $S_0 = 0.0637$, $a = 0.6$, $\beta_0 = 0.1$, $\omega_0 = 1$, $x_y = 1$.

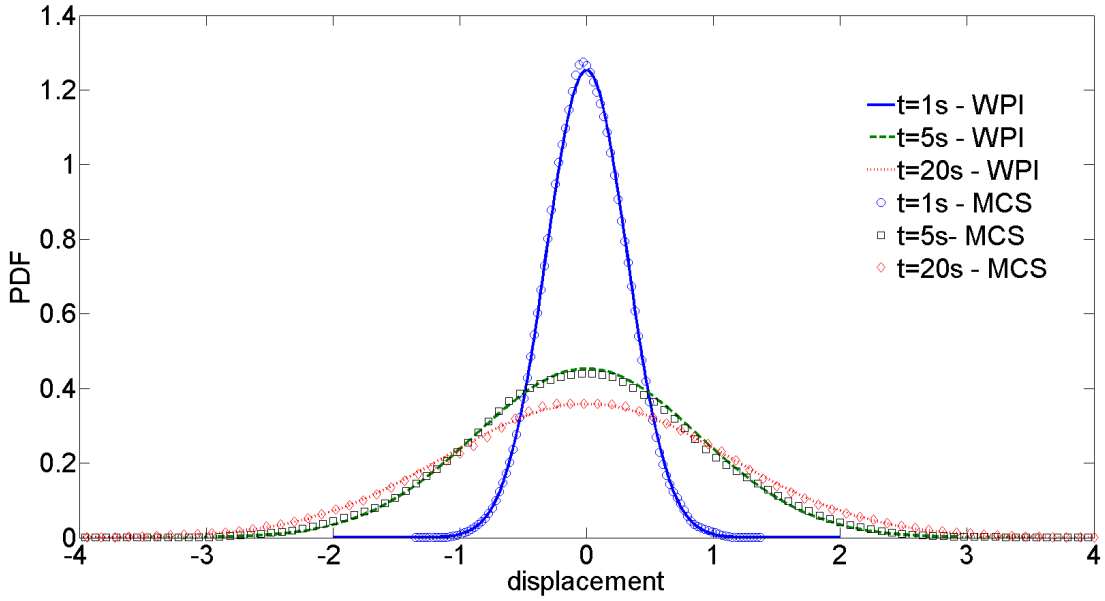

Figure 4.12: Response displacement PDF for a bilinear oscillator under white noise excitation with parameters values $S_0 = 0.0637$, $a = 0.6$, $\beta_0 = 0.1$, $\omega_0 = 1$, $x_y = 1$ for various time instants; comparison with pertinent Monte Carlo simulations (10000 realizations).

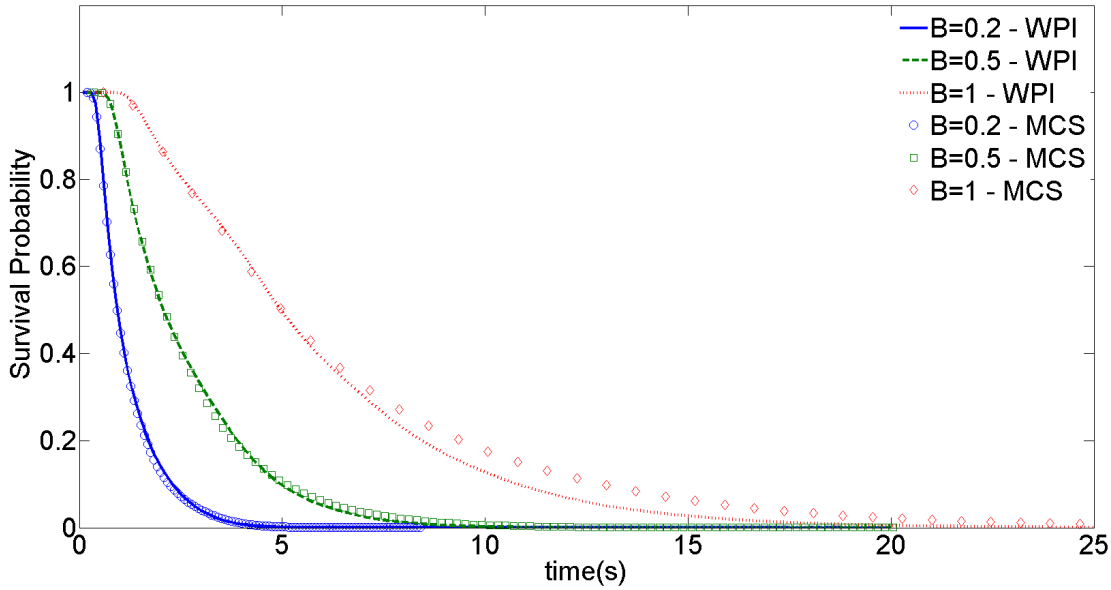

Figure 4.13: Survival probability for a bilinear hysteretic oscillator under white noise excitation with parameters values $S_0 = 0.0637$, $a = 0.6$, $\beta_0 = 0.1$, $\omega_0 = 1$, $x_y = 1$ for various barrier levels; comparison with pertinent Monte Carlo simulations (10000 realizations).

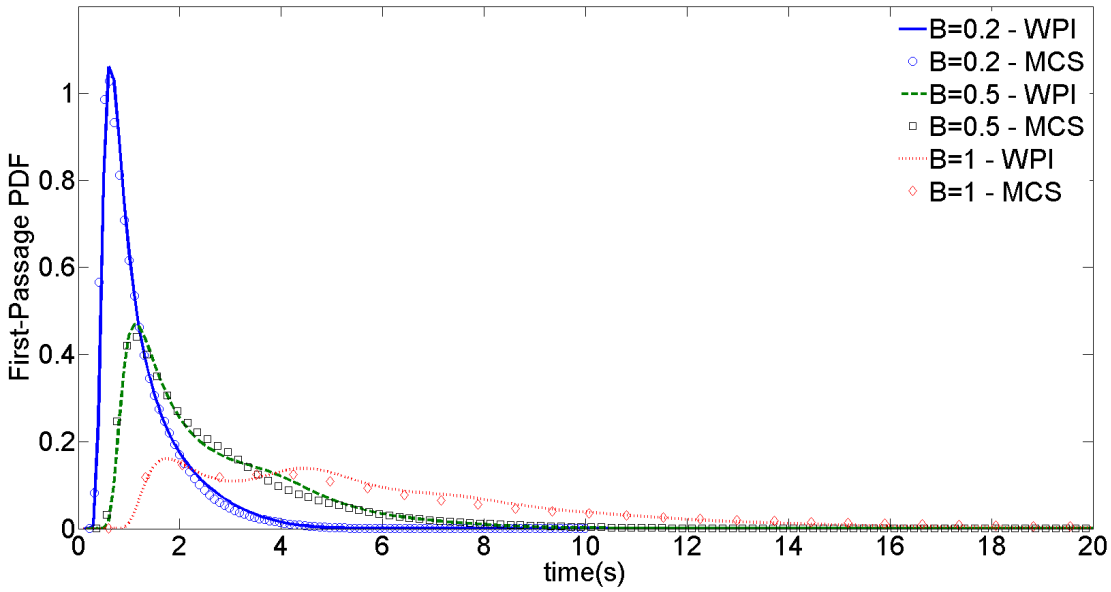

Figure 4.14: First-passage PDF for a bilinear hysteretic oscillator under white noise excitation with parameters values $S_0 = 0.0637$, $a = 0.6$, $\beta_0 = 0.1$, $\omega_0 = 1$, $x_y = 1$ for various barrier levels; comparison with pertinent Monte Carlo simulations (10000 realizations).

son with existing, albeit more versatile, numerical path integral schemes, a significant advantage of the proposed WPI technique is that the computationally demanding task of numerically integrating for every time step the high-dimensional convolution integrals involved in the C-K equation has been circumvented. Besides, the WPI based approach takes into account the correlation of the displacement x and velocity $\dot{x}$, which is important for the accuracy of the response analysis especially during the transient phase where the oscillator response displacement and velocity are correlated. Two different oscillators, Duffing and bilinear models, are considered to demonstrate the accuracy and effectiveness of proposed method. In both examples, WPI method shows a quite satisfactory agreement with pertinent Monte Carlo simulations. Due to the approximation of the linerization of nonlinearity, it is expected that the error between the WPI and MCS becomes larger when the degree of nonlinearity is increasing. In above two numerical examples, it only takes less than 20 minutes to calculate the results for the analytical method, while MC takes hours due to the large number of MC times.

Chapter 5

Uncertainty propagation: softening Duffing oscillator reliability assessment subject to evolutionary stochastic excitation

5.1 Preliminary remarks

In chapter 4, a WPI technique was developed (see also [141]) for determining the survival probability and first-passage PDF of nonlinear oscillators in a computationally efficient manner. In this chapter, the softening Duffing oscillator is discussed due to the negative restoring force, which makes the above WPI method inapplicable in this case.

The softening Duffing oscillator is a nonlinear oscillator possessing a linear-plus-cubic restoring force so that the spring has a softening characteristic. This oscillator has received considerable attention in the literature primarily due to its importance in describing the roll motion of a ship model in beam seas (e.g. [123], [6]). Note, however, that the softening Duffing oscillator has found applications in diverse other fields of engineering dynamics such as structural system vibration isolation (e.g. [82]), energy harvesting (e.g. [131]) and dynamics of timber structures (e.g. [95]).

Further, although several research efforts have focused on studying the oscillator response under deterministic excitation (e.g. [127], [79], [9]), limited results exist regarding the response analysis of the oscillator when it is subjected to stochastic excitation (e.g. [98], [101], [26]). Specifically, most of the results are based on rather heuristic approaches which inherently assume stationarity and that the probability the response leaves the stable region is extremely small; thus, neglecting important aspects of the analysis such as the possible unbounded response behavior when the restoring force acquires negative values. Recently, a numerical path integral approach was developed in [68] for determining the survival probability of a softening Duffing oscillator subject to stochastic excitation. The unbounded character of the response was rigorously taken into account by introducing a special form for the conditional response PDF, while the solution

was propagated by utilizing a discrete version of the C-K equation. Note, however, that, in general, numerical path integral schemes based on discrete versions of the C-K equation can be computationally demanding; this is due to the fact that the solution needs to be advanced in short time steps, while convolution integrals need to be numerically evaluated at every time step as well.

In this chapter, an efficient approximate analytical technique for determining the survival probability of a softening Duffing oscillator subject to evolutionary stochastic excitation is developed. Specifically, relying on a stochastic averaging treatment of the problem and introducing a special form for the oscillator response PDF, the technique developed in [118] is adapted and generalized herein to account for the special case of the softening Duffing oscillator. A significant advantage of the technique is that it can readily handle cases of evolutionary stochastic excitation with arbitrary evolutionary power spectrum (EPS) forms, even of the non-separable kind. Numerical examples include a softening Duffing oscillator under evolutionary earthquake excitation, as well as a softening Duffing oscillator with nonlinear damping modeling the nonlinear ship roll motion in beam seas. Comparisons with pertinent Monte Carlo simulations demonstrate the reliability of the technique.

5.2 Mathematical formulation

5.2.1 Softening Duffing oscillator response analysis

Consider the softening Duffing oscillator whose motion is governed by the equation

$$\ddot{x}_n(t) + 2\zeta_0\omega_0\dot{x}_n(t) + \omega_0^2 x_n(t) + \varepsilon\omega_0^2 x_n^3(t) = w_x(t),\ \varepsilon < 0 \tag{5.1}$$

where a dot over a variable denotes differentiation with respect to time t; ε denotes a negative constant representing the magnitude of the nonlinearity degree; ζ_0 is the ratio of critical damping; ω_0 is the natural frequency corresponding to the linear oscillator (i.e. $\varepsilon = 0$) and $w_x(t)$ represents a Gaussian, zero-mean non-stationary stochastic process possessing an evolutionary broad-band power spectrum $S_w(\omega, t)$. Examining Eq.(5.1), it can be readily seen that there exist values of the response displacement $x(t)$ for which the oscillator restoring force $F_r(x_n) = \omega_0^2 x_n + \varepsilon\omega_0^2 x_n^3 = \omega_0^2 x_n(1 + \varepsilon x_n^2)$ reaches zero, and even negative values. Clearly, this may lead to unbounded system response, and a special treatment is necessary to account for this behavior. Next, bearing this qualitative behavior in mind, and focusing on lightly damped systems (i.e. $\zeta_0 \ll 1$), it can be argued (e.g. [119]) that for $F_r(x_n) = \omega_0^2 x_n(1 + \varepsilon x_n^2) \geq 0$, or equivalently $x_n^2 \geq -1/\varepsilon$, the oscillator response exhibits a pseudo-harmonic behavior described by the equations Eqs. (4.2-4.4), where ϕ and A represent a slowly varying with time phase and a slowly varying with time response amplitude, respectively.

It is primarily the assumption of light damping that allows a combination of deterministic and

stochastic averaging to be performed next and to approximate the second-order stochastic differential equation (SDE) (Eq.(5.1)) by a first-order SDE governing the response amplitude process A. A more detailed presentation/discussion of the assumptions involved and the corresponding assumed pseudo-harmonic behavior of the response process $x(t)$ can be found in references (e.g. [119], [99], [142], [63]). Next, following a stochastic averaging/linearization approach (e.g. [63], [100]) a linearized version of Eq.(5.1) becomes

$$\ddot{x}(t) + 2\zeta_0\omega_0\dot{x}(t) + \omega^2(A)x(t) = w_x(t) \tag{5.2}$$

where the equivalent natural frequency $\omega(A)$ is given by the expression

$$\omega^2(A) = \frac{\omega_0^2}{\pi A}\int_0^{2\pi}\cos\psi(A\cos\psi + \varepsilon(A\cos\psi)^3)d\psi = \omega_0^2(1 + \frac{3}{4}\varepsilon A^2) \tag{5.3}$$

Examining Eq.(5.3) it can be readily seen that the stiffness element of the equivalent linear oscillator becomes zero at the critical response amplitude value $A_cr = \sqrt{-4/(3\varepsilon)}$. In this regard, the requirement $x^2 \geq -1/\varepsilon$ for the oscillator of Eq.(5.1) to have a bounded response is equivalently expressed in the following by the requirement $A < A_{cr}$. Bearing this qualitative aspect in mind, a special form for the non-stationary response amplitude PDF $p(A,t)$ is introduced next; that is,

$$p(A,t) = \frac{A}{c(t)}\text{exp}\left(\frac{-A^2}{2c(t)}\right)\text{rect}(A) + S_r(t)\delta(A - A_\infty) \tag{5.4}$$

where $\text{rect}(A) = H_u(A) - H_u(A - A_{cr})$, $H_u(.)$ denotes the unit step function, $c(t)$ is a time-dependent coefficient to be determined, $\delta(.)$ denotes the Dirac delta function, and A_∞ represents an arbitrary response amplitude value with the property $A_\infty \gg A \in [0, A_{cr}]$. Further, the time-dependent factor $S(t)$ can be determined by applying the normalization condition $\int_0^\infty p(A,t)dA = 1$; this yields

$$S_r(t) = 1 - \int_0^{A_{cr}}\frac{A}{c(t)}\text{exp}\left(\frac{-A^2}{2c(t)}\right)dA = \text{exp}\left(\frac{-A_{cr}^2}{2c(t)}\right) \tag{5.5}$$

Examining the form of the non-stationary response amplitude PDF of Eq.(5.4), it can be readily seen that it comprises two conceptually different terms. The first one represents a truncated Rayleigh PDF for amplitude values in the range $[0, A_{cr}]$, whereas the factor $S(t)$ in the second term represents the probability at a specific time instant that the response grows unbounded, namely the system response asymptotically approaches infinity. The rationale behind the choice of the truncated time-dependent Rayleigh PDF of Eq.(5.4) relates to the fact that the linear oscillator stationary response amplitude PDF is a Rayleigh one (see also [113]). In fact, as it was shown in [119], the non-stationary response amplitude PDF of a linear oscillator subject to Gaussian white noise excitation is a time-dependent Rayleigh PDF of the form $p(A,t) = \frac{A}{c(t)}\text{exp}\left(\frac{-A^2}{2c(t)}\right)$ with

the property $\lim_{t\to 0} p(A,t) = \frac{A}{\sigma^2}\exp\left(\frac{-A^2}{2\sigma^2}\right)$; where σ^2 represents the linear oscillator stationary response variance. In [63] it was further shown that the Rayleigh representation is suitable for nonlinear oscillators also and under evolutionary stochastic excitation as well. It is pointed out that a significant difference between adopting a PDF of the form $p(A,t) = \frac{A}{c(t)} exp(\frac{-A^2}{2c(t)})$ in [63] and introducing a PDF form of Eq.(5.4) in the herein developed technique, is that in the former case $c(t)$ accounts for the variance of the non-stationary response process x, whereas in the latter case $c(t)$ is simply a time-varying coefficient to be determined. Further, note that for the case where the oscillator is assumed to be initially at rest, i.e. $p(A_0, t_0 = 0) = \delta(A_0)$, the amplitude PDF $p(A,t)$ values will be concentrated around $A = 0$ for the very early part of the oscillation duration, or in other words, $\lim_{t\to 0^+} c(t) = 0$ which yields $\lim_{t\to 0^+} S_r(t) = 0$; that is, the probability that the system response will grow unbounded goes to zero as $t \to 0^+$.

Next, relying on Eq.(5.4), it can be argued that an alternative to Eq.(5.2) equivalent linear system is given in the form

$$\ddot{x}(t) + 2\zeta_0\omega_0\dot{x}(t) + \omega_{eq}^2(t)x(t) = w_x(t) \tag{5.6}$$

where the time-dependent stiffness element $\omega_{eq}^2(t)$ is defined as (see also [63], [118])

$$\omega_{eq}^2(t) = \int_0^{+\infty} \omega^2(A)p(A,t)dA \tag{5.7}$$

Note that taking into account the form of the amplitude PDF of Eq.(5.4), the time-varying equivalent stiffness element of Eq.(5.7) also has two parts. Specifically, for $A \in [0, A_{cr}]$, $\omega_{eq}^2(t)$ has a bounded part, i.e. $\omega_{eq,B}^2(t)$, whereas for $A > A_{cr}$ the stiffness element $\omega_{eq}^2(t)$ exhibits negative values; thus, yielding negative restoring force values resulting potentially in an unbounded system response behavior. In this regard, utilizing Eq.(5.4) the bounded part $\omega_{eq,B}^2(t)$ is determined as

$$\omega_{eq,B}^2(t) = \int_0^{A_{cr}} \omega^2(A)p(A,t)dA \tag{5.8}$$

Analytical determination of the integral in Eq.(5.8) yields

$$\omega_{eq,B}^2(t) = \omega_0^2\left[1 + \frac{3}{2}\varepsilon c(t)\left(1 - S_r(t)\right)\right] \tag{5.9}$$

Examining Eq.(5.9) it can be readily seen that the stiffness element $\omega_{eq,B}^2(t)$ is bounded between the values 0 and ω_0^2. Specifically, assuming that the oscillator is initially at rest yields $\lim_{t\to 0^+} p(A,t) = \delta(A_0)$, or in other words, $\lim_{t\to 0^+} c(t) = 0$, which yields $\lim_{c(t)\to 0^+} \omega_{eq,B}^2(t) = \omega_0^2$. This means that for the very early part of the oscillation duration the oscillator features an approxi-

mately linear restoring force. Further, as time increases and the transient phase progresses, the truncated Rayleigh PDF of Eq.(5.4) broadens as the oscillator exhibits higher amplitude values $A(t)$. Equivalently, the time-varying coefficient $c(t)$ increases with time, whereas the equivalent stiffness part $\omega_{eq,B}^2(t)$ decreases with time. Taking into account Eqs.(5.4) and (5.9) it can be readily shown that in the extreme case $\lim_{c(t)\to+\infty} \omega_{eq,B}^2(t) = 0$. Thus, the equivalent stiffness part $\omega_{eq,B}^2(t)$ is a non-negative and bounded quantity varying with time between the values 0 and ω_0^2. This is in agreement with the fact that $\omega_{eq,B}^2(t)$ corresponds to amplitude values $A \in [0, A_{cr}]$ where the oscillator response is assumed to behave in a bounded manner.

Further, focusing on the case where $A \in [0, A_{cr}]$ and based on a stochastic averaging approach Eq.(5.6) can be cast in a first-order SDE governing the evolution in time of the amplitude $A(t)$; see [119], [99], [142], [63] for a more detailed presentation. Related to this SDE is the Fokker-Planck (F-P) partial differential equation as Eq.(4.11), where

$$K_1(A,t) = -\zeta_0\omega_0 A + \frac{\pi S(\omega_{eq,B}(t),t)}{2A\omega_{eq,B}^2(t)} \tag{5.10}$$

and

$$K_2(A,t) = \sqrt{\frac{\pi S(\omega_{eq,B}(t),t)}{\omega_{eq,B}^2(t)}} \tag{5.11}$$

The F-P Eq.(4.11) governs the evolution in time of the transition PDF $p(A,t|A_1,t_1)$ for $A \in [0, A_{cr}]$ and $A_1 \in [0, A_{cr}]$. Next, a solution of the associated F-P equation $p(A,t|A_1 = 0, t_1 = 0) = p(A,t)$ is attempted in the form of the truncated Rayleigh PDF of Eq.(5.4). Specifically, substituting the truncated Rayleigh PDF into the associated F-P equation, assuming that the oscillator is initially at rest (i.e. $p(A, t = 0) = \delta(A)$), and manipulating yields the first-order nonlinear differential equation

$$\dot{c}(t) = -2\zeta_0\omega_0 c(t) + \frac{\pi S(\omega_{eq,B}(t),t)}{\omega_{eq,B}^2(t),t)} \tag{5.12}$$

to be solved numerically for the time-varying coefficient $c(t)$. Obviously, once the time-varying coefficient $c(t)$ is determined, the time-dependent coefficient $S(t)$ can be evaluated via Eq.(5.5). Further, equations similar to Eq.(5.12) can be derived for the case of the response amplitude transition PDF in a straightforward manner. Specifically, following a similar analysis as in [121], the transition amplitude PDF $p(A,t|A_1,t_1)$ is sought in the form

$$p(A,t|A_1,t_1) = \begin{cases} p_{tr}(A,t|A_1,t_1) + R(t,t_1)\delta(A - A_\infty) & ,0 < A_1 < A_{cr} \\ \delta(A - A_\infty) & ,A_1 > A_{cr} \end{cases} \tag{5.13}$$

where

$$p_{tr}(A,t|A_1,t_1) = \frac{A}{c(t,t_1)}\exp\left(-\frac{A^2+h^2(t,t_1)}{2c(t,t_1)}\right) I_0\left(\frac{Ah(t,t_1)}{c(t,t_1)}\right) rect(A) \tag{5.14}$$

and $c(t,t_1)$ and $h(t,t_1)$ are time-varying coefficients to be determined. Further, applying the normalization condition $\int_0^{+\infty} p(A,t|A_1,t_1)dA = 1$ yields the time-varying coefficient

$$R(t,t_1) = 1 - \int_0^{A_{cr}} p_{tr}(A,t|A_1,t_1)dA \tag{5.15}$$

where $I_0(.)$ denotes the modified Bessel function of the first kind and of zero order. In a similar manner as before, under the condition that $A \in [0, A_{cr}]$ and $A_1 \in [0, A_{cr}]$ substituting the bounded part of Eq.(5.13) into Eq.(4.11) and manipulating yields the first-order differential equations (see [121] for a more detailed derivation)

$$\frac{dc(t,t_1)}{dt} + 2\zeta_0\omega_0 c(t,t_1) - \frac{\pi S(\omega_{eq,B}(t),t)}{\omega^2_{eq,B}(t),t)} = 0 \tag{5.16}$$

and

$$\frac{dh(t,t_1)}{dt} + \zeta_0\omega_0 h(t,t_1) = 0 \tag{5.17}$$

Eqs.(5.16-5.17) are subject to the initial condition $p(A_2,t_2|A_1,t_1) = \delta(A_2 - A_1)$, which states that no change of state can occur if the transition time is zero.

5.2.2 Softening Duffing oscillator reliability assessment

In this section the approach developed in [118] is adapted and generalized herein to account for the special case of the softening Duffing oscillator and to determine the oscillator time-dependent survival probability. This is defined as the probability $P_B(t)$ that the amplitude a stays below the threshold A_cr over a given time interval $[t_0,T]$; that is, Prob$[A(t) \leq A_{cr}, \text{over}[t_0,T]|A(t_0) < A_{cr}]$. In the following, adopting the dicretization scheme applied in [118] the time domain is divided into intervals of the form

$$[t_{m-1},t_m],\ m = 1,2,...,M, t_0 = 0, t_M = T \text{ and } t_m = t_{m-1} + d_T T_{eq}(t_{m-1}) \tag{5.18}$$

where T_{eq} denotes the equivalent natural period of the oscillator given by

$$T_{eq}(t) = \frac{2\pi}{\omega_{eq,B}(t)} \tag{5.19}$$

and d_T is a constant to be selected with the property $d_T \in (0, 1]$. In the ensuing analysis, the survival probability is determined assuming that it is approximately constant over the time interval $[t_{m-1}, t_m]$. Clearly, for $d_T = 1$ the time interval $[t_{m-1}, t_m]$ corresponds to the equivalent time-dependent natural period of the oscillator. The choice is justified by the fact that the response amplitude A is assumed to be approximately constant over the interval $[t_{m-1}, t_m]$, owing to its slowly varying character with respect to time (see section 5.2.1). Thus, the survival probability $P_B(T)$ is assumed to be constant over $[t_{m-1}, t_m]$ as well. Of course, if higher accuracy is required a smaller value for d_T can be chosen. This is especially important for the case of the herein considered softening Duffing oscillator. Specifically, taking into account Eq.(5.9) it can be readily seen that for large enough values of the excitation intensity and/or of the nonlinearity magnitude, the equivalent time-varying natural frequency $\omega_{eq,B}(t)$ decreases significantly, or equivalently considering Eq.(5.19), the natural period $T_{eq}(t)$ increases considerably. Thus, the time interval $[t_{m-1}, t_m]$ of Eq.(5.18) increases substantially yielding potentially unrealistically large time intervals where the survival probability $P_B(T)$ is assumed to be constant. This phenomenon can be readily mitigated by selecting a small enough value for the coefficient d_T.

Further, taking into account the discretization of Eq.(5.18), the survival probability $P_B(T)$ is given by the equation

$$P_B(T = t_M) = \prod_{m=1}^{M} (1 - F_m) \tag{5.20}$$

where F_m is defined as the probability that A will cross the barrier A_{cr} in the time interval $[t_{m-1}, t_m]$, given that no crossings have occurred prior to time t_{m-1}. Next, invoking the Markovian property for the process A and utilizing the standard definition of conditional probability yields

$$F_m = \frac{\text{Prob}[A(t_m) \geq A_{cr} \bigcap A(t_{m-1}) \leq A_{cr}]}{\text{Prob}[A(t_{m-1}) \leq A_{cr}]} = \frac{Q_{m-1,m}}{H_m} \tag{5.21}$$

where

$$H_{m-1} = \int_0^{A_{cr}} p(A_{m-1}, t_{m-1}) dA_{m-1} \tag{5.22}$$

and, by utilizing the relationship $p(A_1, t_1; A_2, t_2) = p(A_1, t_1)p(A_2, t_2|A_1, t_1)$,

$$Q_{m-1,m} = \int_0^{A_{cr}} \left(\int_{A_{cr}}^{+\infty} p(A_m, t_m|A_{m-1}, t_{m-1}) dA_m \right) p(A_{m-1}, t_{m-1}) dA_{m-1} \tag{5.23}$$

Next, taking into account Eqs.(5.4) and (5.13), Eqs.(5.22-5.23) become

$$H_{m-1} = 1 - \exp\left(\frac{A_{cr}^2}{2c(t_{m-1})} \right) \tag{5.24}$$

and

$$Q_{m-1,i} = \int_0^{A_{cr}} \left(\int_{A_{cr}}^{+\infty} [p_{tr}(A_m, t_m | A_{m-1}, t_{m-1}) + R(t_m, t_{m-1})\delta(A_m - A_\infty)] dA_m \right) \cdot p(A_{m-1}, t_{m-1}) dA_{m-1} \tag{5.25}$$

respectively. Taking into account the properties of the Dirac delta function, Eq.(5.25) becomes

$$Q_{m-1,m} = \int_0^{A_{cr}} R(t_m, t_{m-1}) p(A_{m-1}, t_{m-1}) dA_{m-1} \tag{5.26}$$

and utilizing Eq.(5.15) yields

$$\begin{aligned} Q_{m-1,m} = & \int_0^{A_{cr}} p(A_{m-1}, t_{m-1}) dA_{m-1} \\ & - \int_0^{A_{cr}} \left(\int_0^{A_{cr}} p_{tr}(A_m, t_m | A_{m-1}, t_{m-1}) dA_m \right) p(A_{m-1}, t_{m-1}) dA_{m-1} \end{aligned} \tag{5.27}$$

Next, considering Eqs.(5.22), Eq.(5.27) takes the form

$$Q_{m-1,m} = H_{m-1} - \int_0^{A_{cr}} \left(\int_0^{A_{cr}} p_{tr}(A_m, t_m | A_{m-1}, t_{m-1}) dA_m \right) p(A_{m-1}, t_{m-1}) dA_{m-1} \tag{5.28}$$

Relying further on the assumption that $\omega_{eq,B}(t)$ follows a slowly varying with time behavior, the following approximation over a small time interval $[t_{m-1}, t_m]$ is introduced; i.e., $\omega_{eq,B}(t) = \omega_{eq,B}(t_{m-1})$ for $t \in [t_{m-1}, t_m]$. Next, based on the slowly varying with time behavior of the EPS, $S_w(\omega, t)$ is also treated as a constant over the interval $[t_{m-1}, t_m]$. Further, based on the above assumptions, introducing the variable $\tau_m = t_m - t_{m-1}$, and applying a first-order Taylor expansion around point $\tau_m = 0$, Eqs.(5.16-5.17) become (see [118] for a detailed derivation)

$$c(t_{m-1}, t_m) = \frac{\pi S_w(\omega_{eq,B}(t_{m-1}), t_{m-1})}{\omega_{eq,B}^2(t_{m-1})} \tau_m \tag{5.29}$$

and

$$h(t_{m-1}, t_m) = A_{m-1} \sqrt{1 - 2\zeta_0 \omega_0 \tau_m} \tag{5.30}$$

respectively. Furthermore, considering Eqs.(5.16) and (5.29) and applying a first-order Taylor expansion for the time-varying coefficient $c_m(t)$ around point $t = t_{m-1}$ yields

$$c(t_m) = c(t_{m-1}, t_m) + c(t_{m-1})(1 - 2\zeta_0 \omega_0 \tau_m) \tag{5.31}$$

Next, setting

$$r_m^2 = \frac{c(t_{m-1})}{c(t_m)}(1 - 2\zeta_0\omega_0\tau_m) \tag{5.32}$$

Eq.(5.31) yields

$$c(t_{m-1}, t_m) = c(t_m)(1 - r_m^2) \tag{5.33}$$

Further, taking into account Eq.(5.28) and expanding the Bessel function $I_0(x)$ in the form (e.g. [118])

$$I_0(x) = \sum_{k=0}^{\infty} \frac{(x/2)^{2k}}{k!\Gamma(k+1)} \tag{5.34}$$

analytical treatment of the involved double integral of Eq.(5.28) is possible yielding

$$Q_{m-1,i} = H_{m-1} - \left(A_0 + \sum_{n=1}^{N} A_n\right) \tag{5.35}$$

where

$$A_0 = \left[1 - \exp\left(-\frac{A_{cr}^2}{2c(t_m)(1-r_m^2)}\right)\right]\left[1 - \exp\left(-\frac{A_{cr}^2}{2c(t_{m-1})(1-r_m^2)}\right)\right](1 - r_m^2) \tag{5.36}$$

$$A_n = \frac{r_m^{2n}(1-r_m^2)}{\prod_{k=1}^{n}(k)^2} L_n = \frac{r_m^{2n}(1-r_m^2)}{(n!)^2} L_n \tag{5.37}$$

and

$$\begin{aligned} L_n = &\left\{\Gamma[1+n, 0] - \Gamma\left[1+n, \frac{A_{cr}^2}{2c(t_{m-1})(1-r_m^2)}\right]\right\} \\ &\cdot \left\{\Gamma[1+n, 0] - \Gamma\left[1+n, \frac{A_{cr}^2}{2c(t_m)(1-r_m^2)}\right]\right\} \end{aligned} \tag{5.38}$$

In Eq.(5.38) $\Gamma[\gamma, z]$ represents the incomplete Gamma function defined as $\Gamma[\gamma, z] = \int_z^{+\infty} t^{\gamma-1}e^{-t}dt$. A more detailed presentation of the derivations in this section can be found in [118].

Concisely, the developed technique comprises the following steps:

a) Determination of the time-varying coefficient $c(t)$ via numerical solution of Eq.(5.12).

b) Determination of the bounded equivalent time-varying natural frequency $\omega_{eq,B}(t)$ via Eq.(5.9).

c) Determination of the effective natural period $T_{eq}(t)$ (Eq.(5.19)) and discretization of the time domain via Eq.(5.18).

d) Determination of the parameters H_{m-1} and $Q_{m-1,m}$ via Eqs.(5.24) and (5.35).

e) Determination of the survival probability $P_B(T)$ via Eq.(5.20).

5.3 Numerical examples

5.3.1 Softening Duffing oscillator under earthquake excitation

The softening Duffing oscillator has also been used in conjunction with structural dynamics/earthquake engineering applications such as the rocking response of a rigid block (e.g. [120]), and dynamics of timber structures (e.g. [95]). In this regard, the non-separable earthquake excitation EPS of the form

$$S_w(\omega,t)=S_0(\frac{\omega}{5\pi})^2\text{exp}(-0.2t)t^2\text{exp}\left[-(\frac{\omega}{10\pi})^2t\right] \tag{5.39}$$

is considered in this example. This spectrum, plotted in Fig.(5.1) for $S_0=1$, comprises some of the main characteristics of seismic shaking, such as decreasing of the dominant frequency with time (e.g. [104]). Further, survival probabilities determined via the herein developed approximate technique are compared with pertinent Monte Carlo simulation data (10,000 realizations). To this aim, realizations compatible with the EPS of Eq.(5.39) are generated based on a spectral representation approach (e.g. [71]), while a standard fourth-order Runge-Kutta scheme is employed for solving the nonlinear equation of motion (Eq.(5.1)). The initial distribution chosen for the response amplitude PDF is the Dirac delta function, i.e., $p(A_0,t_0=0)=\delta(A_0)$, assuming the system is initially at rest. In the ensuing analysis the value $N=60$ is chosen in Eq.(5.35) for the terms to be included in the expansion.

In Fig.(5.2), the bounded equivalent natural frequencies (Eq.(5.13)) of the oscillators with parameter values ($S_0=1$, $\omega_0^2=\pi^2$, $\zeta_0=0.01$, $\varepsilon=-1$), ($S_0=1$, $\omega_0^2=\pi^2$, $\zeta_0=0.01$, $\varepsilon=-2$), and ($S_0=1$, $\omega_0^2=\pi^2$, $\zeta_0=0.01$, $\varepsilon=-3$) are plotted. In Fig.(5.3), the equivalent natural periods for the above oscillators are plotted, whereas in Fig.(5.4) the survival probabilities determined by Eqs.(5.20) are plotted for various barrier levels $A_{cr}=\sqrt{-\frac{4}{3\varepsilon}}$; comparisons with MCS (10,000 realizations) demonstrate a quite satisfactory agreement.

5.3.2 Softening Duffing oscillator under sea wave excitation

Considering the rolling motion of a ship in unidirectional beam waves enables one to approximate reasonably the motion as uncoupled with respect to other motions such as sway, pitch and heave; see [123], [6], [1], [55] for a detailed presentation of the topic. Further, to take into account the viscous and vortex components of roll damping, a nonlinear expression for the damping force of

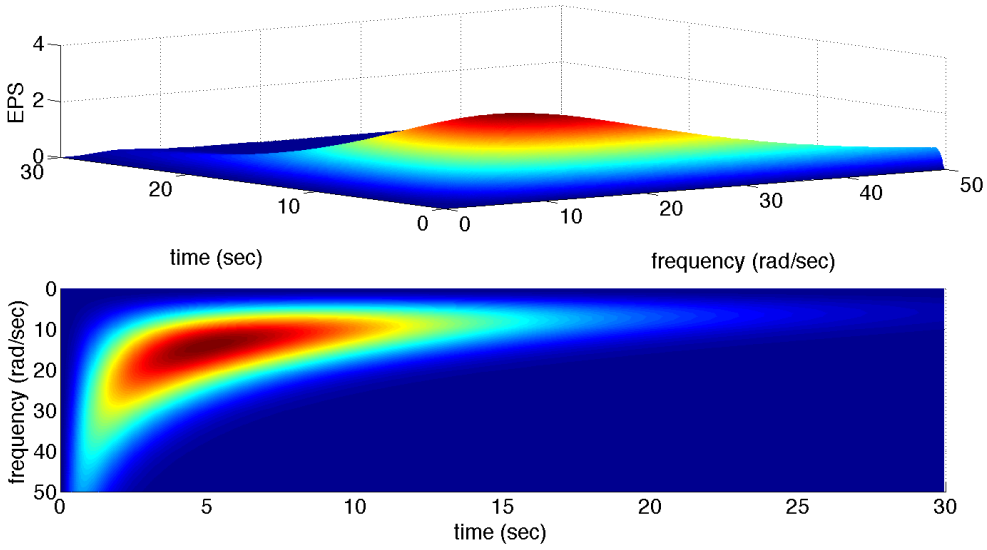

Figure 5.1: Non-separable earthquake excitation evolutionary power spectrum

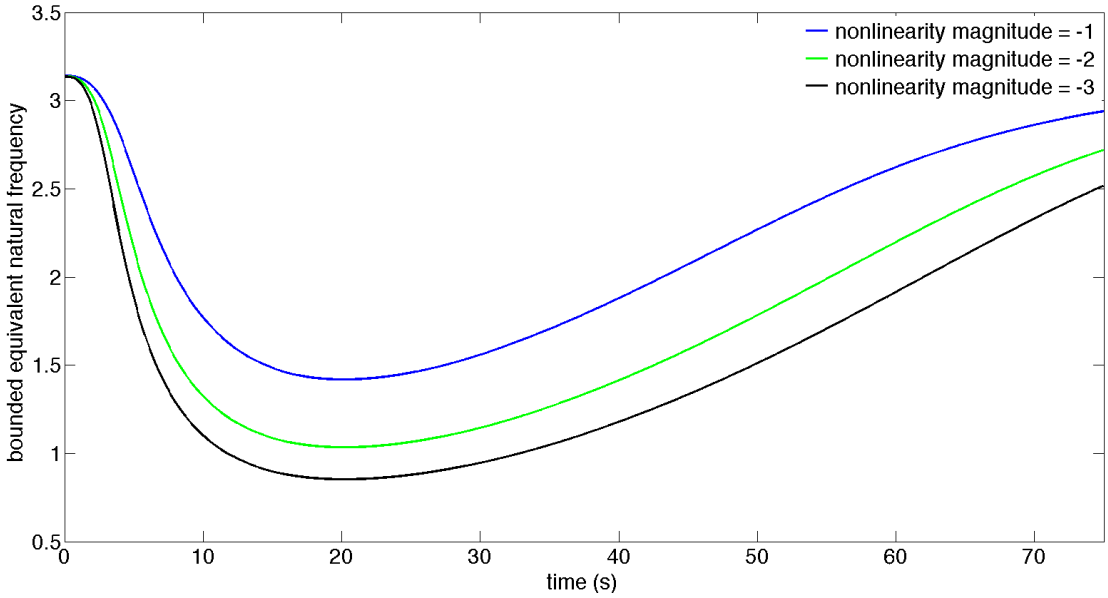

Figure 5.2: Bounded equivalent time-varying natural frequency $\omega_{eq,B}(t)$ for a softening Duffing oscillator ($S_0 = 1$, $\omega_0^2 = \pi^2$, $\zeta_0 = 0.01$) under earthquake excitation

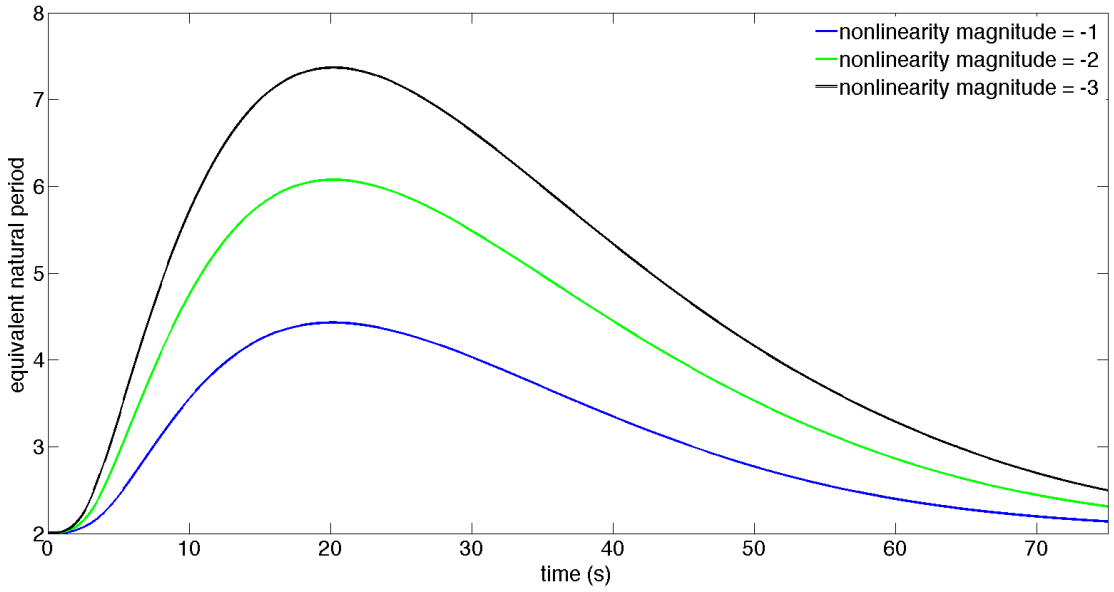

Figure 5.3: Equivalent natural period $T_{eq}(t)$ for a softening Duffing oscillator ($S_0 = 1$, $\omega_0^2 = \pi^2$, $\zeta_0 = 0.01$) under earthquake excitation

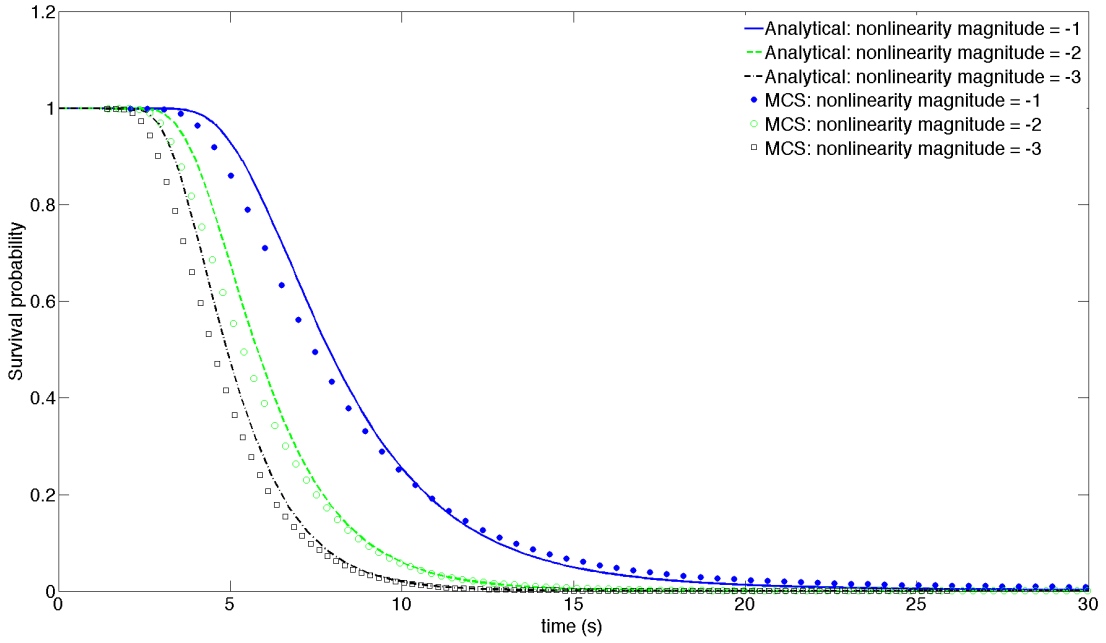

Figure 5.4: Survival probability for a softening Duffing oscillator ($S_0 = 1$, $\omega_0^2 = \pi^2$, $\zeta_0 = 0.01$, $d_T = 0.125$) under earthquake excitation; comparisons with MCS (10,000 realizations)

the form $M_D = 2\zeta_0\omega_0(\dot{\phi} + \varepsilon_1\dot{\phi}^3)$, $\varepsilon_1 > 0$ where ϕ is the ship rolling angle, is commonly adopted in the literature; indicatively, see also [114], [30], [129], [74] for some alternative polynomial and other approximations. As far as the nonlinear restoring moment is concerned, several approximations exist in the literature with the expression $M_D = \omega_0^2(\phi + \varepsilon_2\phi^3)$, $\varepsilon_2 < 0$, being among the most commonly adopted choices (e.g. Taylan 1999); see also [108], [126]. The aforementioned expression, although phenomenological, manages to capture to an adequate degree the qualitative behavior and basic physics of nonlinear ship rolling motion under beam waves (e.g. [123], [6]).

In this regard, consider next the uncoupled ship roll motion given by the equation

$$\ddot{\phi} + 2\zeta_0\omega_0\dot{\phi} + 2\varepsilon_1\zeta_0\omega_0\dot{\phi}^3 + \omega_0^2\phi + \varepsilon_2\omega_0^2\phi^3 = w(t),\ \varepsilon_1 > 0,\ \varepsilon_2 < 0 \tag{5.40}$$

where $w(t)$ represents a Gaussian, zero-mean non-stationary stochastic process possessing an evolutionary broad-band power spectrum $S_w\omega, t$ of the form

$$S_w(\omega, t) = |g(t)|^2|F_{roll}(\omega)|^2 S_E(\omega) \tag{5.41}$$

In Eq.(5.41) $S_E(\omega)$ denotes the stationary wave energy spectrum, whereas the function $F_{roll}(\omega)$ relates the wave energy spectrum to the roll moment excitation spectrum (e.g. [59]). Although, in general, wave energy spectra, such as the Jonswap (e.g. [52]), are narrow-band with a distinct peak, it has been shown that the resulting roll moment excitation spectrum is significantly more broad-band than the corresponding wave energy spectrum (e.g. [108]). This broad-band characteristic of the stationary roll moment excitation power spectrum $|F_{roll}(\omega)|^2 S_E(\omega)$ is in agreement with the assumptions and justifies to a certain extent the applicability of the approach developed in section 5.2. In the following, the Pierson-Moskowitz (P-M) spectrum [88], i.e. a special case of the Jonswap spectrum of the form

$$S_E(\omega) = \frac{D}{\omega^5}\exp\left(-\frac{G}{\omega^4}\right) \tag{5.42}$$

is used for the wave energy spectrum $S_E(\omega)$, where $D = 1 \times 10^{-2}g^2$, $G = 120(\frac{g}{u})^4$, $u = 15m/s$, $g = 9.8m/s^2$. As far as the function $F_{roll}(\omega)$ is concerned, this is chosen to be of the rather general form (e.g. [108]) $|F_{roll}(\omega)|^2 = C\omega^4$ where the constant C is associated with beam sea and oscillator characteristics. In the following, the value $C = 3$ is used. Thus, due to the effect of multiplying Eq.(5.42) with the term "ω^4" the resulting stationary roll moment excitation spectrum $|F_{roll}(\omega)|^2 S_E(\omega)$ becomes relatively broad-band as shown in Fig.(5.5).

Further, to demonstrate the versatility of the technique for addressing cases of non-stationary

excitations, a time-modulating function $g(t)$ of the form

$$g(t) = \left\{ 0.2 + 0.8 \cdot \left[\frac{t}{a} \exp\left(1 - \frac{t}{a}\right) \right]^b \right\}^{0.5} \tag{5.43}$$

is utilized next, where $a = 20,\ b = 5$. As it is shown in Fig.(5.6) the function $g(t)$ varies slowly with time suggesting a low level of non-stationarity. In Fig.(5.7) the excitation EPS of Eq.(5.41) is plotted.

It can be readily seen that the only qualitative difference between Eq.(5.40) and the softening Duffing oscillator of Eq.(5.1) is the nonlinear damping term; thus, following [63] (see also [118]) an equivalent linear oscillator is given in the form

$$\ddot{x}(t) + \beta_{eq}(t)\dot{x}(t) + \omega_{eq}^2(t)x(t) = w_x(t) \tag{5.44}$$

where the time-dependent stiffness element $\omega_{eq}^2(t)$ is given by Eq.(5.7), and the time-dependent damping element $\beta_{eq}(t)$ is given by

$$\beta_{eq}(t) = E[\beta(A)] = \int_0^{+\infty} \beta(A) p(A,t) dA \tag{5.45}$$

Following a stochastic averaging/linearization treatment (e.g. [118], [63]) $\beta(A)$ in Eq.(5.45) is given by

$$\begin{aligned} \beta(A) =& 2\zeta_0\omega_0 - \frac{1}{\pi A \omega(A)} \int_0^{2\pi} \sin\psi [2\varepsilon_1\zeta_0\omega_0(-\omega(A)A\sin\psi)^3 \\ &+ \omega_0^2 A\cos\psi + \omega_0^2\varepsilon_1(A\cos\psi)^3] d\psi \\ =& 2\zeta_0\omega_0 \left(1 + \frac{3}{4}\varepsilon_1\omega^2(A)A^2\right) \end{aligned} \tag{5.46}$$

It can be readily seen that the time-dependent damping element $\beta_{eq}(t)$ depends on $\beta(A)$ which in turn depends on the stiffness element $\omega^2(A)$; thus, following the development in section 5.2, a bounded part $\beta_{eq,B}(t)$ is defined as

$$\beta_{eq,B}(t) = \int_0^{A_{cr}} \beta(A) p(A,t) dA \tag{5.47}$$

Substituting Eq. (5.46) into (5.47), and taking into account Eq.(5.4) yields

$$\begin{aligned} \beta(A) =& 2\zeta_0\omega_0\{1 - S(t) + \frac{3}{4}\varepsilon_1\omega_0^2[2c(t) - S(t)(2c(t) + A_{cr}^2)] \\ &+ \frac{9}{16}\omega_0^2\varepsilon_1\varepsilon_2[8c^2(t) - S(t)(A_{cr}^4 + 4c(t)A_{cr}^2 + 8c^2(t))]\} \end{aligned} \tag{5.48}$$

Further, Eqs. (5.10), (5.12), (5.16), (5.17), and (5.32) are updated accordingly (see also [118], [63]) taking the form

$$K_1(A,t) = -\frac{1}{2}\beta_{eq,B}(t)A + \frac{\pi S(\omega_{eq,B}(t),t)}{2A\omega^2_{eq,B}(t)} \tag{5.49}$$

$$\dot{c}(t) = -\beta_{eq,B}(t)c(t) + \frac{\pi S(\omega_{eq,B}(t),t)}{\omega^2_{eq,B}(t)} \tag{5.50}$$

$$\frac{dc(t,t_1)}{dt} + \beta_{eq,B}(t)c(t,t_1) - \frac{\pi S(\omega_{eq,B}(t),t)}{\omega^2_{eq,B}(t)} = 0 \tag{5.51}$$

$$\frac{dh(t,t_1)}{dt} + \frac{1}{2}\beta_{eq,B}(t)h(t,t_1) = 0 \tag{5.52}$$

and

$$r^2_m = \frac{c(t_{m-1})}{c(t_m)}(1 - \beta_{eq,B}(t_{m-1})\tau_m) \tag{5.53}$$

respectively. As in section 5.3.1 survival probabilities are determined via the herein developed approximate technique and are further compared with spectral representation based (e.g. [71]) pertinent Monte Carlo simulation data (10,000 realizations). The oscillator is assumed to be initially at rest, whereas the value $N = 60$ is chosen in Eq.(5.35) for the terms to be included in the expansion. In Fig.(5.8) and Fig.(5.9), the bounded equivalent natural frequencies $\omega_{eq,B}(t)$ and equivalent natural period $T_{eq}(t)$ of the oscillators of Eq.(5.40) with parameter values ($\zeta_0 = 0.01$, $\omega_0^2 = \pi^2$, $\varepsilon_1 = 0.1$, $\varepsilon_2 = -1$), ($\zeta_0 = 0.01$, $\omega_0^2 = \pi^2$, $\varepsilon_1 = 0.1$, $\varepsilon_2 = -2$) and ($\zeta_0 = 0.01$, $\omega_0^2 = \pi^2$, $\varepsilon_1 = 0.1$, $\varepsilon_2 = -4$) are plotted, respectively. In Fig.(5.10), the equivalent natural periods for the above oscillators are plotted, whereas in Fig.(5.11) the survival probabilities determined by Eq.(5.20) are plotted for various barrier levels $A_{cr} = \sqrt{-\frac{4}{3\varepsilon_2}}$; comparisons with MCS (10000 realizations) demonstrate an acceptable agreement due to the softening nonlinearity.

5.4 Summary

In chapter 5, an approximate analytical technique has been developed for determining the survival probability of a softening Duffing oscillator subject to evolutionary stochastic excitation. Herein, introducing a special form for the oscillator non-stationary response amplitude PDF and relying on stochastic averaging, a rigorous and computationally efficient treatment of the problem has been provided to deal with the negative stiffness issue. Taking advantage of this special response amplitude PDF form, a bounded transition probability function is obtained. Further, survival probability estimates have been determined for various levels of nonlinearity magnitude. A significant advantage of the technique relates to the fact that it can readily handle cases of stochastic excitations that exhibit strong variability in both the intensity and the frequency content. Two different examples, are considered to demonstrate the accuracy and effectiveness of proposed method. In

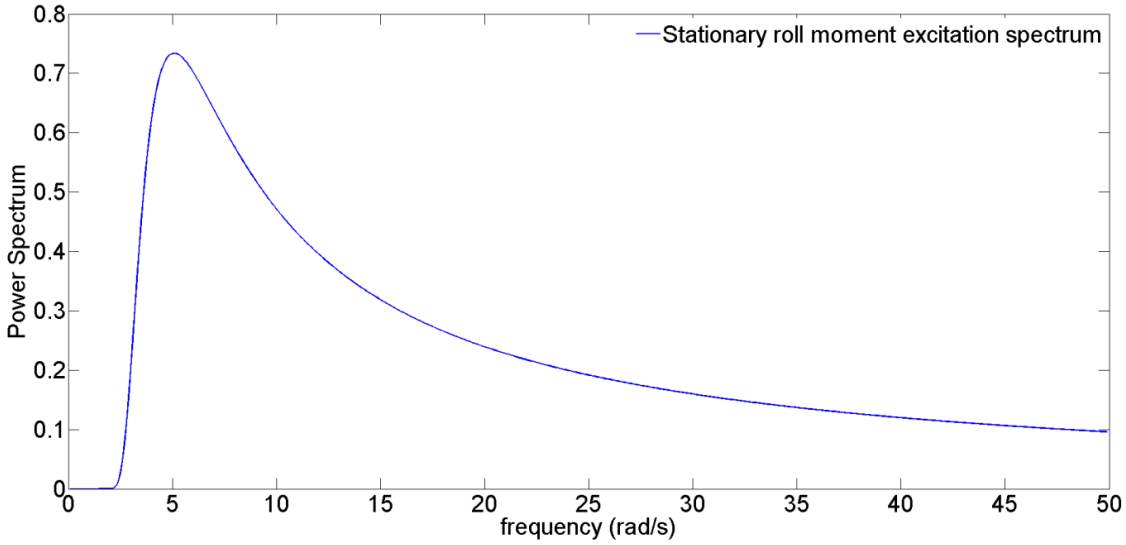

Figure 5.5: Stationary roll moment excitation spectrum $|F_{roll}(\omega)|^2 S_E(\omega)$

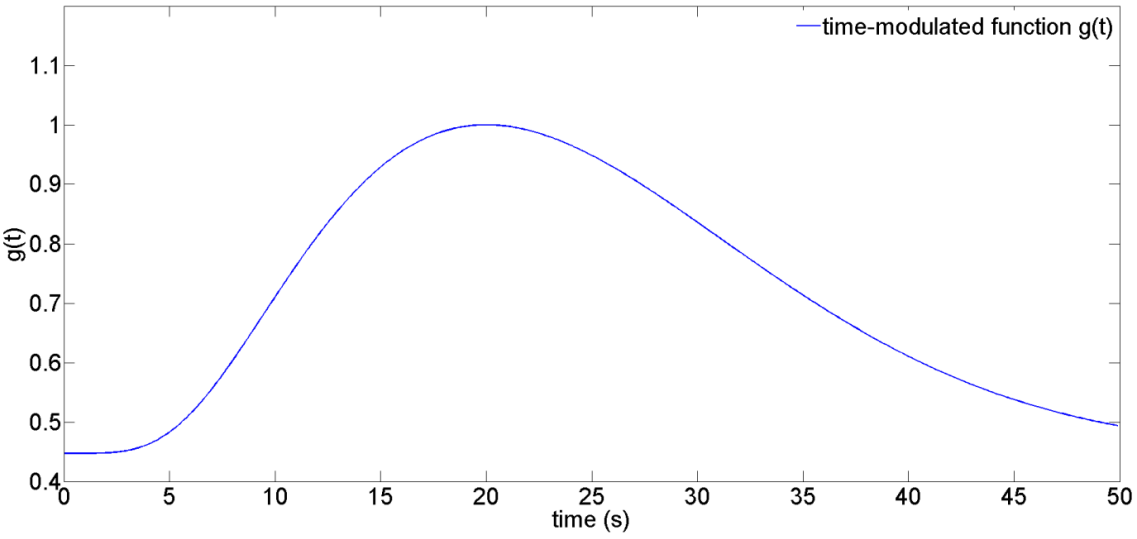

Figure 5.6: Time-modulating function $g(t)$

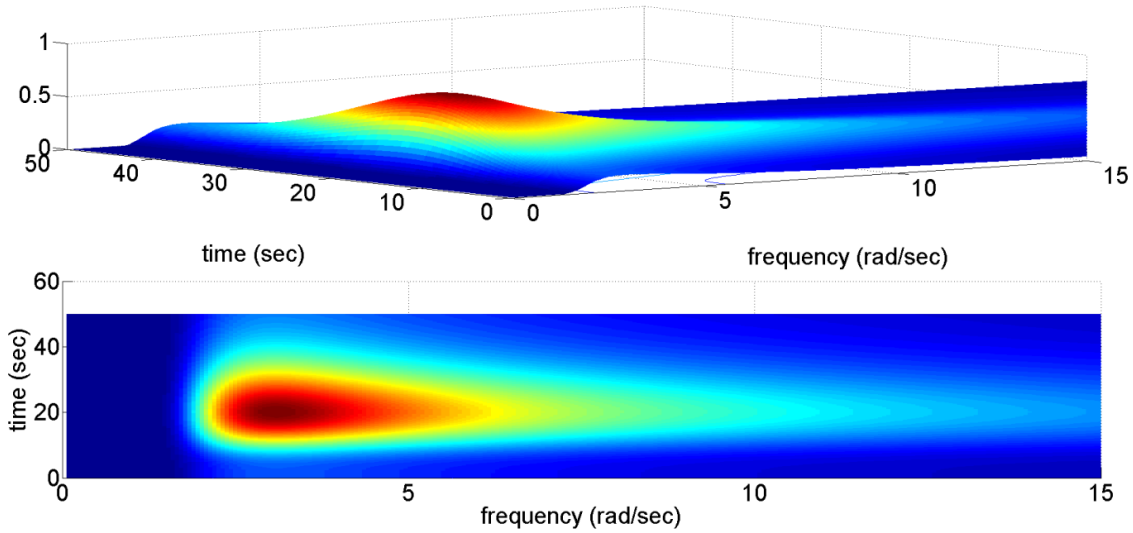

Figure 5.7: Time-modulated roll moment excitation spectrum

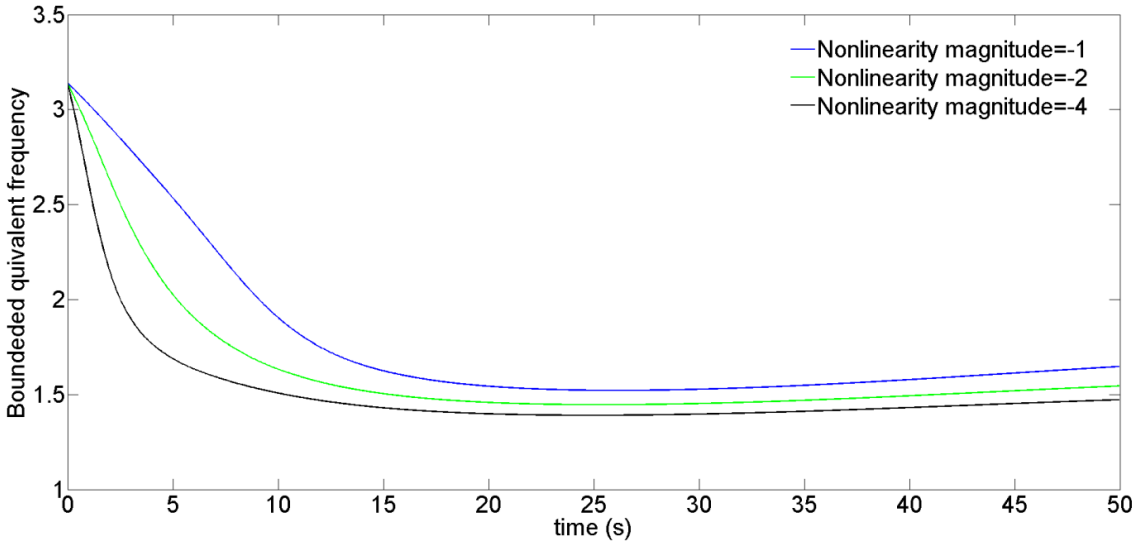

Figure 5.8: Bounded equivalent time-varying natural frequency $\omega_{eq,B}(t)$ for a softening Duffing oscillator with nonlinear damping ($\varepsilon_1 = 0.1$, $\omega_0^2 = \pi^2$, $\zeta_0 = 0.01$) under sea wave excitation

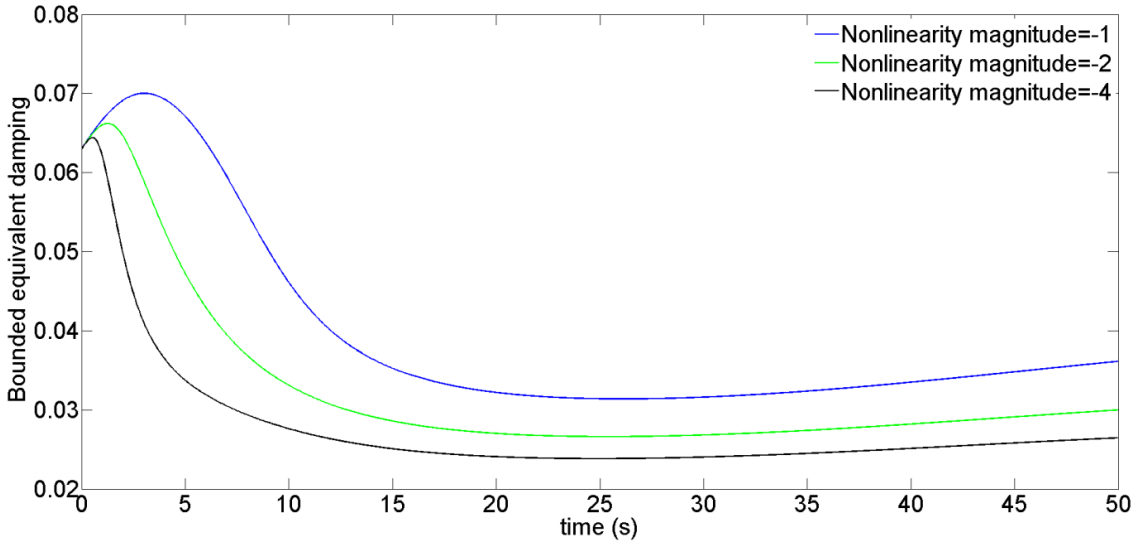

Figure 5.9: Bounded equivalent time-varying damping $\beta_{eq,B}(t)$ for a softening Duffing oscillator with nonlinear damping ($\varepsilon_1 = 0.1$,$\omega_0^2 = \pi^2$, $\zeta_0 = 0.01$) under sea wave excitation

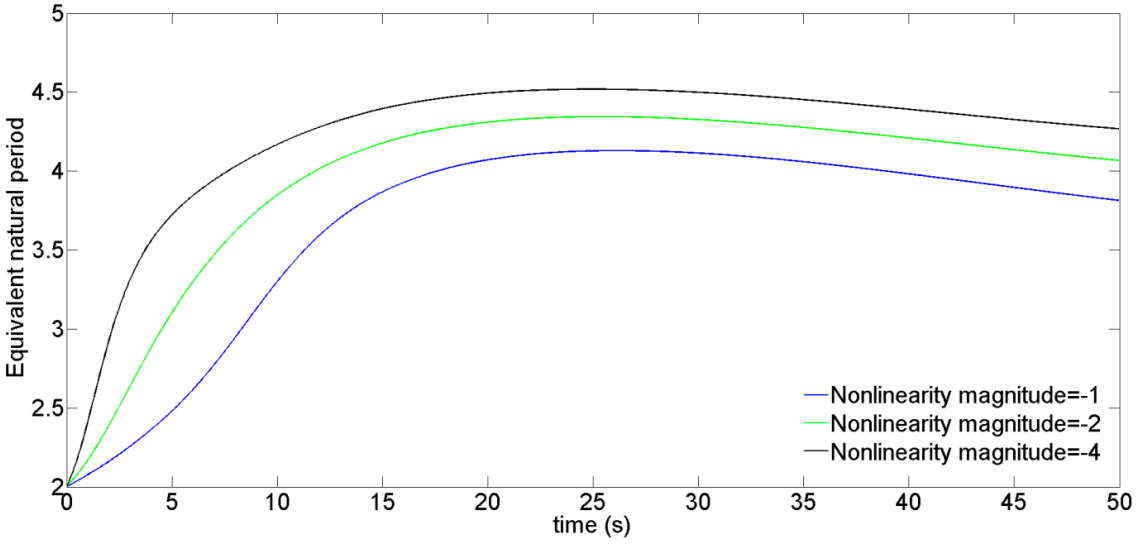

Figure 5.10: Equivalent natural period $T_{eq}(t)$ for a softening Duffing oscillator with nonlinear damping ($\varepsilon_1 = 0.1$,$\omega_0^2 = \pi^2$, $\zeta_0 = 0.01$) under sea wave excitation

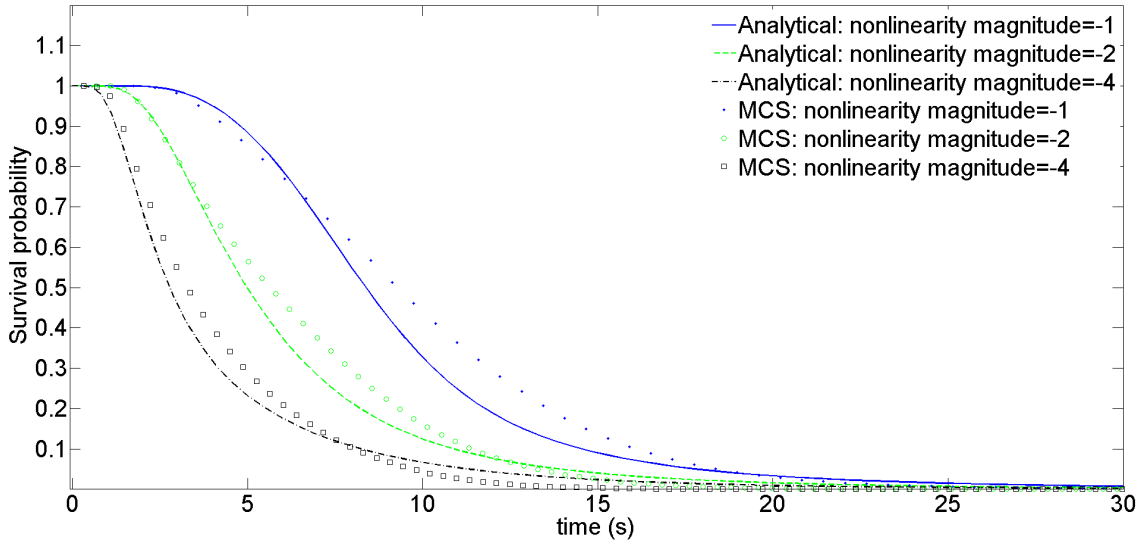

Figure 5.11: Survival probability for a softening Duffing oscillator with nonlinear damping ($\varepsilon_1 = 0.1$,$\omega_0^2 = \pi^2$, $\zeta_0 = 0.01$, $d_T = 0.125$) under sea wave excitation; comparisons with MCS (10,000 realizations)

both examples, the proposed method shows an acceptable agreement with pertinent Monte Carlo simulations. Due to the approximation of the linerization of negative stiffness, it is expected that the error between this method and MCS becomes larger when the degree of negative stiffness is increasing.

Chapter 6

Concluding remarks

In this chapter, the main contents of the thesis along with discussions of results are summarized and presented. Then, suggestions of future developments for the proposed methods are also discussed.

In chapter 2, a general L_p norm $(0 < p \leq 1)$ minimization approach has been proposed for estimating stochastic process power spectra subject to realizations with missing data. In particular, focusing on the L_1 and $L_{1/2}$ norms, it has been shown that the approach can be significantly enhanced by an adaptive basis re-weighting scheme, while it can satisfactorily estimate the power spectra of stationary, non-stationary, and multi-dimensional processes. It is shown that there are clear advantages to utilizing $L_{1/2}$ norm over L_1 norm minimization in signal reconstruction for power spectrum estimation. In particular, when dealing with single process records for which the presented adaptive basis re-weighting procedure cannot be applied, $L_{1/2}$ norm minimization exhibits superior performance to L_1 norm. In addition, where multiple realizations are available for basis re-weighting, $L_{1/2}$ norm is shown to provide more accurate spectrum estimations when large sample sizes are utilized. Nevertheless, differences in the effect of re-weighting have been observed. Although the improvement in spectrum estimation accuracy was significant for both $L_{1/2}$ and L_1 norm minimization when utilizing the re-weighting procedure, L_1 norm minimization has been shown to exhibit a greater magnitude of improvement after re-weighting when compared to $L_{1/2}$. This is due to the fact that the re-weighting procedure has a sparsity enhancing effect, which leaves less room for an $L_{1/2}$ solution to exhibit greater sparsity than an L_1 solution. Nevertheless, despite the re-weighting, the $L_{1/2}$ solution still succeeds in producing sparser spectral estimates. For a signal that is not truly sparse, this additional sparsity can be an advantage or disadvantage depending on the number of samples available. For large sample sizes, the $L_{1/2}$ norm minimization has produced superior results across all of the examples. However, in the stationary and the two-dimensional cases, for small sample sizes the opposite has been true. Thus, for small sample numbers in particular, when dealing with reconstruction of processes for which limited information regarding their degree of sparsity is available, estimates from both minimization schemes should be utilized within a decision-making process.

In chapter 3, an analytical approach for quantifying the uncertainty in stochastic process power spectrum estimates based on samples with missing data has been developed. Specifically, the cor-

relations between the missing data are considered by employing a Kriging model, while utilizing fundamental concepts from probability theory, and resorting to a Fourier based representation of stationary stochastic processes, a closed form expression has been derived for the power spectrum estimate PDF at each frequency. Next, the approach has been extended for determining the PDF of spectral moments estimates as well. This is of considerable significance to reliability assessment methodologies as well, where spectral moments are used for evaluating the survival probability of the system. Further, it has been shown that utilizing a Cholesky kind decomposition for the PDF related integrals the computational cost is kept at a minimal level.

In chapter 4, a WPI based technique for determining the non-stationary response PDF, the survival probability and the first-passage PDF of nonlinear/hysteretic oscillators subject to stochastic excitation has been developed. Specifically, based on a stochastic averaging/linearization treatment of the problem, the nonlinear oscillator has been cast into an equivalent linear time-variant oscillator. In this regard, equivalent linear time-dependent stiffness and damping elements have been also determined as part of the solution procedure. Further, relying on a variational formulation and on the concept of the most probable path, a closed-form analytical expression has been derived for the oscillator short-time transition PDF. Next, utilizing the short-time transition PDF and the C-K equation, a closed-form expression for the oscillator transient joint response PDF has been derived as well. Thus, the solution can be propagated in short time steps yielding not only the non-stationary response PDF, but also the survival probability and the first-passage PDF of the nonlinear oscillator. In comparison with existing, albeit more versatile, numerical path integral schemes, a significant advantage of the proposed WPI technique is that the computationally demanding task of numerically integrating for every time step the high-dimensional convolution integrals involved in the C-K equation has been circumvented. This is due to the fact that closed-form analytical expressions have been derived for the involved multi-dimensional convolution integrals; thus, the computational cost is kept at a minimum level. Besides, the WPI based approach takes into account the correlation of the displacement x and velocity $\dot{x}$, which is important for the accuracy of the response analysis especially during the transient phase where the oscillator response displacement and velocity are correlated.

In chapter 5, an approximate analytical technique has been developed for determining the survival probability of a softening Duffing oscillator subject to evolutionary stochastic excitation. In the context of nonlinear stochastic dynamics, the Duffing oscillator with softening nonlinearity has been so far treated in a manner which disregarded important aspects of the analysis, such as the unbounded behavior the response process experiences when the restoring force acquires negative values. Herein, introducing a special form for the oscillator non-stationary response amplitude PDF and relying on stochastic averaging, a rigorous and computationally efficient treatment of the problem has been provided. Taking advantage of this special response amplitude PDF form, a bounded transition probability function is obtained. Further, survival probability estimates have been determined for various levels of nonlinearity magnitude. A significant advantage of the tech-

nique relates to the fact that it can readily handle cases of stochastic excitations that exhibit strong variability in both the intensity and the frequency content.

Some future work can be done in both the missing data problem and first passage problem, discussed in this thesis.

For the missing data problem, the idea of reweighting could actually improve the performance of spectral estimation. L_p norm $(0 < p \leq 1)$ minimization approach can potential serve as a tool for develop a power spectrum estimation for the case of sub-Nyquist sampling to reduce the cost. Apart from the least square based reweighting procedure described in chapter 2, other potential alternative sparsity promoting schemes can also be utilized, such as L_1. Obviously, comprehensive comparisons of all the potential methods are required to be done as a benchmark.

As far as future extensions for first passage problem, the WPI technique based survival probability determination protains to explore its applicability in the context of multiple degree of freedom, for different oscillator models. In this regard, the dimension reduction technique [65] is potentially applied to improve the effectiveness of the method. Another potential direction is to extend the proposed analytical techniques to determine directly the survival probability without employing the short-time propagator as shown in chapter 4 and 5. In this regard, the accuracy of the solution is anticipated to increase due to the fact that no approximations related to the linearization of the system will be made.

Appendix A

By factorizing part of the integrand of Eq.(3.30) (given as Y in Eq.(3.31), the solution of Eq.(3.30) may be greatly simplified. In the following, a 2-variable case is given as an example.

For a 2-variable case, Eq. (3.29) becomes

$$\lambda_m = ax_1^2 + bx_1x_2 + cx_2^2 + dx_1 + ex_2 + f \tag{A.1}$$

where a, b, c, d, e, f are real constant with $a > 0, c > 0, f > 0$. Eq.(A.1) can be also recast into a matrix form as

$$\lambda_m = \begin{pmatrix} x_1 & x_2 & 1 \end{pmatrix} \begin{pmatrix} a & 0.5b & 0.5d \\ 0.5b & c & 0.5e \\ 0.5d & 0.5e & f \end{pmatrix} \begin{pmatrix} x_1 \\ x_2 \\ 1 \end{pmatrix} \tag{A.2}$$

Further, according to Eq.(3.31), Y has the form

$$Y = \frac{1}{2}x_1^2 + \frac{1}{2}x_2^2 - i\omega(ax_1^2 + bx_1x_2 + cx_2^2 + dx_1 + ex_2 + f) \tag{A.3}$$

The object of step 3 is to recast Eq.(A.3) into the form given by Eq.(3.34). To achieve this goal, second order terms of Y are separated and then factorized as follows,

$$\begin{aligned} Y_1 &= \frac{1}{2}x_1^2 + \frac{1}{2}x_2^2 - i\omega(ax_1^2 + bx_1x_2 + cx_2^2) \\ &= \begin{pmatrix} x_1 & x_2 \end{pmatrix} \begin{pmatrix} 0.5 - i\omega a & -0.5i\omega b \\ -0.5i\omega b & 0.5 - i\omega c \end{pmatrix} \begin{pmatrix} x_1 \\ x_2 \end{pmatrix} \\ &= \begin{pmatrix} x_1 & x_2 \end{pmatrix} A'_{Y_1} A_{Y_1} \begin{pmatrix} x_1 \\ x_2 \end{pmatrix} \end{aligned} \tag{A.4}$$

where $A_{Y_1} = \begin{pmatrix} \sqrt{0.5 - i\omega a} & -\dfrac{i\omega b}{2\sqrt{0.5 - i\omega a}} \\ 0 & \sqrt{\dfrac{\omega^2 b^2}{2 - 4i\omega a} + 0.5 - i\omega c} \end{pmatrix}$, and A'_{Y_1} is the non-conjugate transpose of A_{Y_1}, i.e., $A'_{Y_1} A_{Y_1} = \begin{pmatrix} 0.5 - i\omega a & -0.5i\omega b \\ -0.5i\omega b & 0.5 - i\omega c \end{pmatrix}$. This calculation can use the same numerical implementation steps as a Cholesky factorization algorithm with the note that $\begin{pmatrix} 0.5 - i\omega a & -0.5i\omega b \\ -0.5i\omega b & 0.5 - i\omega c \end{pmatrix}$ is not a Hermitian positive-definite matrix. Then, extending Y_1 to account for the first order terms in Eq.(A.3), Y may be written as,

$$\begin{aligned} Y &= \frac{1}{2}x_1^2 + \frac{1}{2}x_2^2 - i\omega(ax_1^2 + bx_1x_2 + cx_2^2 + dx_1 + ex_2 + f) \\ &= \begin{pmatrix} x_1 & x_2 \end{pmatrix} A'_{Y_1} A_{Y_1} \begin{pmatrix} x_1 \\ x_2 \end{pmatrix} - i\omega(dx_1 + ex_2 + f) \\ &= (A_Y \begin{pmatrix} x_1 \\ x_2 \\ 1 \end{pmatrix})'(A_Y \begin{pmatrix} x_1 \\ x_2 \\ 1 \end{pmatrix}) + c_Y \end{aligned} \tag{A.5}$$

where $A_Y = \begin{pmatrix} \sqrt{0.5 - i\omega a} & -\dfrac{i\omega b}{2\sqrt{0.5 - i\omega a}} & -\dfrac{i\omega d}{2\sqrt{0.5 - i\omega a}} \\ 0 & \sqrt{\dfrac{\omega^2 b^2}{2 - 4i\omega a} + 0.5 - i\omega c} & \dfrac{\dfrac{bd\omega^2}{1 - 2i\omega a} - i\omega e}{2\sqrt{\dfrac{\omega^2 b^2}{2 - 4i\omega a} + 0.5 - i\omega c}} \\ 0 & 0 & 0 \end{pmatrix}$, $c_Y = -(-\dfrac{i\omega d}{2\sqrt{0.5 - i\omega a}})^2 - (\dfrac{\dfrac{bd\omega^2}{1 - 2i\omega a} - i\omega e}{2\sqrt{\dfrac{\omega^2 b^2}{2 - 4i\omega a} + 0.5 - i\omega c}})^2 - i\omega f.$

Calculating the first term in Eq.(A.5), it can be seen that $(A_Y \begin{pmatrix} x_1 \\ x_2 \\ 1 \end{pmatrix})'(A_Y \begin{pmatrix} x_1 \\ x_2 \\ 1 \end{pmatrix})$ takes the

form

$$(A_Y \begin{pmatrix} x_1 \\ x_2 \\ 1 \end{pmatrix})'(A_Y \begin{pmatrix} x_1 \\ x_2 \\ 1 \end{pmatrix}) = (m_1x_1 + m_2x_2 + m_3)^2 + (m_4x_2 + m_5)^2 \tag{A.6}$$

where the constants m_1, m_2, m_3, m_4, m_5 are calculated by A_Y. Hence, Y may be written as

$$Y = (m_1x_1 + m_2x_2 + m_3)^2 + (m_4x_2 + m_5)^2 + c_Y \tag{A.7}$$

The form Eq.(A.7) is particularly useful in calculating the integral in Eq.(3.30), allowing it to be simplified as shown

$$\begin{aligned} \Phi_{\lambda_i}(\omega) &= E[e^{i\omega\lambda_i}] = \int_{-\infty}^{+\infty} (2\pi)^{-\frac{u}{2}} exp(-Y) dx_g \\ &= (2\pi)^{-1} \iint_{-\infty}^{+\infty} exp[-(m_1x_1 + m_2x_2 + m_3)^2 - (m_4x_2 + m_5)^2 - c_Y] dx_1 dx_2 \\ &= (2\pi)^{-1} \frac{\sqrt{\pi}}{m_1} \int_{-\infty}^{+\infty} exp[-(m_4x_2 + m_5)^2 - c_Y] dx_2 \\ &= \frac{1}{2m_1m_4} exp(-c_Y) \end{aligned} \tag{A.8}$$

For the general multi-variable case, the above steps are the same.

Appendix B

In this Appendix, analytical expressions are provided for several coefficients used in expressions derived in the main text. In this regard, with the aid of the symbolic toolbox of $MATLAB$ the analytical expressions for the coefficients C_1, C_2, C_3, C_4 of Eq.(4.25) are given by

$$\begin{aligned}
C_1 = [&\dot{x}_{m-1}e^{\zeta\omega(2t_m+t_{m-1})}sin(\omega t_{m-1}) + (x_m\zeta\omega - \dot{x}_m)e^{3\zeta\omega t_m}sin(\omega t_m) + (x_{m-1}\zeta\omega - \dot{x}_{m-1}) \\
&e^{3\zeta\omega t_{m-1}}sin(\omega t_{m-1}) + \dot{x}_m e^{\zeta\omega(t_m+2t_{m-1})}sin(\omega t_m) - (\dot{x}_{m-1}\zeta + x_{m-1}\omega + x_{m-1}\zeta^2\omega) \\
&e^{\zeta\omega(2t_m+t_{m-1})}cos(\omega t_{m-1}) - (\dot{x}_m\zeta + x_m\omega + x_m\zeta^2\omega)e^{\zeta\omega(t_m+2t_{m-1})}cos(\omega t_m) \\
&+ (\dot{x}_m + x_m\zeta\omega)\zeta e^{\zeta\omega(t_m+2t_{m-1})}cos(\omega(t_m - 2t_{m-1})) + (\dot{x}_{m-1} + x_{m-1}\zeta\omega)\zeta e^{\zeta\omega(2t_m+t_{m-1})} \\
&cos(\omega(2t_m - t_{m-1})) + x_{m-1}\omega e^{3\zeta\omega t_{m-1}}cos(\omega t_{m-1}) + x_m\omega e^{3\zeta\omega t_m}cos(\omega t_m) \\
&- x_{m-1}\zeta\omega e^{\zeta\omega(2t_m+t_{m-1})}sin(\omega(2t_m - t_{m-1})) + x_m\zeta\omega e^{\zeta\omega(t_m+2t_{m-1})}sin(\omega(t_m - 2t_{m-1}))] \\
&/[\omega(e^{4\zeta\omega t_m} + e^{4\zeta\omega t_{m-1}} - 2(1 + \zeta^2 - \zeta^2 cos(2\omega(t_m - t_{m-1})))e^{2\zeta\omega(t_m+t_{m-1})})]
\end{aligned} \tag{B.1}$$

$$\begin{aligned}
C_2 = -[&\dot{x}_{m-1}e^{\zeta\omega(2t_m+t_{m-1})}cos(\omega t_{m-1}) + (x_m\zeta\omega - \dot{x}_m)e^{3\zeta\omega t_m}cos(\omega t_m) + (x_{m-1}\zeta\omega - \dot{x}_{m-1}) \\
&e^{3\zeta\omega t_{m-1}}cos(\omega t_{m-1}) + \dot{x}_m e^{\zeta\omega(t_m+2t_{m-1})}cos(\omega t_m) + (+\dot{x}_{m-1}\zeta + x_{m-1}\omega + x_{m-1}\zeta^2\omega) \\
&e^{\zeta\omega(2t_m+t_{m-1})}sin(\omega t_{m-1}) + (\dot{x}_m\zeta + x_m\omega + x_m\zeta^2\omega)e^{\zeta\omega(t_m+2t_{m-1})}sin(\omega t_m) \\
&+ (-\dot{x}_m - x_m\zeta\omega)\zeta e^{\zeta\omega(t_m+2t_{m-1})}sin(\omega(t_m - 2t_{m-1})) + (\dot{x}_{m-1} - x_{m-1}\zeta\omega)\zeta e^{\zeta\omega(2t_m+t_{m-1})} \\
&sin(\omega(2t_m - t_{m-1})) - x_{m-1}\omega e^{3\zeta\omega t_{m-1}}sin(\omega t_{m-1}) - x_m\omega e^{3\zeta\omega t_m}sin(\omega t_m) \\
&- x_{m-1}\zeta\omega e^{\zeta\omega(2t_m+t_{m-1})}cos(\omega(2t_m - t_{m-1})) + x_m\zeta\omega e^{\zeta\omega(t_m+2t_{m-1})}sin(\omega(t_m - 2t_{m-1}))] \\
&/[\omega(e^{4\zeta\omega t_m} + e^{4\zeta\omega t_{m-1}} - 2(1 + \zeta^2 - \zeta^2 cos(2\omega(t_m - t_{m-1})))e^{2\zeta\omega(t_m+t_{m-1})})]
\end{aligned} \tag{B.2}$$

$$C_3 = -[\dot{x}_{m-1}(e^{\zeta\omega(4t_m+t_{m-1})} - e^{\zeta\omega(2t_m+3t_{m-1})})sin(\omega t_{m-1}) - \dot{x}_m(e^{\zeta\omega(3t_m+2t_{m-1})}$$
$$- e^{\zeta\omega(t_m+4t_{m-1})})sin(\omega t_m) + (\dot{x}_{m-1} - x_{m-1}\zeta\omega)\zeta e^{\zeta\omega(2t_m+3t_{m-1})}cos(\omega(2t_m - t_{m-1}))$$
$$- x_{m-1}\omega e^{\zeta\omega(4t_m+t_{m-1})}cos(\omega t_{m-1}) - x_m\omega e^{\zeta\omega(t_m+4t_{m-1})}cos(\omega t_m)$$
$$+ (x_{m-1}\omega - \dot{x}_{m-1}\zeta + x_{m-1}\zeta^2\omega)e^{\zeta\omega(2t_m+3t_{m-1})}cos(\omega t_{m-1}) + (x_m\omega - \dot{x}_{m-1}\zeta)$$
$$e^{\zeta\omega(3t_m+2t_{m-1})}cos(\omega t_m) + (\dot{x}_m - x_m\omega\zeta)\zeta e^{\zeta\omega(3t_m+2t_{m-1})}cos(\omega(t_m - 2t_{m-1})) + x_m\omega\zeta$$
$$e^{\zeta\omega(3t_m+2t_{m-1})}(sin(t_m - 2t_{m-1}) + \zeta cos(\omega t_m)) - x_{m-1}\zeta\omega e^{\zeta\omega(2t_m+3t_{m-1})}sin(\omega(2t_m - t_{m-1}))$$
$$+ x_{m-1}\zeta\omega e^{\zeta\omega(4t_m+t_{m-1})}sin(\omega t_{m-1}) + x_m\zeta\omega e^{\zeta\omega(t_m+4t_{m-1})}sin(\omega t_m)]$$
$$/[\omega(e^{4\zeta\omega t_m} + e^{4\zeta\omega t_{m-1}} - 2(1 + \zeta^2 - \zeta^2 cos(2\omega(t_m - t_{m-1})))e^{2\zeta\omega(t_m+t_{m-1})})] \tag{B.3}$$

$$C_4 = -[\dot{x}_{m-1}e^{\zeta\omega(2t_m+3t_{m-1})}cos(\omega t_{m-1}) + \dot{x}_m e^{\zeta\omega(3t_m+2t_{m-1})}cos(\omega t_m) - (\dot{x}_{m-1} + x_{m-1}\zeta\omega)$$
$$e^{\zeta\omega(4t_m+t_{m-1})}cos(\omega t_{m-1}) - (\dot{x}_m + x_m\zeta\omega)e^{\zeta\omega(t_m+4t_{m-1})}cos(\omega t_m) + (\dot{x}_{m-1} - x_{m-1}\zeta\omega)\zeta$$
$$e^{\zeta\omega(2t_m+3t_{m-1})}sin(\omega(2t_m - t_{m-1})) - x_{m-1}\omega e^{\zeta\omega(4t_m+t_{m-1})}sin(\omega t_{m-1})$$
$$- x_m\omega e^{\zeta\omega(t_m+4t_{m-1})}sin(\omega t_m) + (x_{m-1}\omega + x_{m-1}\omega\zeta^2 - \dot{x}_{m-1}\zeta)e^{\zeta\omega(2t_m+3t_{m-1})}sin(\omega t_{m-1})$$
$$+ (x_m\omega + x_m\omega\zeta^2 - \dot{x}_m\zeta)e^{\zeta\omega(3t_m+2t_{m-1})}sin(\omega t_m) + (x_m\zeta\omega - \dot{x}_m)\zeta e^{\zeta\omega(3t_m+2t_{m-1})}$$
$$sin(\omega(t_m - 2t_{m-1})) + x_m\zeta\omega e^{\zeta\omega(3t_m+2t_{m-1})}cos(\omega(t_m - 2t_{m-1}))$$
$$+ x_{m-1}\zeta\omega e^{\zeta\omega(2t_m+3t_{m-1})}cos(\omega(2t_m - t_{m-1}))]$$
$$/[\omega(e^{4\zeta\omega t_m} + e^{4\zeta\omega t_{m-1}} - 2(1 + \zeta^2 - \zeta^2 cos(2\omega(t_m - t_{m-1})))e^{2\zeta\omega(t_m+t_{m-1})})] \tag{B.4}$$

where ω denotes $\omega_{eq,m}$ and ζ denotes $\zeta_{eq,m}$ for simplification.

Further, to determine the analytical expression of the transition PDF of Eq.(4.28), a Taylor series expansion has been employed to expand the expression of Eq.(4.25) for the most probable path around point $t = t_{m-1}$. For instance, for a 3th order Taylor expansion of the form

$$f(t) \approx f(t_{m-1}) + f'(t_{m-1})(t - t_{m-1}) + \frac{f''(t_{m-1})}{2!}(t - t_{m-1})^2 + \frac{f^{(3)}(t_{m-1})}{3!}(t - t_{m-1})^3 \tag{B.5}$$

$p(x_m, \dot{x}_m, t_m | x_{m-1}, \dot{x}_{m-1}, t_{m-1})$ takes the form of Eq.(4.28), whereas the coefficients $n_{1,m}$, $n_{2,m}$,

$n_{3,m}$, $n_{4,m}$, $n_{5,m}$, $n_{6,m}$, $n_{7,m}$ are given by

$$\begin{aligned} n_{4,m} =&[-(47\zeta^4\Delta t^4\omega^4 + 96\zeta^3\Delta t^3\omega^3 + 18\zeta^2\Delta t^4\omega^4 + 42\zeta^2\Delta t^2\omega^2 + 16\zeta\Delta t^4\omega^4 - \Delta t^4\omega^4 \\ &+ 10\Delta t^2\omega^2 - 12)/(12\pi S\Delta t)]^{0.5} \end{aligned} \tag{B.6}$$

$$\begin{aligned} n_{1,m} =& -(338\zeta^5\Delta t^5\omega^5 + 809\zeta^4\Delta t^4\omega^4 + 34\zeta^3\Delta t^5\omega^5 + 768\zeta^3\Delta t^3\omega^3 + 23\zeta^2\Delta t^4\omega^4 \\ &+ 408\zeta^2\Delta t^2\omega^2 - 24\zeta\Delta t^5\omega^5 + 84\zeta\Delta t^3\omega^3 + 72\zeta\Delta t\omega - 10\Delta t^4\omega^4 \\ &+ 42\Delta t^2\omega^2 - 36)/(24\pi S\Delta t^2 n_{4,m}) \end{aligned} \tag{B.7}$$

$$\begin{aligned} n_{3,m} =&(342\zeta^5\Delta t^5\omega^5 + 811\zeta^4\Delta t^4\omega^4 + 60\zeta^3\Delta t^5\omega^5 + 768\zeta^3\Delta t^3\omega^3 + 62\zeta^2\Delta t^4\omega^4 \\ &+ 408\zeta^2\Delta t^2\omega^2 - 18\zeta\Delta t^5\omega^5 + 96\zeta\Delta t^3\omega^3 + 72\zeta\Delta t\omega - 9\Delta t^4\omega^4 \\ &+ 48\Delta t^2\omega^2 - 36)/(24\pi S\Delta t^2 n_{4,m}) \end{aligned} \tag{B.8}$$

$$\begin{aligned} n_{2,m} =& -(87\zeta^4\Delta t^4\omega^4 + 169\zeta^3\Delta t^3\omega^3 + 19\zeta^2\Delta t^4\omega^4 + 111\zeta^2\Delta t^2\omega^2 + 19\zeta\Delta t^3\omega^3 \\ &+ 30\zeta\Delta t\omega - 2\Delta t^4\omega^4 + 14\Delta t^2\omega^2 - 6)/(12\pi S\Delta t n_{4,m}) \end{aligned} \tag{B.9}$$

$$\begin{aligned} n_{7,m} =&(3 - 12\zeta^2\Delta t^2\omega^2 - 12\zeta\Delta t\omega - 4\Delta t^2\omega^2)^{0.5} * (73\zeta^4\Delta t^4\omega^4 + 152\zeta^3\Delta t^3\omega^3 \\ &+ 6\zeta^2\Delta t^4\omega^4 + 148\zeta^2\Delta t^2\omega^2 + 8\zeta\Delta t^3\omega^3 + 48\zeta\Delta t\omega + \Delta t^4\omega^4 - 4\Delta t^2\omega^2 \\ &+ 12)/(24\pi S\Delta t^2 n_{4,m}) \end{aligned} \tag{B.10}$$

$$\begin{aligned} n_{6,m} =&[(310\zeta^5\Delta t^5\omega^5 + 605\zeta^4\Delta t^4\omega^4 - 14\zeta^3\Delta t^5\omega^5 + 492\zeta^3\Delta t^3\omega^3 - 47\zeta^2\Delta t^4\omega^4 \\ &+ 288\zeta^2\Delta t^2\omega^2 - 32\zeta\Delta t^5\omega^5 + 60\zeta\Delta t^3\omega^3 + 72\zeta\Delta t\omega - 18\Delta t^4\omega^4 + 66\Delta t^2\omega^2 \\ &- 36)/(24\pi S\Delta t^2) - n_{3,m}n_{2,m}]/n_{7,m} \end{aligned} \tag{B.11}$$

$$\begin{aligned} n_{5,m} =&[(551\zeta^5\Delta t^5 + 1224\zeta^5\Delta t^5\omega^5 - 165\zeta^4\Delta t^6\omega^6 + 1180\zeta^4\Delta t^4\omega^4 - 426\zeta^3\Delta t^5\omega^5 \\ &+ 1056\zeta^3\Delta t^3\omega^3 - 106\zeta^2\Delta t^6\omega^6 - 74\zeta^2\Delta t^4\omega^4 + 672\zeta^2\Delta t^2\omega^2 - 90\zeta\Delta t^5\omega^5 \\ &+ 204\zeta\Delta t^3\omega^3 + 144\zeta\Delta t\omega + 4\Delta t^6\omega^6 - 44\Delta t^4\omega^4 + 120\Delta t^2\omega^2 \\ &- 72)/(24\pi S\Delta t^3) - n_{3,m}n_{1,m}]/n_{7,m} \end{aligned} \tag{B.12}$$

where ω denotes $\omega_{eq,m}$ and ζ denotes $\zeta_{eq,m}$ for simplification.

Note that the transition PDF does not depend on the initial t_{m-1} and final t_m time points, but only on the time interval $\Delta t = t_m - t_{m-1}$. Furthermore, with the aid of the symbolic toolbox of

$MATLAB$ the integration in Eq.(4.32) can be performed analytically to yield the non-stationary response PDF of Eq.(4.33), with the coefficients $k_{1,m}$, $k_{2,m}$, $k_{3,m}$, $k_{4,m}$, $k_{5,m}$, $k_{6,m}$, $k_{7,m}$ given by

$$k_{4,m} = [(n_{4,m}^2(k_{3,m-1}^2 n_{6,m}^2 + k_{4,m-1}^2 k_{7,m-1}^2 - 2k_{4,m-1}k_{3,m-1}n_{6,m}n_{5,m} + k_{4,m-1}^2 n_{5,m}^2 + k_{7,m-1}^2 n_{6,m}^2))/M]^{0.5} \tag{B.13}$$

$$\begin{aligned} k_{1,m} = -[&n_{4,m}(k_{5,m-1}n_{1,m}k_{4,m-1}^2 k_{7,m-1} + k_{1,m-1}n_{2,m}k_{4,m-1}k_{7,m-1}^2 \\ &- k_{3,m-1}k_{5,m-1}k_{4,m-1}k_{7,m-1}n_{2,m} - k_{1,m-1}n_{1,m}k_{4,m-1}n_{6,m}n_{5,m} \\ &+ k_{1,m-1}n_{2,m}k_{4,m-1}n_{5,m}^2 + k_{5,m-1}n_{1,m}k_{7,m-1}n_{6,m}^2 - k_{5,m-1}n_{2,m}k_{7,m-1}n_{6,m}n_{5,m} \\ &+ k_{1,m-1}k_{3,m-1}n_{1,m}n_{6,m}^2 - k_{1,m-1}k_{3,m-1}n_{2,m}n_{6,m}n_{5,m})]/[k_{4,m}M] \end{aligned} \tag{B.14}$$

$$\begin{aligned} k_{3,m} = [&n_{4,m}(n_{3,m}k_{3,m-1}^2 n_{6,m}^2 - n_{2,m}n_{7,m}k_{3,m-1}^2 n_{6,m}^2 - n_{3,m}k_{3,m-1}k_{4,m-1}n_{5,m}n_{6,m} \\ &+ n_{2,m}n_{7,m}k_{3,m-1}k_{4,m-1}n_{5,m} + n_{1,m}n_{7,m}k_{3,m-1}k_{4,m-1}n_{6,m} + n_{3,m}k_{4,m-1}^2 k_{7,m-1}^2 \\ &+ n_{3,m}k_{4,m-1}^2 n_{5,m}^2 - n_{1,m}n_{7,m}k_{4,m-1}^2 n_{5,m} + n_{3,m}k_{7,m-1}^2 n_{6,m}^2 - n_{2,m}n_{7,m}k_{7,m-1}^2 n_{6,m})] \\ &/[k_{4,m}M] \end{aligned} \tag{B.15}$$

$$\begin{aligned} k_{2,m} = -[&n_{4,m}(k_{6,m-1}n_{1,m}k_{6,m-1}^2 n_{7,m} + k_{2,m-1}n_{2,m}k_{4,m-1}k_{7,m-1}^2 \\ &- k_{3,m-1}k_{6,m-1}n_{2,m}k_{4,m-1}k_{7,m-1} + k_{2,m-1}n_{2,m}k_{4,m-1}n_{5,m}^2 \\ &- k_{2,m-1}n_{1,m}k_{4,m-1}n_{5,m}n_{6,m} - k_{6,m-1}n_{2,m}k_{7,m-1}n_{5,m}n_{6,m} + k_{6,m-1}n_{1,m}k_{7,m-1}n_{6,m}^2 \\ &- k_{2,m-1}k_{3,m-1}n_{2,m}n_{5,m}n_{6,m} + k_{2,m-1}k_{3,m-1}n_{1,m}n_{6,m}^2)]/[k_{4,m}M] \end{aligned} \tag{B.16}$$

$$k_{7,m} = [(k_{4,m-1}^2 k_{7,m-1}^2 n_{7,m}^2)/(k_{3,m-1}^2 n_{6,m}^2 - 2k_{3,m-1}k_{4,m-1}n_{5,m}n_{6,m} + k_{4,m-1}^2 k_{7,m-1}^2 + k_{4,m-1}^2 n_{5,m}^2 + k_{7,m-1}^2 n_{6,m}^2)]^{0.5} \tag{B.17}$$

$$\begin{aligned} k_{6,m} = -[&k_{4,m-1}k_{7,m-1}n_{7,m}(k_{4,m-1}k_{6,m-1}n_{5,m} + k_{2,m-1}k_{7,m-1}n_{6,m} - k_{3,m-1}k_{6,m-1}n_{6,m})] \\ &/[k_{7,m}(k_{3,m-1}^2 n_{6,m}^2 - 2k_{3,m-1}k_{4,m-1}n_{5,m}n_{6,m} + k_{4,m-1}^2 k_{7,m-1}^2 + k_{4,m-1}^2 n_{5,m}^2 \\ &+ k_{7,m-1}^2 n_{6,m}^2)] \end{aligned} \tag{B.18}$$

$$k_{5,m} = -[k_{4,m-1}k_{7,m-1}n_{7,m}(k_{4,m-1}k_{5,m-1}n_{5,m} + k_{1,m-1}k_{7,m-1}n_{6,m} - k_{3,m-1}k_{5,m-1}n_{6,m})]$$
$$/[k_{7,m}(k_{3,m-1}^2 n_{6,m}^2 - 2k_{3,m-1}k_{4,m-1}n_{5,m}n_{6,m} + k_{4,m-1}^2 k_{7,m-1}^2 + k_{4,m-1}^2 n_{5,m}^2$$
$$+ k_{7,m-1}^2 n_{6,m}^2)] \tag{B.19}$$

$$k_{i,1} = n_{i,1}, i = 1, 2, 3, ..., 6, 7 \tag{B.20}$$

$$M = (k_{3,m-1}^2 n_{2,m}^2 + k_{3,m-1}^2 n_{6,m}^2 + k_{4,m-1}^2 k_{7,m-1}^2 - 2k_{4,m-1}k_{3,m-1}n_{2,m}n_{1,m}$$
$$- 2k_{4,m-1}k_{3,m-1}n_{6,m}n_{5,m} + k_{4,m-1}^2 n_{1,m}^2 + k_{4,m-1}^2 n_{5,m}^2 + k_{7,m-1}^2 n_{2,m}^2 + k_{7,m-1}^2 n_{6,m}^2$$
$$+ n_{1,m}^2 n_{6,m}^2 - 2n_{2,m}n_{1,m}n_{6,m}n_{5,m} + n_{2,m}^2 n_{5,m}^2) \tag{B.21}$$

List of Publications

Journal Papers:

- Y. Zhang, I. A. Kougioumtzoglou (2015). Nonlinear oscillator stochastic response and survival probability determination via the Wiener path integral, ASCE-ASME Journal of Risk and Uncertainty in Engineering Systems, Part B. Mechanical Engineering, (1): 021006:1-15.

- I. A. Kougioumtzoglou, Y. Zhang, Beer M., 2015. Softening Duffing oscillator reliability assessment subject to evolutionary stochastic excitation, ASCE-ASME Journal of Risk and Uncertainty in Engineering Systems, Part A. Civil Engineering, 10.1061/AJRUA6.0000828, C4015001: 1-10 (Special Issue, Invited).

- Y. Zhang, L. Comerford, I. A. Kougioumtzoglou, M. Beer, -norm minimization for stochastic process power spectrum estimation subject to incomplete data, Mechanical Systems and Signal Processing (Under Review)

- Y. Zhang, L. Comerford, I. A. Kougioumtzoglou, E. Patelli, M. Beer, Uncertainty quantification of power spectrum and spectral moments estimates subject to missing data, ASCE-ASME Journal of Risk and Uncertainty in Engineering Systems, Part A. Civil Engineering (Under Review)

Conference Papers:

- Y. Zhang, I. A. Kougioumtzoglou, Wiener path integral based nonlinear oscillator survival probability determination, Proceedings of the 7th International Conference on Computational Stochastic Mechanics (CSM 7), Santorini, Greece, 15-18 June, 2014, G. Deodatis, P. D. Spanos (Eds.), Research Publishing, ISBN:978-981-09-5348-5, 789-800.

- Y. Zhang, I. A. Kougioumtzoglou, An approximate approach for assessing the reliability of a stochastically excited softening Duffing oscillator, Proceedings of the 12th International Conference on Applications of Statistics and Probability in Civil Engineering (ICASP 12), Vancouver, Canada, 12-15 July, 2015.

- Y. Zhang, L. Comerford, I. A. Kougioumtzoglou, M. Beer, Compressive sensing for power spectrum estimation of multi-dimensional processes under missing data, Proceedings of the

22nd International Conference on Systems, Signals and Image Processing (IWSSIP 2015), London, UK, 10-12 September, 2015, ISBN:978-1-4673-8353-0.

- Y. Zhang, L. Comerford, I. A. Kougioumtzoglou, E. Patelli, M. Beer, Spectral moments estimates uncertainty quantification under incomplete data, Proceedings of the 6th Asia-Pacific Symposium on Structural Reliability and its Applications (APSSRA 2016), H.W. Huang, J. Li, J. Zhang & J.B. Chen (editors), May 28-30, 2016, Shanghai, China, ISBN 978-7-5608- 6303-0, 377-384.

- Y. Zhang, L. Comerford, I. A. Kougioumtzoglou, M. Beer, Enhancing sparsity in compressive sensing based power spectrum estimation of gappy processes, Proceedings of the 12th International Conference On Structural Safety And Reliability (ICOSSAR 2017), 6-10 August, 2017, TU Wien, Vienna, Austria, (Accepted).

Bibliography

[1] L. Arnold, I. Chuesov, and G. Ochs. Stability and capsizing of ships in random sea – a survey. *Nonlinear Dynamics*, 36:135–179, 2004.

[2] S.-K. Au and J.L. Beck. Estimation of small failure probabilities in high dimensions by subset simulation. *Prob. Eng. Mech.*, 16(4):263–277, 2001.

[3] S.-K. Au, Ching J., and J.L. Beck. Estimation of small failure probabilities in high dimensions by subset simulation. *Structural Safety*, 29:183–193, 2007.

[4] S. Baisch and G. Bokelmann. Spectral analysis with incomplete time series: an example from seismology. *Computers & Geosciences*, 25(7):739–750, 1999.

[5] A. Bandeira, E. Dobriban, D. Mixon, and W. Sawin. Certifying the restricted isometry property is hard. *IEEE Transactions on Information Theory*, 59(6):3448–3450, 2013.

[6] V. L. Belenky and N. B. Sevastianov. *Stability and safety of ships: Risk of capsizing*. The Society of Naval Architects and Marine Engineers, 2007.

[7] P. Billingsley. *Probability and measure*. John Wiley & Sons, 2008.

[8] P. Bocchini and G. Deodatis. Critical review and latest developments of a class of simulation algorithms for strongly non-gaussian random fields. *Probabilistic Engineering Mechanics*, 23(4):393–407, 2008.

[9] M. J. Brennan, I. Kovacic, A. Carrella, and T. P. Waters. On the jump-up and jump-down frequencies of the duffing oscillator. *Journal of Sound and Vibration*, 318:1250–1261, 2008.

[10] P. Broersen and R. Bos. Time-series analysis if data are randomly missing. *IEEE Trans.Instrum.Meas*, 55(1):79–84, 2006.

[11] C. Bucher. Simulation methods in structural reliability. *Marine Technology and Engineering*, 2:1071–1086, 2011.

[12] E. J. Candes, J. Romberg, and T. Tao. Robust uncertainty principles: Exact signal reconstruction from highly incomplete frequency information. *IEEE Transactions on Information Theory*, 52(2):489–509, 2006.

[13] T. K. Caughey. Random excitation of a system with bilinear hysteresis. *Journal of Applied Mechanics*, 27(4):649–652, 1960.

[14] M. Chaichian and A. Demichiev. *Path Integrals in Physics, vol.1*. Institute of Physics Publishing, Bristol and Philadelphia, 2001.

[15] R. Chartrand. Exact reconstruction of sparse signals via nonconvex minimization. *IEEE SIGNAL PROCESSING LETTERS*, 14(10):707–710, 2007.

[16] R. Chartrand and V. Staneva. Restricted isometry properties and nonconvex compressive sensing. *Inverse Problems*, 24(3):035020, 2008.

[17] R. Chartrand and W. Yin. Iteratively reweighted algorithms for compressive sensing. *2008 IEEE International Conference on Acoustics, Speech and Signal Processing*, pages 3869–3872, 2008.

[18] Pranesh Chatterjee and Biswajit Basu. Nonstationary seismic response of a tank on a bilinear hysteretic soil using wavelet transform. *Probabilistic Engineering Mechanics*, 21(1):54–63, 2006.

[19] J. Chen and J. Li. Optimal determination of frequencies in the spectral representation of stochastic processes. *Computational Mechanics*, 51(5):791–806, 2013.

[20] J. Chen, W. Sun, and J. Li, J.and Xu. Stochastic harmonic function representation of stochastic processes. *Journal of Applied Mechanics*, 80(1):2013, 2013.

[21] R.W. Clough and J. Penzien. *Dynamics of structures*. McGraw-Hill, 1975.

[22] L. Comerford, I. A. Kougioumtzoglou, and M. Beer. Compressive sensing based power spectrum estimation from incomplete records by utilizing an adaptive basis. In *Proceedings of IEEE SSCI 2014*, pages 117–124, 2014. doi:10.1109/CIES.2014.7011840.

[23] L. Comerford, I. A. Kougioumtzoglou, and M. Beer. Uncertainty quantification in power spectrum estimation of stochastic processes subject to missing data. In *Proceedings of the 2nd International Conference on Vulnerability and Risk Analysis and Management (ICVRAM 2014) & 6th International Symposium on Uncertainty Modelling and Analysis (ISUMA 2014), University of Liverpool, Liverpool, UK, July 13 – 16, 2014, M. Beer, S.-K. Au, J. W. Hall, (Eds.)*, pages 370–377. American Society of Civil Engineers (ASCE), 2014. doi: 10.1061/9780784413609.038.

[24] L. Comerford, I. A. Kougioumtzoglou, and M. Beer. An artificial neural network approach for stochastic process power spectrum estimation subject to missing data. *Structural Safety*, 52:150–160, 2015.

[25] L. Comerford, I. A. Kougioumtzoglou, and M. Beer. Compressive sensing based stochastic process power spectrum estimation subject to missing data. *Probabilistic Engineering Mechanics*, 2016. doi:10.1016/j.probengmech.2015.09.015.

[26] G. Cottone, M. Di Paola, R. Ibrahim, A. Pirrotta, and R. Santoro. Stochastic ship roll motion via path integral method. *International Journal of Naval Architecture and Ocean Engineering*, 2:119–126, 2010.

[27] H. Cramér and R. Leadbetter. *Stationary and related stochastic processes: sample function properties and their applications*. Wiley, 1967.

[28] S. H. Crandall. First-crossing probabilities of the linear oscillator. *Journal of Sound Vibration*, 12(3):285, 1970.

[29] R. Dahlhaus. itting time series models to nonstationary processes. *The annals of Statistics*, 25(1):1–37, 1997.

[30] J. Dalzell. A note on the form of ship roll damping. *Journal of Ship Research*, 22:178–185, 1978.

[31] M. A. Davenport, M. F. Duarte, Y. C. Eldar, and G. Kutyniok. *Introduction to Compressed Sensing, Compressed Sensing: Theory and Applications*. Cambridge University Press, 2012.

[32] H. Dekker. Time-local gaussian processes, path integrals and nonequilibrium nonlinear diffusion. *Physica*, 85(2):363–373, 1976.

[33] G. Deodatis and R. C. Micaletti. Simulation of highly skewed non-gaussian stochastic processes. *Journal of engineering mechanics*, 127(12):1284–1295, 2001.

[34] A. Di Matteo, I. A. Kougioumtzoglou, P. D. Pirrotta, A.and Spanos, and M. Di Paola. Stochastic response determination of nonlinear oscillators with fractional derivatives elements via the wiener path integral. *Probabilistic Engineering Mechanics*, 38:127–135, 2014.

[35] M. Di Paola and R. Santoro. Path integral solution for nonlinear system enforced by poisson white noise. *Probab. Eng. Mech.*, 23(2-3):164–169, 2008.

[36] D. L. Donoho. Compressed sensing. *IEEE Transactions on Information Theory*, 52(4):1289–1306, 2006.

[37] Y.C. Eldar and G. Kutyniok. *Compressed Sensing: Theory and Apps*. Cambridge Uni Press, 2012.

[38] G. M. Ewing. *Calculus of Variations with Applications*. Dover Publications, Mineola, 1985.

[39] G. Fahlman and T. Ulrych. A new method for estimating the power spectrum of gapped data. *Monthly Notices of the Royal Astronomical Society*, 199(1):53–65, 1982.

[40] R. P. Feynman. Space-time approach to non-relativisic quantum mechanics. *R. M. Phys*, 20:367–387, 1948.

[41] R. P. Feynman and A. R Hibbs. *Quantum mechanics and path integrals*. McGraw-Hill, New York, 1965.

[42] D. Gamerman. *Markov Chain Monte Carlo: a stochastic simulation for Bayesian interference*. Taylor and Francis, 2006.

[43] B. Gaspar, A. P. Teixeira, and Soares C. Guedes. Assessment of the efficiency of kriging surrogate models for structural reliability analysis. *Probabilistic Engineering Mechanics*, 37:24–34, 2014.

[44] Gene H. Golub and Charles F Van Loan. *Matrix Computations*. Johns Hopkins, Baltimore, 1996.

[45] I. F. Gorodnitsky and B. D. Rao. Sparse signal reconstruction from limited data using focuss: A re-weighted minimum norm algorithm. *IEEE Transactions on signal processing*, 45(3):600–616, 1997.

[46] P. Green, K. Worden, K. Atallah, and N. D. Sims. The benefits of duffing-type nonlinearities and electrical optimisation of a mono-stable energy harvester under white gaussian excitations. *Journal of Sound and Vibration*, 331(20):4504–4517, 2012.

[47] M. Grigoriu. *Applied non-Gaussian processes: Examples, theory, simulation, linear random vibration, and MATLAB solutions*. Prentice Hall, 1995.

[48] M. Haile and A. Ghoshal. Application of compressed sensing in full-field structural health monitoring. In *SPIE Smart Structures and Materials+ Nondestructive Evaluation and Health Monitoring*, pages 834618–834618. International Society for Optics and Photonics, 2012.

[49] J. M. Hammersley and D. C. Handscomb. *Monte Carlo Methods*. Chpman and Hall Ltd, 1979.

[50] J. B. Harley, A. C. Schmidt, and J. M. Moura. Accurate sparse recovery of guided wave characteristics for structural health monitoring. *IEEE International Ultrasonics Symposium*, pages 158–161, 2012.

[51] K. Hasselmann. *Measurements of wind-wave-growth and swell decay during the joint North Sea wave project: (JONSWAP)*. Deutches Hydrographisches Institut., 1973.

[52] K. Hasselmann, D B Ross, P Mueller, and W. Sell. A parametric wave prediction model. *Journal of Physical Oceanography*, 6:200–228, 1976.

[53] J.A. Hogbom. Aperture synthesis with a non-regular distribution of interferometer baselines. *Astronomy and Astrophysics Supplement*, 15:417, 1974.

[54] Y. Huang, J. L. Beck, and H. Wu, S.and Li. Robust bayesian compressive sensing for signals in structural health monitoring. *Computer-Aided Civil and Infrastructure Engineering*, 29(3):160–170, 2014.

[55] R. A. Ibrahim, N. G. Ghalhoub, and J. Falzarano. Interaction of ships and ocean structures with ice loads and stochastic ocean waves. *Applied Mechanics Review*, 60:246–289, 2007.

[56] D. Iourtchenko, E. Mo, and A. Naess. Reliability of strongly nonlinear single degree of freedom dynamic systems by the path integration method. *Journal of Applied Mechanics*, 75:061016–1 061016–8, 2008.

[57] W.D. Iwan. The steady-state response of a two-degree-of-freedom bilinear hysteretic system. *J. Appl. Mech.*, 32:151–156, 1965.

[58] G. Jia and A. Taflanidis. Kriging metamodeling for approximation of high-dimensional wave and surge responses in real-time storm/hurricane risk assessment. *Computer Methods in Applied Mechanics and Engineering*, 261-262:24–38, 2013.

[59] C. Jiang, A. W. Troesch, and S. W. Shaw. Capsize criteria for ship models with memory-dependent hydrodynamics and random excitation. *Phil. Trans. R. Soc. Lond. A*, 358:1761–1791, 2000.

[60] I. Kaymaz. Application of kriging method to structural reliability problems. *Struct. Saf.*, 27(2):133–151, 2005.

[61] I. A Kougioumtzoglou. Stochastic joint time-frequency response analysis of nonlinear structural systems. *Journal of Sound and Vibration*, 332:7153–7173, 2013.

[62] I. A. Kougioumtzoglou, F. Kong, P. D. Spanos, and J. Li. Some observations on wavelets based evolutionary power spectrum estimation. In *Proceedings of the Stochastic Mechanics Conference (SM12)*, pages 37–44, 2012. ISSN: 2035-679X.

[63] I. A. Kougioumtzoglou and P. D. Spanos. An approximate approach for nonlinear system response determination under evolutionary stochastic excitation. *Current Science*, 97:1203–1211, 2009.

[64] I. A. Kougioumtzoglou and P. D. Spanos. An analytical wiener path integral technique for nonstationary response determination of nonlinear oscillators. *Prob. Eng. Mechanics*, 28:125–131, 2012.

[65] I. A. Kougioumtzoglou and P. D. Spanos. Nonlinear mdof system stochastic response determination via a dimension reduction approach. *Computers and Structures*, 126:135–148, 2013.

[66] I. A. Kougioumtzoglou and P. D. Spanos. Response and first-passage statistics of nonlinear oscillators via a numerical path integral approach. *J. Eng. Mech.*, 139:1207–1217, 2013.

[67] I. A. Kougioumtzoglou and P. D. Spanos. Nonstationary stochastic response determination of nonlinear systems: A wiener path integral formalism. *J. Eng. Mech.*, pages 04014064–1 04014064–14, 2014.

[68] I. A. Kougioumtzoglou and P. D. Spanos. Stochastic response analysis of the softening duffing oscillator and ship capsizing probability determination via a path integral approach. *Probabilistic Engineering Mechanics*, 35(67-74), 2014.

[69] R. M. Levine, J. E. Michaels, S. J. Lee, D. O. Thompson, and D. E. Chimenti. Guided wave localization of damage via sparse reconstruction. *AIP Conference Proceedings-American Institute of Physics*, 1430:647, 2012.

[70] J. Li and J Chen. *Stochastic Dynamics of structures*. J. Wiley & Sons, 2009.

[71] J. Liang, S. R. Chaudhuri, and M. Shinozuka. Simulation of non-stationary stochastic processes by spectral representation. *Journal of Engineering Mechanics*, 133:616–627, 2007.

[72] N. Lomb. Least-squares frequency-analysis of unequally spaced data. *Astrophysics and Space Science*, 39(2):447–462, 1976.

[73] L. D. Lutes and S. Sarkani. *Random vibrations: analysis of structural and mechanical systems*. Elsevier, 2004.

[74] E. Mamontov and A. Naess. An analytical-numerical method for fast evaluation of probability densities for transient solutions of nonlinear ito's stochastic differential equations. *International Journal of Engineering Science*, 47:116–130, 2009.

[75] D. Mascarenas, A. Cattaneo, J. Theiler, and C. Farrar. Compressed sensing techniques for detecting damage in structures. *Structural Health Monitoring*, 2013. 1475921713486164.

[76] R. A. Muller and G. J. MacDonald. *Ice ages and astronomical causes : Data, Spectral Analysis and Mechanisms*. Praxis Publishing, Chichester, UK, 2 edition, 2002.

[77] A. Naess and J. M Johnsen. Response statistics of nonlinear, compliant offshore structures by the path integral solution method. *Probab. Eng. Mech.*, 8(2):91–106, 1993.

[78] G. P. Nason, R. von Sachs, and G. Kroisandt. Wavelet processes and adaptive estimation of the evolutionary wavelet spectrum. *Journal of the Royal Statistical Society.Series B (Statistical Methodology)*, 62(2):271–292, 2000.

[79] A. H. Nayfeh and N. E. Sanchez. Bifurcations in a forced softening duffing oscillator. *Int. J. Non-Linear Mech.*, 24:483–497, 1989.

[80] D. E. Newland. *An introduction to random vibrations, spectral and wavelet analysis*. Dover Publications, 1993.

[81] D. E. Newland. Harmonic and musical wavelets. In *Proceedings of the Royal Society of London Series A-Mathematical Physical and Engineering Sciences*, volume 444, pages 605–620, 1994.

[82] Fu Niu, Lingshuai Meng, Wenjuan Wu, Jinggong Sun, Wenming Zhang, Guang Meng, and Zhushi Rao. Design and analysis of a quasi-zero stiffness isolator using a slotted conical disk spring as negative stiffness structure. *Journal of Vibroengineering*, 16(4):1769–1785, June 2014.

[83] S. M. O'Connor, J. P. Lynch, and A. C. Gilbert. Implementation of a compressive sampling scheme for wireless sensors to achieve energy efficiency in a structural health monitoring system. In *SPIE Smart Structures and Materials+ Nondestructive Evaluation and Health Monitoring*, pages 86941L–86941L. International Society for Optics and Photonics, 2013.

[84] K. B. Oldham and J. Spanier. *The Fractional Calculus*. Academic Press, New York, 1974.

[85] A. Papoulis and S. U. Pillai. *Probability, Random Variables and Stochastic Processes*. McGraw-Hill, 2002.

[86] V. M. Patel and R. Chellappa. *Sparse representations and compressive sensing for imaging and vision*. Springer Science & Business Media, 2013.

[87] A. Perelli, L. De Marchi, L. Flamigni, A. Marzani, and G. Masetti. Best basis compressive sensing of guided waves in structural health monitoring. *Digital Signal Processing*, 42:35–42, 2015.

[88] W J Pierson and L. Moskowitz. A proposed spectral form for fully developed wind seas based on the similarity theory of s. a. kitaigorodskii. *Journal of Geophysical Research*, 69:5181–5190, 1964.

[89] A. Pirrotta and R. Santoro. Probabilistic response of nonlinear systems under combined normal and poisson white noise via path integral method. *Probabilistic Engineering Mechanics*, 26:26–32, 2011.

[90] N. P. Politis, A. Giaralis, and P. D. Spanos. Joint time-frequency representation of simulated earthquake accelerograms via the adaptive chirplet transform. In *Proc. Computational stochastic Mechanics*, pages 549–557, 2007.

[91] B. Priestley. *Spectral analysis and time series*. Academic Press, 1982.

[92] M Priestley. Evolutionary spectra and non-stationary processes. *Journal of the Royal Statistical Society Series B-Statistical Methodology*, 27(2):204–237, 1965.

[93] S Qian. *Introduction to Time-Frequency and Wavelet Transforms*. Prentice Hall, 2002.

[94] Bhaskar D. Rao and Kenneth Kreutz-Delgado. An affine scaling methodology for best basis selection. *IEEE TRANSACTIONS ON SIGNAL PROCESSING*, 47(1):187–200, 1999.

[95] Thomas Reynolds, Richard Harris, and Wen-Shao Chang. Nonlinear pre-yield modal properties of timber structures with large-diameter steel dowel connections. *Engineering Structures*, 76:235–244, 2014.

[96] C. P. Robert and G. Casella. *Monte Carlo Statistical Methods*. Springer, 2004.

[97] D. Roberts, J. Lehar, and J. Dreher. Time-series analysis with clean .1. derivation of a spectrum. *Astronomical Journal*, 93(4):968–989, 1987.

[98] J. B. Roberts. Response of an oscillator with nonlinear damping and a softening spring to non-white excitation. *Probabilistic Engineering Mechanics*, 1:40–48, 1986.

[99] J. B. Roberts and P. D. Spanos. Stochastic averaging: An approximate method of solving random vibration problems. *Int. J. Nonlinear Mech.*, 21(2):111–134, 1986.

[100] J. B. Roberts and P. D. Spanos. *Random vibration and statistical linearization*. Dover Publications, 2003.

[101] J. B. Roberts and M. Vasta. Markov modeling and stochastic identification for nonlinear ship rolling in random waves. *Phil. Trans. R. Soc. Lond. A*, 358, 2000.

[102] R. Y. Rubinstein. *Simulation and the Monte Carlo method*. Wiley, 1981.

[103] R. Y. Rubinstein and D. P. Kroese. *Simulation and the Monte Carlo method*. Wiley, 2008.

[104] F. Sabetta, , and A. Pugliese. Estimation of response spectra and simulation of non-stationary earthquake ground motions. *Bull. Seismol. Soc. Am.*, 86:337–352, 1996.

[105] J. Scargle. Studies in astronomical time-series analysis. ii -statistical aspects of spectral-analysis of unevenly spaced data. *Astrophysical Journal*, 263(2):835–853, 1982.

[106] G. I. Schueller, H. J. Pradlwarter, and Koutsourelakis P. S. A critical appraisal of reliability estimation procedures for high dimensions. *Probabilistic Engineering Mechanics*, 19:463–474, 2004.

[107] G. I. Schueller and P. D. Spanos. *Monte Carlo simulation: proceedings of the International Conference on Monte Carlo simulation*. Principality of Monaco, 2000.

[108] I. Senjanovic, G. Cipric, and J. Parunov. Survival analysis of fishing vessels rolling in rough seas. *Phil. Trans. R. Soc. Lond. A*, 358:1943–1965, 2000.

[109] M. Shields, G. Deodatis, and P. Bocchini. A simple and efficient methodology to approximate a general non-gaussian stationary stochastic process by a translation process. *Probabilistic Engineering Mechanics*, 26(4):511–519, 2011.

[110] M. Shinozuka and G. Deodatis. Simulation of stochastic processes by spectral representation. *Appl. Mech. Rev.*, 44(4):192–203, 1991.

[111] M. Shinozuka and G. Deodatis. Simulation of multi-dimensional gaussian stochastic elds by spectral representation. *Applied Mechanics Reviews*, 49(1):29–53, 1996.

[112] G. P. Solomos and P. D. Spanos. Oscillator response to nonstationary excitation. *Appl. Mech.*, 51(4):907–912, 1984.

[113] P. D. Spanos. Non-stationary random vibration of a linear structure. *International Journal of Solids and Structures*, 14:861–867, 1978.

[114] P. D. Spanos and T. W. Chen. Response of a dynamic system to flow-induced load. *International Journal of Non-Linear Mechanics*, 15:115–116, 1980.

[115] P. D. Spanos and G. Failla. Evolutionary spectra estimation using wavelets. *Journal of Engineering Mechanics*, 130(8):952–960, 2004.

[116] .P. D. Spanos and Agathoklis Giaralis. Third-order statistical linearization-based approach to derive equivalent linear properties of bilinear hysteretic systems for seismic response spectrum analysis. *Structural Safety*, 44:59–69, 2013.

[117] P. D. Spanos and I. A. Kougioumtzoglou. Harmonic wavelets based statistical linearization for response evolutionary power spectrum determination. *Probabilistic Engineering Mechanics*, 27(1):57–68, 2012.

[118] P. D. Spanos and I. A. Kougioumtzoglou. Survival probability determination of nonlinear oscillators subject to evolutionary stochastic excitation. *Journal of Applied Mechanics*, 81(5):051016–1 051016–9, 2014.

[119] P. D. Spanos and L. D. Lutes. Probability of response to evolutionary process. *J. Engrg. Mech. Div.*, 106(2):213–224, 1980.

[120] .P. D. Spanos, P. C. Roussis, and N. P. Politis. Dynamic analysis of stacked rigid blocks. *Soil Dynamics and Earthquake Engineering*, 21:559±578, 2001.

[121] P. D. Spanos and G. P. Solomos. Markov approximation to transient vibration. *Journal of Engineering Mechanics*, 109:1134–1150, 1983.

[122] .P. D. Spanos, J. Tezcan, and P. Tratskas. Stochastic processes evolutionary spectrum estimation via harmonic wavelets. *Computer Methods in Applied Mechanics and Engineering*, 194(12-16):1367–1383, 2005.

[123] K. J. Spyrou and J. M. T. Thomson. The nonlinear dynamics of ship motions: a field overview and some recent developments. *Phil. Trans. R. Soc. Lond. A*, 358:1735–1760, 2000.

[124] Srdjan Stankovic, Irena Orovic, and Sejdic Ervin. *Multimedia signals and systems*. Springer Science & Business Media, 2012.

[125] Michael Stein. *Interpolation of Spatial Data: Some Theory for Kriging*. Springer-Verlag, New York, 1999.

[126] S. Surendran, S. K. Lee, and K. H. Sohn. Simplified model for predicting the onset of parametric rolling. *Ocean Engineering*, 34:630–637, 2007.

[127] W. Szemplinska-Stupnicka. Bifurcations of harmonic solution leading to chaotic motion in the softening type duffing oscillator. *Int. J. Non-Linear Mech.*, 23:257–277, 1988.

[128] T. Taniguchi and E. G. D. Cohen. Inertial effects in non-equilibrium work fluctuations by a path integral approach. *J. Stat. Physics*, 130:1–26, 2008.

[129] M. Taylan. The effect of nonlinear damping and restoring in ship rolling. *Ocean Engineering*, 27:921–932, 2000.

[130] K. Teferra, S. R. Arwade, and G. Deodatis. Generalized variability response functions for two-dimensional elasticity problems. *Computer Methods in Applied Mechanics and Engineering*, 272:121–137, 2014.

[131] L. A. Vandewater and S. D. Moss. Probability of existence of vibro-impact regimes in a nonlinear vibration energy harvester. *Smart Mater. Struct.*, 22:094025, 2013.

[132] P. Vanicek. Approximate spectral analysis by least-squares fit - successive spectral analysis. *Astrophysics and Space Science*, 4(4):387–391, 1969.

[133] E. H. Vanmarcke. Properties of spectral moments with applications to random vibration. *Journal of Engineering Mechanics Division*, 98:425, 1972.

[134] E. H. Vanmarcke. On the distribution of the first-passage time for normal stationary random processes. *ASME Journal of Applied Mechanics*, 42:215–220, 1975.

[135] Y. Wang and H. Hao. Damage identification scheme based on compressive sensing. *Journal of Computing in Civil Engineering*, 2013. 04014037.

[136] Y. Wang, J. Li, and P. Stoica. *Spectral Analysis of Signals, the Mising Data Case*. Morgan & Caypool, 2005.

[137] M. F. Wehner and W. G Wolfer. Numerical evaluation of path integral solutions to fokker-planck equations. *Phys. Rev. A*, 27(5):2663–2670, 1983.

[138] N. Wiener. The average of an analytic functional. *Proceedings of the National Academy of Sciences of the United States of America*, 7(9):253–260, 1921.

[139] Zongben Xu, Hai Zhang, Yao Wand, Xiangyu Chang, and Yong Liang. L1/2 regularization. *Sci. China Inf. Sci.*, 53:1159–1169, 2010.

[140] Y. Yang and S. Nagarajaiah. Output-only modal identification by compressed sensing: Non-uniform low-rate random sampling. *Mechanical Systems and Signal Processing*, 56:15–34, 2015.

[141] Y. Zhang and I. A Kougioumtzoglou. Nonlinear oscillator stochastic response and survival probability determination via the wiener path integral. *ASCE-ASME Journal of Risk and Uncertainty in Engineering Systems, Part B. Mechanical Engineering*, 1(2):021005, 2015.

[142] W. Q. Zhu. Recent developments and applications of the stochastic averaging method in random vibration. *Applied Mechanics Reviews*, 49:72–80, 1996.

[143] Z. Zou, Bao Y., Li H., B. F. Spencer, and J. Ou. Embedding compressive sensing-based data loss recovery algorithm into wireless smart sensors for structural health monitoring. *IEEE Sensors Journal*, 15(2):797–808, 2015.